Development and study of direct-bonded silicon carbide bricks as a lining material for the blast furnace stack

DEVELOPMENT AND STUDY OF DIRECT-BONDED SILICON CARBIDE BRICKS AS A LINING MATERIAL FOR THE BLAST FURNACE STACK

J.T. van Konijnenburg

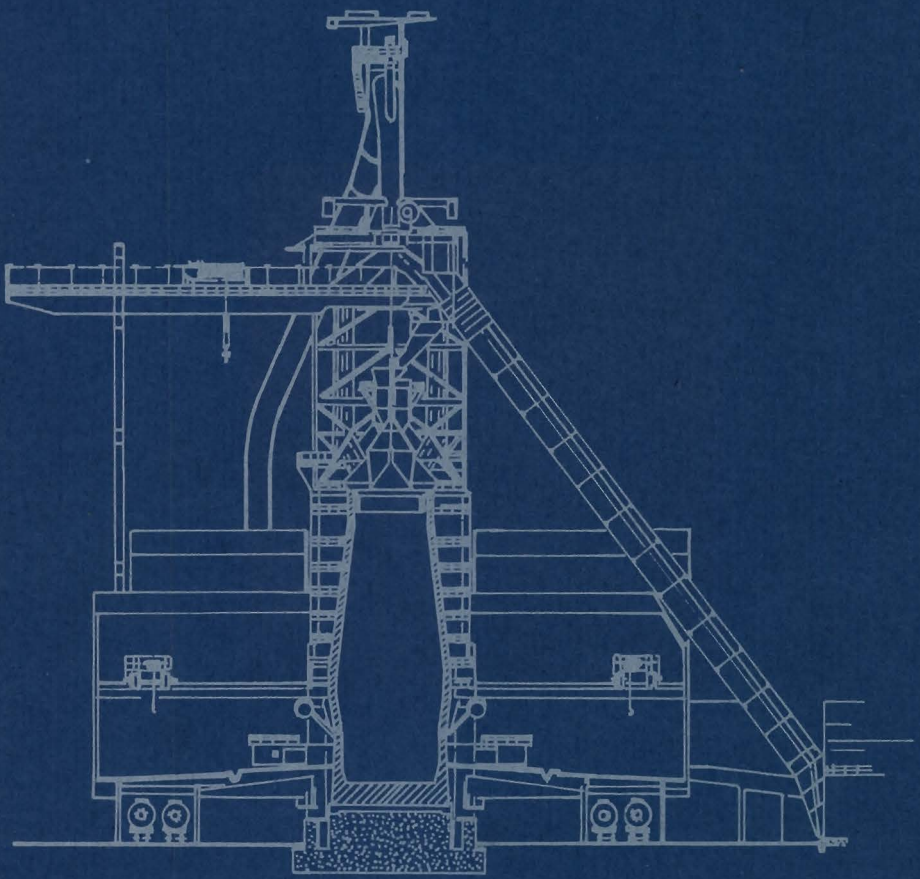

DEVELOPMENT AND STUDY OF DIRECT-BONDED SILICON CARBIDE BRICKS AS A LINING MATERIAL FOR THE BLAST FURNACE STACK

PROEFSCHRIFT

ter verkrijging van de graad van doctor in de technische wetenschappen aan de Technische Hogeschool Eindhoven, op gezag van de rector magnificus, prof.dr. P. van der Leeden, voor een commissie aangewezen door het college van dekanen in het openbaar te verdedigen op vrijdag 1 juli 1977 te 16.00 uur

door

Jan Teun van Konijnenburg
geboren te Voorburg

Dit proefschrift is goedgekeurd door de promotoren
Prof.Ir. A.L. Stuyts en Dr. H.N. Stein

Aan mijn vrouw

Aan mijn ouders

C O N T E N T S

PART TWO - STUDY OF SILICON CARBIDE REFRACTORY BRICKS

Chapter 1 - INTRODUCTION

1.1 - The Blast Furnace, a Chemical Reactor

The *blast furnace** is a vertical chemical reactor in which iron ore is reduced to *pig iron* (in the liquid state called *hot metal*). The blast furnace is a shaft kiln in which the iron ore is reduced by carbon directly or by reducing gases. In principle the furnace is a counter current reactor, as the movement of solid matter is downwards and the gas stream is upwards.
Because of the high temperatures in the reactor a protection of the reactor shell is necessary. Therefore a refractory lining is built against the inside of the shell.
This thesis deals with the problem of finding a suitable refractory lining for that part of the furnace (the middle and lower *stack*) where the *burden* of the furnace is still abrasive and the liquids and gases locally formed are chemically extremely reactive.

For an integrated steelplant a smooth and safe operation of the blast furnace is of the utmost importance. Especially nowadays, where large blast furnaces are used with high specific production rates, a good refractory lining and a good cooling system are the cornerstones of successful operation. Good operation means no relining of the furnace for a period of at least four years. For large blast furnaces this means a production of about 10.10^6 tons of hot metal. In older furnaces in Europe relining after about four years with a production of 3.10^6 tons was normal. From the data given it can be seen, that the quality of the refractory lining of large blast furnaces is very important.

In this chapter the blast furnace process will be discussed in view of the demands on the materials of the refractory wall in the different parts of the furnace.

The work described here was directed to the problems encountered at Hoogovens IJmuiden BV. As will be described later it is thought that the refractory problems have been solved for most of the furnace except the middle and lower stack. It is hoped that the work presented here will help to solve these problems as well.

---

* Words in italics are explained in Appendix I.

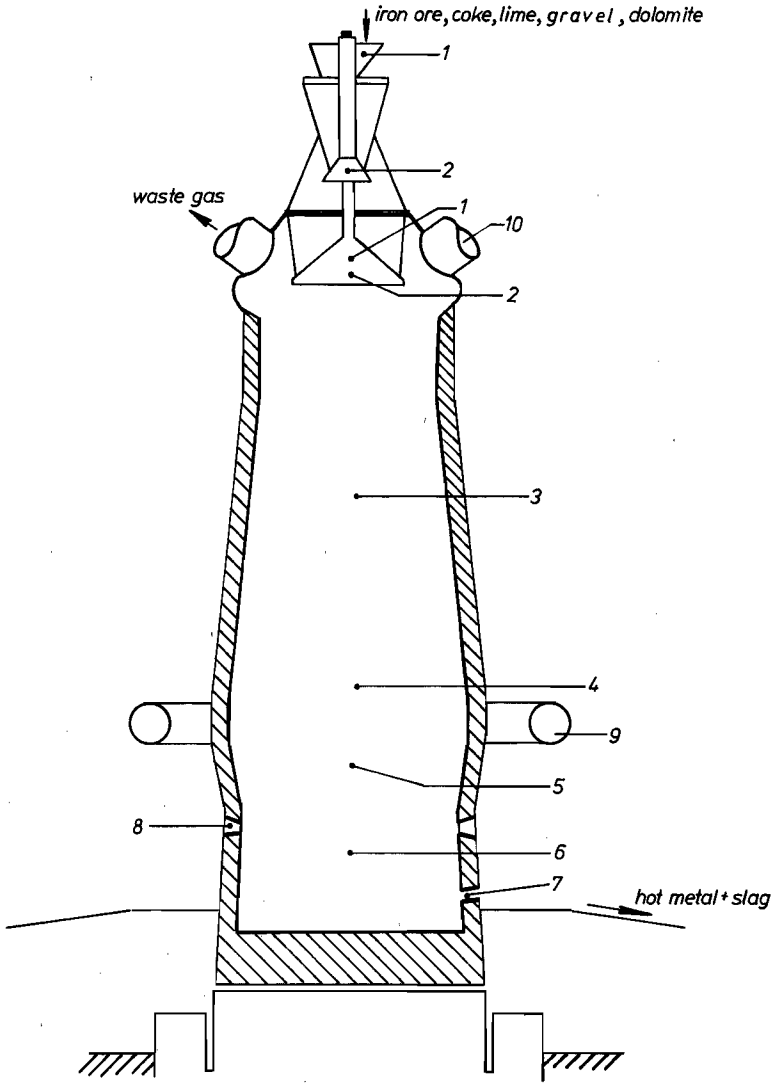

FIGURE 1.1 - The blast furnace. The furnace is a counter current reactor in which iron ore, coke, lime, gravel and dolomite are charged in a charging system (1) on the top of the furnace. The furnace atmosphere is sealed from the outside by means of a double bell system (2). The burden enters the furnace stack (3) by way of those bells. From the stack it comes in the major reaction zone, the belly (4) and the bosh (5). From there the hot metal and the slag drip through the still solid coke into the hearth (6), from where the hot metal and the slag are removed from the furnace through the taphole (7). At the level where the hearth meets

the bosh the tuyeres (8) are situated, which bring in the preheated air. This air is transported from the cowpers to the furnaces through the hot blast main and circulated around the furnace through the bustle pipe (9). The gases in the furnace flow upwards and leave the furnace near the big bell through the waste gas uptakes (10).

1.2 - The Blast Furnace Process

For a good understanding of the subject it is necessary to give a short description of hot metal production in a blast furnace. Hot metal is produced by means of charging iron ore, coke and some suitable additives into a shaft kiln. In principle the hot metal is formed out of iron ore due to reduction of the ore by the coke directly or by CO gas. The reduction takes place at high temperatures which are reached by burning part of the coke with preheated air in the lower part of the furnace. The hot metal and the *slag* are tapped through a taphole near the bottom of the furnace. The iron so produced can be used as a basis for steel production or for iron foundries. Figure 1.1 gives a schematic picture of the blast furnace with the names of the major part of the kiln.
To describe the blast furnace process the flow of gas through the furnace will be followed. The main reaction zone is found where the hearth and the bosh meets. Here a blast of hot air (with temperatures of 900°-1200°C) is blown into the furnace via the tuyeres (figure 1.1, No 7). The coke at this level burns with oxygen from the air and a temperature of about 2000°C can be reached. In principle a mixture of CO and CO_2 is formed following the reaction equation:

$$C + CO_2 = 2\ CO \quad \text{(Boudouard-equation)} \qquad [1.1]$$

Due to the high temperature the equilibrium is far to the right. As we can see from figure 1.2, at the temperatures concerned nearly 99 % (V/V) CO is formed.
If the furnace is filled with coke only, the furnace atmosphere at the tuyere level will be 33 % (V/V) CO and 67 % (V/V) N_2. The furnace, however, is filled with iron ore, coke and slag-forming components. Firstly the influence of the iron ore on the gas atmosphere in the furnace will be discussed.
In the stack the upstreaming gases will heat the burden. From temperatures higher than 700°C on, a direct reduction of the prereduced iron

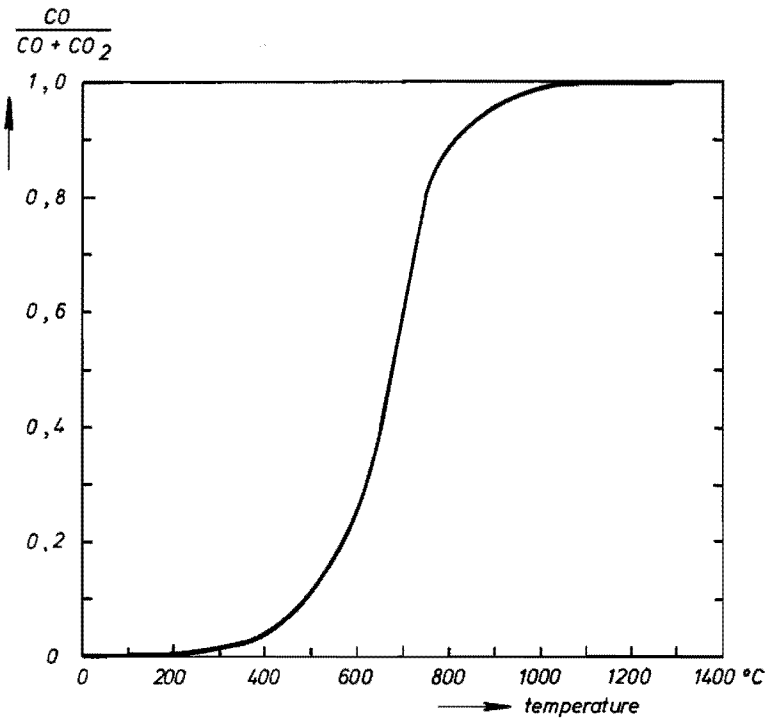

FIGURE 1.2 - Variation with temperature of the concentration of carbon monoxide in equilibrium with carbon dioxide and solid carbon at a total pressure of 1 atm.

ore will take place, following the equation:

$$FeO + C = Fe + CO \qquad [1.2]$$

Due to this second reaction the total CO content will be around 40 % (V/V). The gas mixture CO + N_2 flows upwards in the furnace. The CO content will decrease at higher levels in the furnace (starting somewhere in the lower stack) due to two phenomena:

1) Fe_2O_3 and Fe_3O_4 from the iron ore will react with CO, according to:

$$3\ Fe_2O_3 + CO = 2\ Fe_3O_4 + CO_2 \qquad [1.3]$$

and

$$Fe_3O_4 + CO = 3\ FeO + CO_2 \qquad [1.4]$$

From these equations it can be seen, that part of the CO will be replaced by CO_2.

2) Due to lower temperatures in the stack, the Boudouard-equilibrium [1.1] will shift to the left.

Figure 1.3 shows the gas composition as a function of the level in the furnace as measured in blast furnaces [1-1].

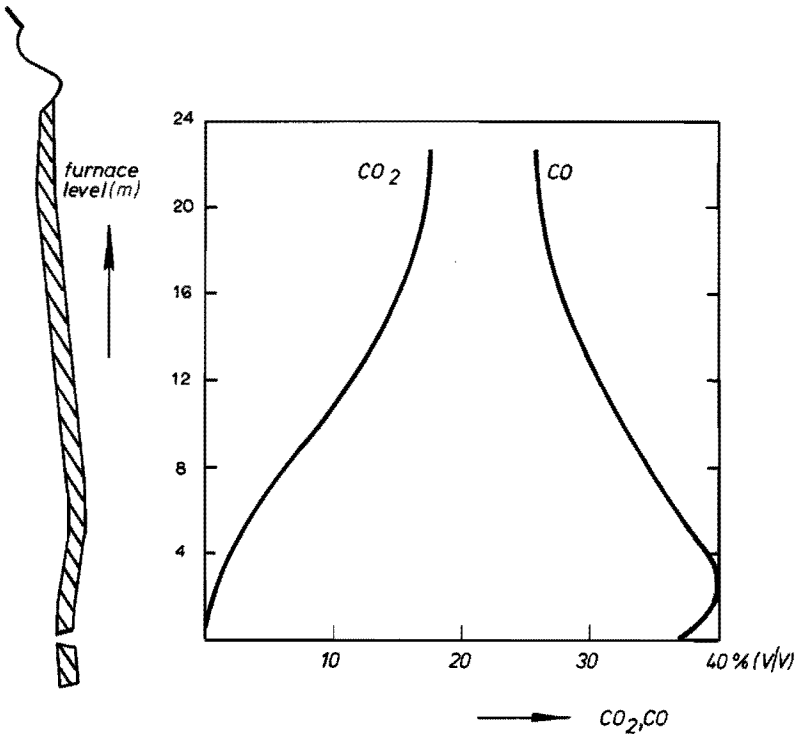

FIGURE 1.3 - The concentration of carbon-monoxide and carbon-dioxide as a function of the level in the blast furnace.

Iron ore has a Fe_2O_3 content of about 80-90 % (m/m). The rest of the ore - the gangue - consists mostly of a clay-like material containing mainly SiO_2, MnO, P_2O_5, Al_2O_3 and small amounts of alkali. In order to form in the furnace a good reservoir (the slag) in which those oxides can dissolve, gravel (SiO_2), limestone ($CaCO_3$) and raw dolomite ($CaCO_3.MgCO_3$) are charged with the ore and the coke. At the stage of the process where Fe_2O_3 is reduced to FeO, the first slag formation takes place. This occurs at a temperature of about 800°C. According to measurements made in blast furnaces this temperature is reached rather high in the furnace as is shown in figure 1.4. This figure also shows that the temperature in the center of the furnace is remarkably higher

than at the furnace wall. The temperature distribution in the furnace is due to the process itself and the system of charging ore and coke.

figure 1.4

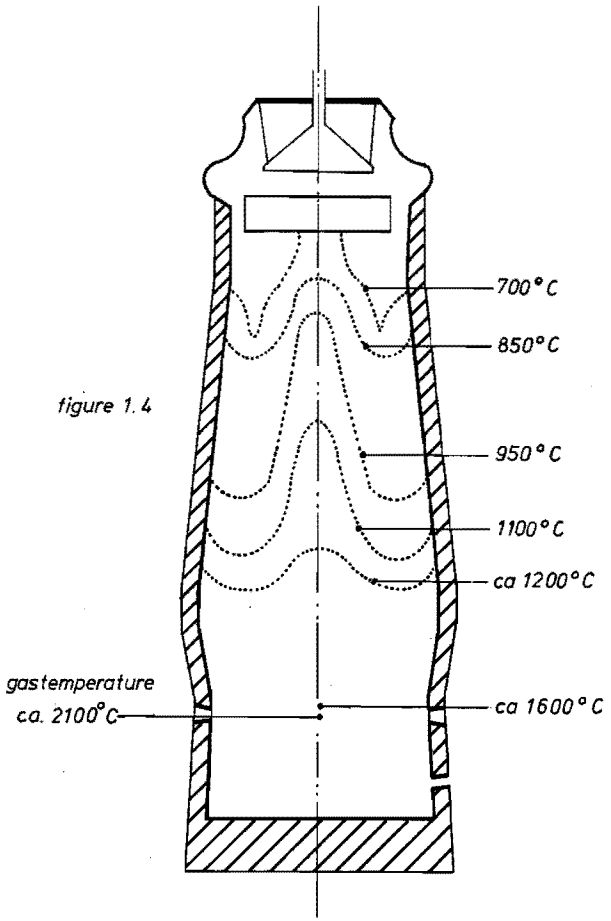

FIGURE 1.4 - The temperature distribution in the blast furnace given for a furnace which is operated at p ≈ 0.2 N.mm^{-2} top pressure [1-2], [1-3]. The isotherms shown represent the burden temperature.

The slag composition can only be determined after the slag has been tapped from the furnace. An average slag composition is given in table 1.1. The composition of the slag in the bosh and the lower stack is slightly different from that after tapping.

In figure 1.5 a schematic diagram of the flow of matter is given.

On the left side the flow of solids is given. This is a downward flow. On the right side the upward flow of gases is given. From the diagram it can be seen where the real slag formation starts, namely in the middle and lower stack where the first reduction of iron ore takes place. In that region also the limestone will decarburize following:

$$CaCO_3 \rightarrow CaO + CO_2 \qquad [1.5]$$

The CO_2 so formed will also increase the total amount of CO_2 present in the furnace.

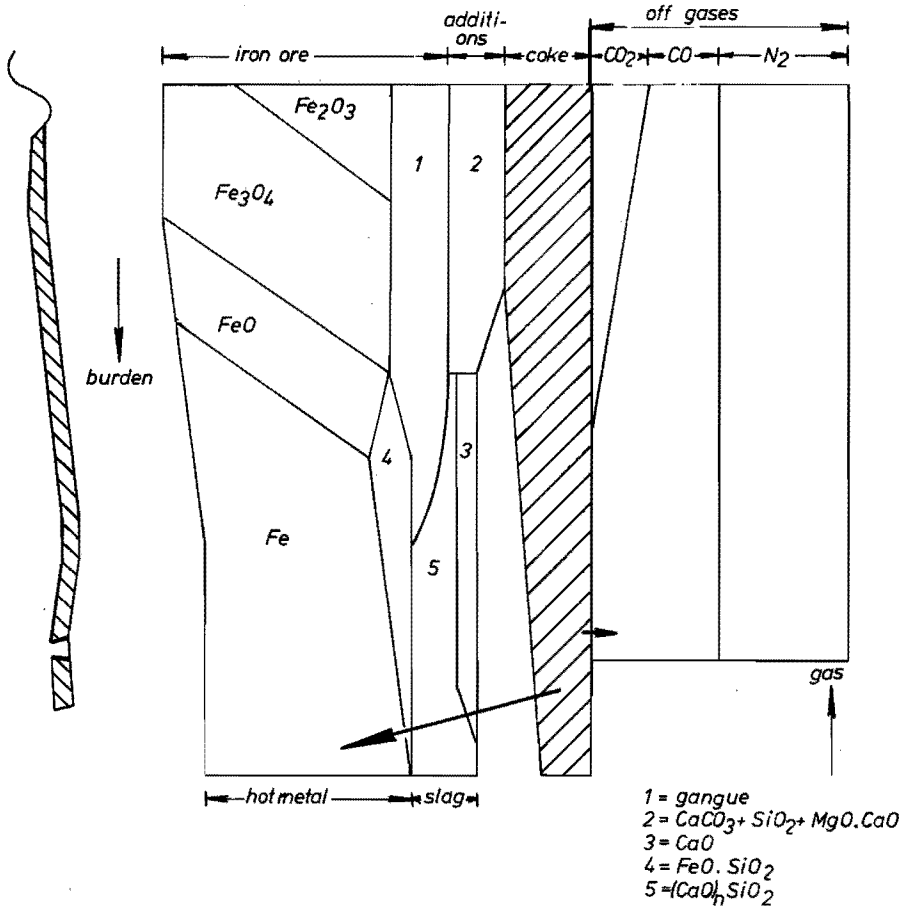

FIGURE 1.5 - A schematical diagram of the flow of solids and gases in a blast furnace. At the left side the mass fractions of the solids and liquids are given, at the right side the volume fractions of the gases.

TABLE 1.1 - Average slag composition

SiO_2	33	% (m/m)
Al_2O_3	12	
FeO	0.5	
CaO	43	
MgO	7	
Na_2O	1	
K_2O	1.5	
MnO	2	
Cs_2O		
Li_2O		
TiO_2		

TABLE 1.2 - Probable slag composition in the lower blast furnace stack

SiO_2	30	% (m/m)
Al_2O_3	16	
FeO	6	
CaO	32	
MgO	10	
Na_2O	1	
K_2O	5	

The lime, dolomite, gravel and the gangue material out of the iron ore become a molten mass at 800°-900°C, the slag [1-4], [1-5], [1-6]. The slag composition in the first stage is dependent on the furnace atmosphere and the temperature. Due to a low melting point of the alkalies, the alkali content of this slag will be relatively high. Studies were made to establish the composition of this early slag. Table 1.2 gives a probable composition of the slag in the lower blast furnace stack [1-7].
The first slag formation takes place in the middle and lower stack, but the major slag formation takes place in the bosh. At a temperature of 1300°C, the slag will be a mixture of molten and unmolten material. At a temperature of 1600°C, all the slag will be molten, as Konopicky [1-5] showed for a simplified slag containing only Al_2O_3, SiO_2 and CaO. Figure 1.6 shows this system in which the slag composition (s1) from table 1.2 is shown. From table 1.1 it can be seen that alkalies are present in the slag. When alkali metals are released from the gangue material, only about one tenth of the amounts of alkali metals which are present in the burden will be removed by the slag. The rest is carried up with the gases and is deposited either in a cooler part of the burden or in the refractory wall, or even removed from the furnace with the off gases [1-8], [1-9]. From broken out blast furnaces and from samples taken out of the blast furnace during the *campaign* it was seen, that only potassium will be deposited in reasonable amounts in the refractory wall. The other alkalies are of no importance. Therefore, in the further work we will

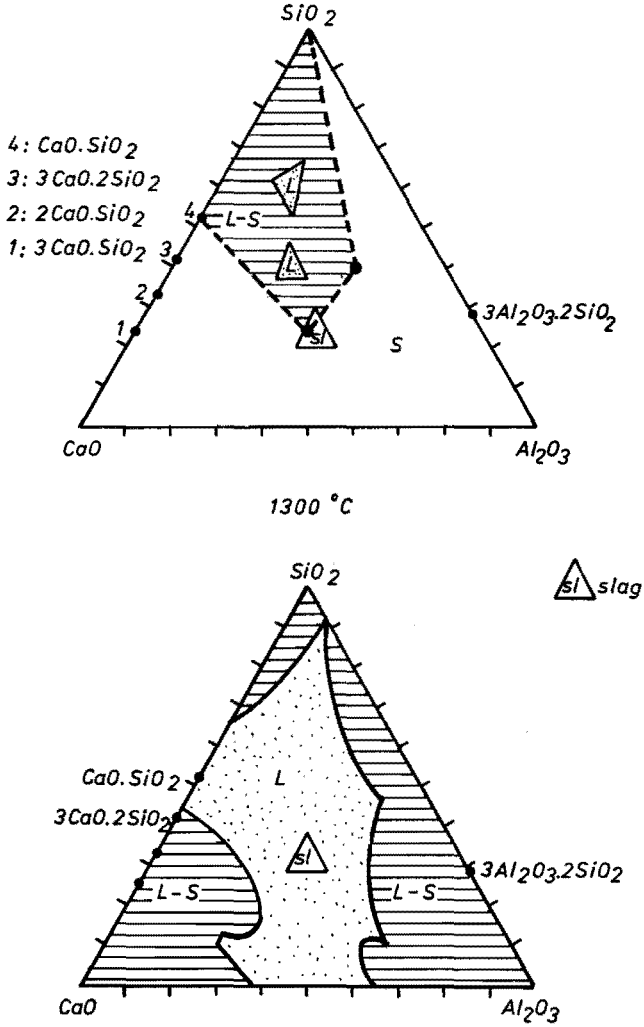

IGURE 1.6 - The quasi ternary system Al_2O_3 - SiO_2 - CaO at 1600°C and 1300°C

L are regions where the material is molten;
L-S are regions where there is a mixture of crystals and molten material;
sl is the region with the slag composition given in table 1.2. Al_2O_3 = Al_2O_3 + Fe_2O_3 + MnO; CaO = CaO + MgO; alkalies are neglected.

(Diagrams according to Konopicky [1-5].)

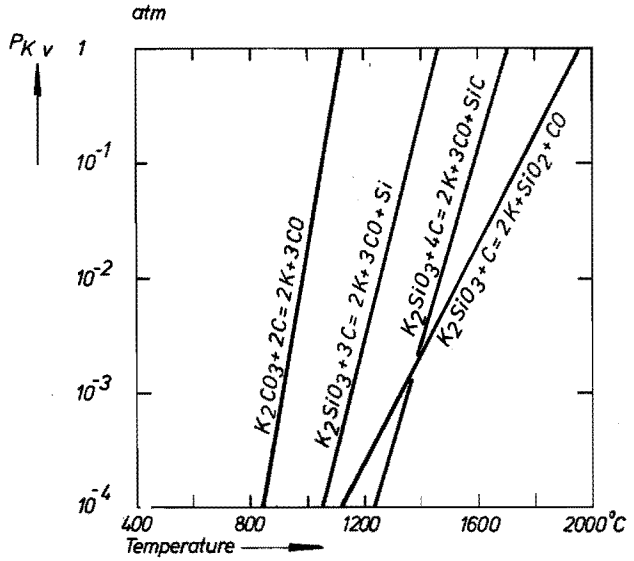

FIGURE 1.7 - The potassium vapour pressure as function of temperature for the reactions:

$$K_2CO_3 + 2\,C = 2\,K + 3\,CO$$
$$K_2SiO_3 + 3\,C = 2\,K + 3\,CO + Si$$
$$K_2SiO_3 + 4\,C = 2\,K + 3\,CO + SiC$$
$$K_2SiO_3 + C = 2\,K + SiO_2 + CO.$$

only consider the role of potassium compounds. The melting point of the early slag will even be lower than shown in figure 1.6 due to the potassium content. In literature [1-8], [1-9], [1-11] various possible reactions with potassium are proposed. In the burden potassium is mostly present as a silicate [1-8] or as K_2O. Due to the reducing atmosphere in the lower stack and the bosh the silicate and the potassium oxyde may be reduced there according to:

$$K_2SiO_3 + C = 2\,K + SiO_2 + CO \qquad [1.6]$$
$$K_2O + C = 2\,K + CO \qquad [1.7]$$
$$K_2O + CO = 2\,K + CO_2 \qquad [1.8]$$
$$K_2O + 3C + N_2 = 2\,KCN + CO \qquad [1.9]$$

In literature [1-9], [1-11], [1-21] different values for the change in Gibbs free energy for these reactions are found. They all indicate the reactions to be possible, but there are large discrepances between the

values given by the different investigators. The best known data are calculated by Richardson and Jeffes [1-9] in 1949. Hawkins et al [1-8] also used those data to calculate the potassium pressure generated at the temperatures reached under blast furnace conditions assuming that the equilibrium is established. The results of their calculations are shown in figure 1.7. The activity values of K_2SiO_3 used in calculating the relations for figure 1.7, correspond to a small amount of potassium as a silicate in the slag (as can be seen from table 1.2, the potassium content of the slag is relatively low).

From figure 1.7 and the reaction [1.6] up to [1.9] it can be seen, that the potassium will be removed from the burden as this descends into the hotter parts of the furnace. From there gaseous potassium will flow upwards in the furnace and either react with carbon and nitrogen or react with CO, according to the reactions:

$$2\ K + 3\ CO = K_2CO_3 + 2\ C \qquad [1.10]$$

$$2\ K + 2\ C + N_2 = 2\ KCN \qquad [1.11]$$

These carbonates and cyanides will be deposited in colder parts of the burden or in the pores of the refractory bricks. Hawkins et al [1-8] state that metallic potassium will be deposited in the pores of the refractory wall as well and will react with the refractory material. To test this hypothesis we carried out experiments with potassium vapour. The equilibrium vapour pressure of potassium at 900°C was created in a tube furnace. The vapour was conducted over test pieces of refractory brick which were placed in the furnace. The test pieces showed severe attack for all the materials tested, even pure graphite, which is unaffected in the blast furnace. When experiments were carried out with K_2CO_3 at the same temperature or slightly higher, the results showed very good agreement with practice. In brick samples out of a blast furnace no K_2CO_3 is found, because it hydrates in wet air. Lately KCN has been found in brick samples from a blast furnace. Therefore it is concluded, that potassium attack takes place via either potassium carbonate or potassium cyanide.

In alumina-silicate bricks with about 42 % (m/m) of Al_2O_3 different potassium compounds may be formed. For our further investigations we will assume that the potassium in the brick is present as K_2O. In that case the compounds formed can be read from figure 1.8. It is assumed that the hot face temperature of the bricks is about 1100°C. The brick

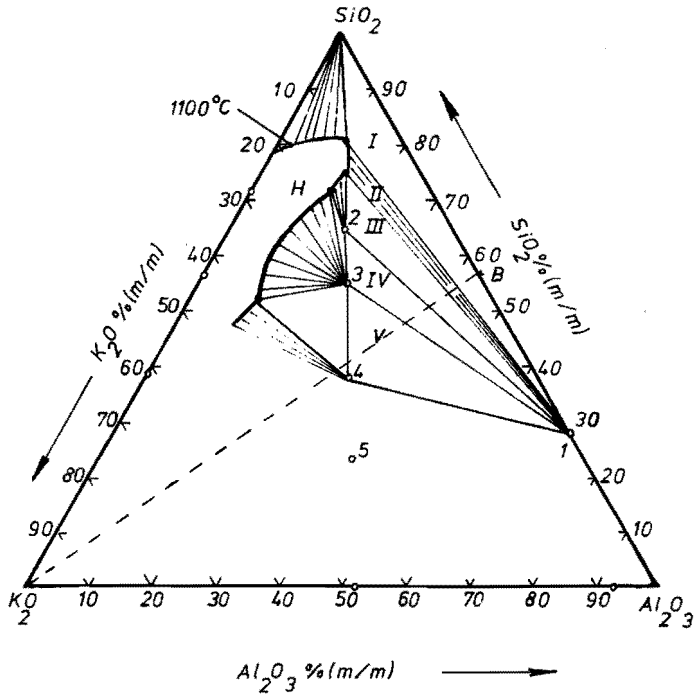

FIGURE 1.8 - The phase diagram of Al_2O_3 - SiO_2 - K_2O at 1100°C derived from Bowen et al [1-10]. Drawn is the 1100°C isotherm. The white triangles are compositions where three phases are in equilibrium. The triangles, in which tie lines have been drawn, are the compositions where one solid phase is in equilibrium with a homogeneous melt.
The area of the homogeneous melt is indicated by H in the diagram. 1 - $3Al_2O_3.2SiO_2$; 2 - $K_2O.Al_2O_3.6SiO_2$; 3 - $K_2O.Al_2O_3.4SiO_2$; 4 - $K_2O.Al_2O_3.2SiO_2$; 5 - $K_2O.Al_2O_3.SiO_2$.

composition is represented by point B in figure 1.8. The drawn triangle is derived from the phase diagram given by Bowen et al [1-10]. The dotted line K_2O - B indicates the chemical composition of the brick plus the impregnated K_2O. As long as the composition is within triangle I three phases will be present assuming that equilibrium can be reached. In that case mullite ($3Al_2O_3.2SiO_2$), cristobalite (SiO_2) and a liquid with a composition indicated by the left angle of triangle I are present. When the amount of K_2O is increased the brick composition enters triangle II, in this case a mixture of solid mullite and the homogeneous liquid, with a composition indicated on the 1100°C isotherm, is found. Further increase of the K_2O content of the brick gives mullite

in equilibrium with potassium feldspar ($K_2O.Al_2O_3.6SiO_2$) and a liquid with the composition indicated by the top angle of triangle III. When the amount of K_2O is further increased the brick composition will enter triangle IV. Now a composition area is entered in which no melt is present at the temperature concerned. In this case mullite will be in equilibrium with potassium feldspar and leucite ($K_2O.Al_2O_3.4SiO_2$). The phase diagram shows that by addition of a little K_2O to a pure Al_2O_3-SiO_2 brick there occurs initially some molten phase in the brick at 1100°C. When the amount of K_2O is increased the quantity of the molten phase will increase, until the brick composition enters triangle III, then the molten phase decreases and is gone when triangle IV is entered. Accordingly one could expect that no wear by melting would occur if the bricks were penetrated with a large amount of K_2O instantaneously. However, instead of wear by melting, the bricks will crack since K_2O penetration gives a volume expansion [1-12] (see also chapter 3).

The description given above shows that the refractory wall of the blast furnace is in contact with molten slag and the gases flowing through the furnace. This causes penetration of the liquid and gases into the pores of the bricks. Due to this, chemical attack of the bricks will take place.

In the following section we will discuss the refractory construction in a blast furnace in more detail.

1.3 - The Blast Furnace Wall Construction

As can be seen from figure 1.1, a blast furnace consists in principle of two conical parts which are placed one on top of the other with the wider open ends joined. The outer construction of a blast furnace consists of a steel shell in which a refractory wall is placed. The wall of this container is used to hold the burden and it must be abrasion resistant and has to insulate the furnace. In the wall construction we find three parts, the *hearth*, the *bosh* and the *stack* or *shaft*. The function of the hearth is to hold the molten metal and slag. The bosh is the major reaction zone and the stack is the container for the burden. A short discussion on the interaction of the furnace content and the lining will be given for the major parts of the furnace.

1.3.1 - The hearth

In the hearth we find the molten metal and the slag. The temperature is rather high as can be seen from figure 1.4. The molten material will partly impregnate the wall and the bottom. If refractory material is used that is not highly slag resistant, rapid wear will occur. In the late sixties the problems with the hearth refractories were solved by using dense *carbon bricks* with a suitable cooling system. In most of the modern highly productive blast furnaces throughout Europe, carbon is used in the hearth.

1.3.2 - The bosh

As was stated before, the bosh is the main reaction zone. The temperature is rather high (burden temperatures from 1300°C to 1600°C). In this region CO and potassium vapour are formed. Nearly all the slag present will be in the liquid state (see also figure 1.6). So the bosh wall has to be highly refractory, resistant against attack by CO, potassium and slag. Since the burden in this part of the furnace is in a semi-plastic state, it will not cause much mechanical erosion of the wall. So what is needed for the bosh area is a highly chemical resistant brick.
After extended studies [1-12], [1-13], [1-14] it was found that carbon with an extremely low ash content (< 1 % (m/m)) is suitable in this part of the furnace, especially when an adequate cooling system is used. For this purpose only *graphite* or *semi-graphite* will suffice.

1.3.3 - The stack

The stack can roughly be divided into two zones. Firstly the charging zone, where the burden is still relatively cold, and secondly the middle and lower stack, where the first reductions of the ore take place.

In the upper stack - the charging zone - the refractory lining has only to be abrasion resistant. The wall temperatures are too low to give trouble with chemical reactions with the burden material or gases. König et al state that no reactions will take place below 400°C [1-15]. In the middle and lower stack higher temperatures are reached as can be seen from figure 1.4. In this area a first chemical attack can take place. Therefore one must have in this region a refractory brick which

is abrasion resistant (since the burden is moving along the wall) and also highly chemical resistant (for reasons described in 1.2). Up till now this problem is unsolved in most furnaces. In the next section we will discuss the requirements for the middle and lower stack in more detail. The main subject of this thesis is to describe requirements for refractory materials for the middle and lower stack, and to outline a possible solution of this problem.

1.4 - The Requirements for a Stack Wall

1.4.1 - The chemical requirements

In section 1.2 a general characteristic of the bosh and stack was given. From that description it can be seen, that the chemical attack in the stack will not come directly from the burden, but from the gases flowing along the wall and from molten slag material. Studies of broken out blast furnaces and studies of cores drilled out of the furnace wall during the campaign learned, that usually a layer of slag is formed on the furnace wall [1-5], [1-12], [1-16], [1-17]. This insulating layer will protect the wall, but when it falls off, as it often does [1-16] it will also tear out small parts of the furnace wall. The studies also showed that low melting metals like zinc and lead will condensate or freeze in the cooler parts of the furnace, for instance the cracks and joints in the wall. It was observed, however, that the major chemical attack in the lower stack and the bosh was due to CO and alkali. For this reason we have neglected the influence of zinc and lead on the furnace wall any further in this work.

During World War II and shortly afterwards CO attack caused a lot of trouble in the refractory linings of the blast furnaces. The *fireclay* bricks (35-60 % Al_2O_3) applied were fired at too low temperatures and the bricks were often contaminated with iron or iron-oxide particles. When iron or iron-oxide particles are present they will increase the reaction rate of the Boudouard reaction [1.1] to a great extent even at rather low temperatures (450°-650°C). The iron or iron-oxide act as a catalyst to the reaction, and C is deposited upon the *iron spots*. The growth of such carbon deposits disrupts the fireclay bricks [1-19], [1-20]. The fireclay bricks used nowadays are fired for an appropriate time at a suitable temperature [1-18].

Intensive studies have been carried out in many steelplants throughout the world to find the reason for the chemical attack in the blast furnace bosh and stack. (See Konopicky [1-5]) and Chesters [1-19]) for detailed reviews on early work; see also section 1.2.) A special study has been carried out by the European Carbon and Steel Community in a small experimental blast furnace in Ougrée - Belgium. In this work Hoogovens also participated. The results of this study have been reviewed by Konopicky [1-13]). In connection with this work trials were carried out at Hoogovens as well. More details are given in Chapter 3.
From the given thermodynamic data on potassium vapour (figure 1.7) it can be seen that potassium is the main component for chemical attack in the middle and lower stack, because in the stack the most aggressive components are the potassium compounds. As is stated before heavy metals will penetrate in joints and cracks. Under the blast furnace conditions CaO can penetrate the wall as well as a calcium silicate compound. But the potassium penetration is the most severe one. Potassium will penetrate the blast furnace lining at temperatures above 900°C as potassium compound vapour and between 900°C and 700°C as liquid potassium carbonate or potassium cyanide as was indicated by Richardson et al [1-9]). Therefore the pores of the bricks will soon be penetrated by alkali.

1.4.2 - Mechanical and thermal resistance of a stack lining

The bricks in the middle and lower stack have to be abrasion resistant, since the burden is slowly passing along the wall. In the middle stack nearly all the burden material is still in a solid state. The iron ore is softening already, but the coke is still very hard when it is well fired in the coke-oven. By charging the burden in a special way it is possible for the iron maker to influence the movement of the burden along the walls. He can choose either for a slow or for a rapid movement along the wall. For a highly productive furnace the latter is mostly used. This also gives the most severe circumstances for the brickwork. Therefore a good stack brick should be very abrasion resistant.

A skull of frozen slag can be formed on the brick surface. Under certain conditions this skull falls off, as was concluded from the rapid temperature changes measured with thermocouples installed in the furnace wall (Van Laar, Maes [1-16])). The temperature differences observed

accounted to over 300°C within 2 minutes. Therefore the refractory material should also be thermal shock resistant.

1.5 - Summary

In this chapter an outline has been given of the processes proceeding in the blast furnace. The influence of the processes on the refractory wall were discussed. The conclusions which can be given now, are:

- the refractory material must be CO and alkali resistant;
- the bricks should have low porosity to avoid rapid penetration of potassium carbonate and potassium cyanide;
- the bricks should be abrasion resistant, since a constant flow of matter grates along the wall;
- the bricks should be thermal shock resistant, since large temperature fluctuations have been observed in a blast furnace wall.

The conclusions derived here will be used as a basis for the material choice, which is made in part 1 of this thesis. In chapter 2 test methods are described, which are used for the material choice made in chapter 3. In the last section of chapter 3 some experiments carried out in practice are described. Part 2 of this thesis describes further study of silicon carbide bricks for use in the blast furnace stack. The thermodynamic data are studied which control the possible formation of silicon carbide out of silicon and carbon. The bonding system and the brick production are studied. In the last chapter some results of experiments in practice with this type of brick are given.

L i t e r a t u r e

[1-1] *Flierman, G.* — *Privat communication*

[1-2] *Homminga, F.* — *Het Hoogovenproces, Internal report Hoogovens, 1975*

[1-3] *Yatsuzuka, T.; Hiragushi, K.* — *Internal Commity paper presented at meeting of Sidérurgie et Produits Réfractaires Europ. Work.-group IV June 1976*

[1- 4] *Jongenburger, P.*	*Kennis der Metalen, Deel 1; 7e druk, Delft, Delftsche Uitgevers Mij., 1963*
[1- 5] *Konopicky, K.*	*Feuerfeste Baustoffe; Düsseldorf, Verlag Stahleisen 1957, 376-387*
[1- 6] *Harders, F.; Kienow, S.*	*Feuerfestkunde; Berlin, Springer Verlag, 1960*
[1- 7] *Van Toor, Ch.*	*Invloed van de verlaging van de slakhoeveelheid bij de hoogovens op de slakvoering en de ontzwaveling van het ruwijzer; Internal report Hoogovens, 1969*
[1- 8] *Hawkins, R.J.; Monte, L.; Waters, J.J.*	*Ironmaking Steelmaking (Quarterly); 1 (1974) No 3, 151-160*
[1- 9] *Richardson, F.D.; Jeffes, J.H.E.*	*J. Iron and Steel Inst. 163 (1949) 397-420*
[1-10] *Bowen, N.L.; Schairer, J.F.*	*Am. J. Sci. 45 (1947), 199-203*
[1-11] *Hiragushi, K.*	*Communication at the SIPRE/GT IV meeting, June 1976 (Comments concerning a paper presented by T. Hayashi called "A few problems in blast furnace wear behaviour")*
[1-12] *Doornenbal, W.; Van Konijnenburg, J.T.; Van Laar, J.; Visser, R.; Waasdorp, A.*	*C.N.R.M. Metallurgical repts. (1970) No 25, 11-20*
[1-13] *Konopicky, K.*	*Stahl und Eisen 92 (1972) 481-487*
[1-14] *Konopicky, K.; Routschka, G.; Van Laar, J.; Visser, R.; Halm, L.*	*Report of the "Centre de Recherches Métallurgiques" (1972) No S.9/72*
[1-15] *König, G.; Weidemüller, Ch.; Pietzke, G.*	*Stahl und Eisen 91 (1971) 63-69*

[1-16] *Van Laar, J.; Maes, J.* — *Stahl und Eisen 91 (1971) 1098-1101*

[1-17] *Workman, G.M.; Davidson, J.A.C.* — *Blast furnace refractories, London Iron and Steel Inst. (1968) Publ. 116 - p.83*

[1-18] *Clews, F.H.; Ball, F. Green, A.T.* — *Trans. British Ceramic Society 45 (1946) 251-255*

[1-19] *Chesters, J.H.* — *Refractories for Iron and Steelmaking; London, Metals Soc., 1974, p.42*

[1-20] *Bohlken, S.F.* — *Bijdrage tot de bepaling van de bestendigheid van vuurvaste Chamottesteenen tegen desintegratie door koolmonoxyde; Amsterdam, NV Noordhollandsche Uitgevers maatschappij, 1946*

[1-21] *Barin, J.; Knacke, O.* — *Thermomechanical properties of inorganic substances Berlin, Springer Verlag, 1973*

PART ONE

Testing Methods

and

Choice of Materials for the Blast Furnace Stack

Chapter 2 - LABORATORY TESTING METHODS FOR REFRACTORIES

Before discussing the possible alternatives for blast furnace stack refractories it seems useful to outline the different testing methods used to characterise refractory bricks. In the next chapters we shall often use data obtained from the tests described. It is also tried to to compare the laboratory data with the performance of the bricks in practice. The tests can be classified into three groups:

2.1 - Physical properties

These tests give a physical characterisation of the refractory bricks concerned. The characteristics mentioned here give the material density, porosity and the *texture* of the brick.

2.2 - Mechanical and thermo-mechanical properties

The tests concerned give the crushing strength or the bending strength of the bricks at room temperature and at elevated temperatures.

2.3 - Thermal properties

The tests give the best obtainable thermal values of the bricks. The properties measured are thermal expansion, thermal conductivity, and heat capacity. From the properties described in 2.1, 2.2, and 2.3 it is possible to give a classification system for the thermal shock resistance of refractory bricks.

When in our investigations a standard test is used only a brief description is given, with reference to the national or international standard. When a revised or a new test is used a more detailed description is given.

2.1 - Physical Properties

Refering to physical properties of refractory bricks in this work the following properties are meant:

2.1.1 true density	ρ	$g.cm^{-3}$
2.1.2 bulk density and	d_s	$g.cm^{-3}$
apparent porosity	π_s	% (V/V)
2.1.3 true porosity	π_w	% (V/V)

2.1.1 - True density

The definition of the true density ρ is according to the ISO standard [2-1]: "the ratio of solid mass to its true volume. The true volume is the volume of the solid material only". The latter means, that the porous ceramic material is ground so far, that no pores are left in the powder grains. In practice this means, that the grains should be smaller than 60 μm. The dry mass of the material to be tested is measured in a dry pycnometer of a known volume. Then the pycnometer is filled with water and that mass is weighed again.
The true density can be calculated from the measured values. The testing method is described in "P.R.E. Refractory Materials" [2-2]. Knowledge of the true density of refractories is of importance for control purposes. Under certain circumstances it is possible to see how far the reactants reacted during firing in the furnace, since in that case the true density of the mixture changes.

2.1.2 - Bulk density and apparent porosity

The definition of the bulk density d_s is according to the ISO standard [2-1]: "the ratio of mass of the material to its bulk volume, where the bulk volume is the volume of the solid material plus the volume of the closed and open pores".
The apparent porosity π_s is: "the ratio of the volume of the open pores to the bulk volume of the material".
The bulk density and apparent porosity are measured in the same test. The dry mass of a cylindrical test piece is determined. The test piece is then soaked in water and the mass of the test piece under water and of the soaked test piece above the water are determined. From the data obtained the bulk density and the apparent porosity can be calculated. The test is described in ISO standard [2-1].

2.1.3 - True porosity

The definition of the true porosity π_w is according to the ISO standard [2-1]: "the ratio of the volume of the open and closed pores to the bulk volume of the material". The true porosity is calculated from the bulk density and the true density as:

$$\pi_w = 100 \cdot \left(1 - \frac{d_s}{\rho}\right) \qquad (2.1)$$

The difference between the true porosity and the apparent porosity gives the volume of closed pores in a brick. These pores do not influence the absorption ability of the brick. However, they do influence the thermal conductivity and the strength of the brick, in the same way as the open pores do.

2.2 - Mechanical and Thermo-Mechanical Tests

In order to characterize refractory materials also mechanical tests have to be carried out. In most of the laboratories the following tests are carried out:

2.2.1 Cold Crushing Strength	(CCS)	$N.m^{-2}$
2.2.2 Hot Modulus of Rupture	(M)	$N.m^{-2}$
2.2.3 Refractories under Load	(RUL)	

and in some cases:

2.2.4 Young's Modulus	(E)	$N.m^{-2}$

2.2.1 - Cold crushing strength

The cold crushing strength (CCS) of a brick is its strength at ambient temperature given per unit surface area.
For our investigations the test was carried out according to DIN 51067 [2-4]. For the test cylindrical test pieces (size 50 mm diam., 50 mm long, or cubes of 40 x 40 x 40 mm^3) are prepared out of a brick. The test pieces are crushed in a hydraulic pressing machine in which the load is applied at a rate of $0.33 \cdot 10^3$ $N.s^{-1}$. This loading rate is maintained until the test piece fails. The maximum recorded load is the crushing load.
The data obtained from this test have no real scientific value, but they give a first indication of the results of firing the bricks.

2.2.2 - Hot modulus of rupture

The modulus of rupture is the transverse strength of a material. It is given by the formula:

$$M = \frac{3 \cdot w \cdot 1}{2 \cdot b \cdot d^2} \qquad (2.2)$$

where: M - modulus of rupture $N.m^{-2}$

w - load at which failure occurs N

l - distance between the supports m

b - the width of the test piece m

d - the thickness of the test piece m

Formula (2.2) is only valid for materials obeying Hooke's Law, for brittle materials formula (2.2) gives a good approximation.
The test is not yet standardized. For our investigations we used test pieces with the following dimensions: length 110 mm, width 30 mm and thickness 10 mm. The distance between the supports (l) was 100 mm. In our case the test piece support and the bending knife are placed in an electric furnace, which is able to heat the test pieces up to a temperature of 1400°C. The test piece is loaded with a constant loading rate of 0.15 $N.mm^{-2}.s^{-1}$ which is obtained by a constant flow of water into a bucket hanging on a lever which is attached to the loading knife. Figure 2.1 shows the arrangement of the test piece in the furnace. Figure 2.2 shows the actual modulus of rupture furnace with its preheating unit.

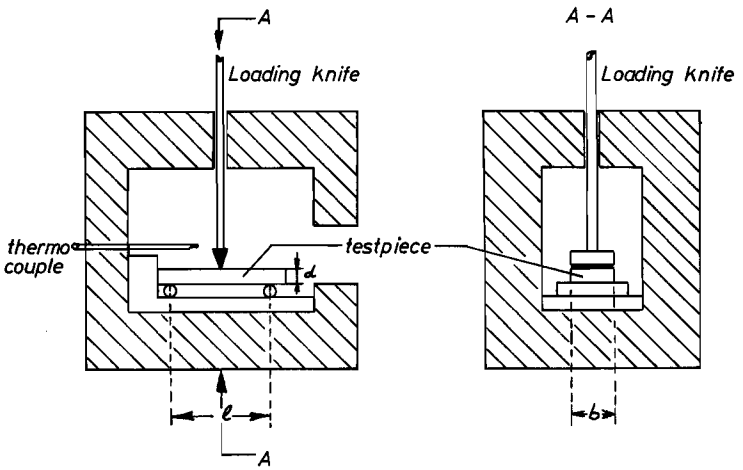

FIGURE 2.1 - The arrangement of the test piece in the furnace for the hot modulus of rupture test.

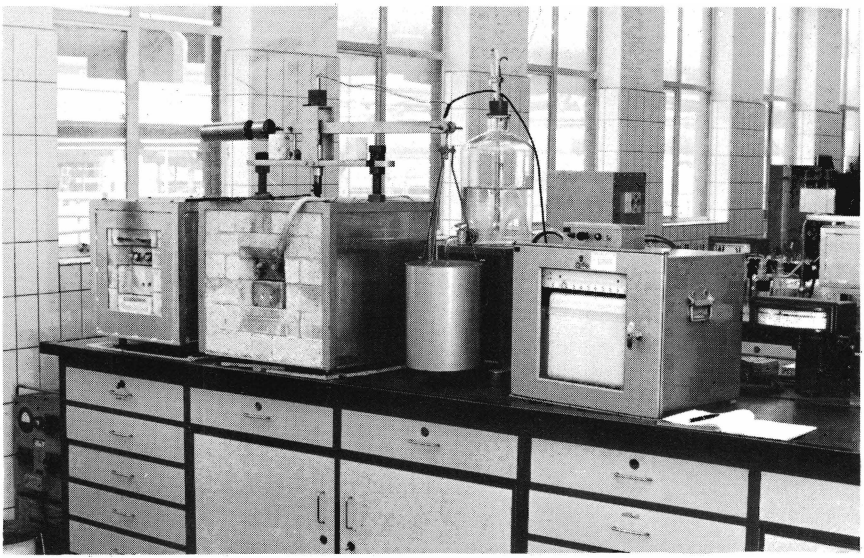

FIGURE 2.2 - The modulus of rupture furnace.

The modulus of rupture load is the load which is applied to the test piece at the moment of failure. It is measured by weighing the water content of the bucket.
The tests carried out at different temperatures (20 - 400 - 800 - 1000 - 1200 and 1400°C) give the strength of the brick at those temperatures. When a reducing atmosphere is required, carbon is introduced into the furnace. It is also possible to measure the bending-through (Δd) at the moment of failure. The comparison between the bending-through and the modulus of rupture gives an indication of the flexibility of the brick at the temperatures concerned.
As a standard for our studies three test pieces out of one brick were measured at each temperature.

2.2.3 - Determination of refractoriness under load

With this test the high temperature deformation of a refractory material is measured when an uniaxial load of 0.2 $N.mm^{-2}$ is applied to a hollow

cylindrical test piece during heating up with a heating rate of 4 to 5 K/min. Cylinder size: outer diam. 50 mm; inner diam. 12 mm; height 50 mm. The deformation during heating up is measured with a differential method. A corundum measuring rod is placed on the bottom support of the test piece through the central hole and a second measuring rod is placed on top of the test piece. The test piece is placed in the center of a vertical tube furnace. The measuring rods are at the outside of the furnace connected with an inductive displacement gauge. For the thermal expansion of the measuring rods corrections are made. The temperature is measured in the center of the test piece. The test is carried out according to ISO and NEN standards [2-5], [2-6].

2.3 - Thermal Properties

The thermal properties characterize a material at higher temperatures. For the construction of furnaces we are interested in the thermal expansion of the material, the heat resistance, mostly defined as the thermal conductivity of the material and in the heat which can be stored in a wall, defined by means of the heat capacity. Since for all refractory materials the heat capacity is about the same and well known from literature, we will use the literature data in this work. In practice also the thermal shock resistance is of importance. In this section we will present a method for a quantitative description of this property.

2.3.1 - Thermal expansion

The thermal expansion is the increase in dimensions of a material when heated. The term is only applied to that part of the expansion which is reversible. The linear thermal expansion (α) is defined as:

$$\alpha = \frac{1}{l} \cdot \frac{dl}{dT} \qquad (2.3)$$

where: dl/l = partial length difference

dT = temperature difference.

It is also possible to define a volume expansion but this property is unimportant for our purpose.

The type of apparatus used is illustrated in figure 2.3. A vertical tube furnace is heated with a silicon carbide heating tube. The

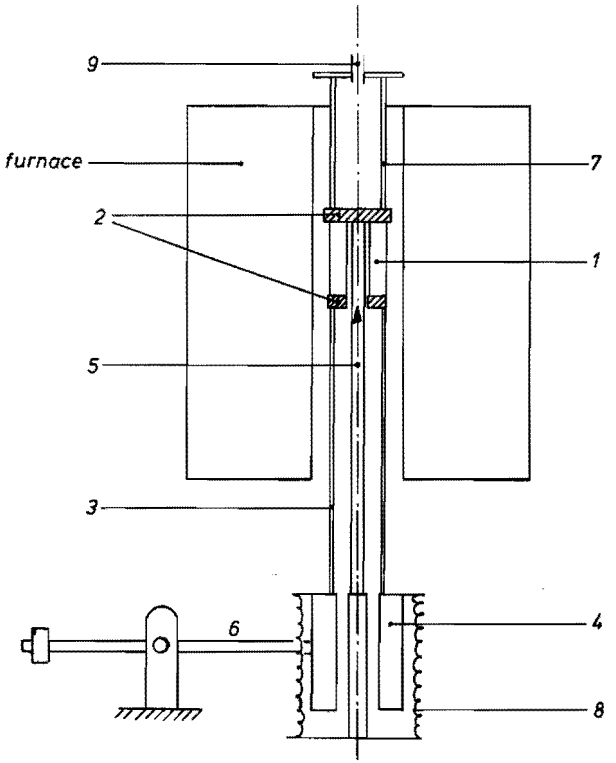

FIGURE 2.3 - Vertical type thermal expansion apparatus. (Design: Netzsch GmbH, Selb, Western Germany)

measuring method of the thermal expansion is in principle the same differential method as used with the refractoriness under load test (see 2.2.3). A test piece (1) (cylinder; outer diameter 35 mm, inner diameter 12 mm, height 50 mm) is placed between two separating disks (2) (thickness about 8 mm) on the outer measuring rod (3). This rod is screwed in a displacement gauge holder (4) and a lever (6) underneath the furnace. The movable metal rod in the inductive displacement gauge is connected with the inner measuring rod (5). This assembly of rods and test piece is softly pressed against the upper column (7) in the furnace by means of the lever (6) and a pair of springs (8).

The heating rate of the furnace can be chosen between $0.2^{\circ}C.min^{-1}$ up to about $10^{\circ}C.min^{-1}$. The maximum temperature is $1550^{\circ}C$. A gas inlet (9) is mounted on top of the furnace, so the test pieces can be heated in an

inert atmosphere if required.

2.3.2 - Thermal conductivity

The thermal conductivity is the property by virtue of which heat is transmitted through matter. A heat flow ϕ_w through a flat wall is described by the formula:

$$\phi_w = - \lambda \cdot \frac{dT}{dx} \qquad (2.4)$$

where: ϕ_w = heatflow through an unit surface area $W.m^{-2}$

$\frac{dT}{dx}$ = temperature gradient over the wall thickness $K.m^{-1}$

λ = thermal conductivity $W.m^{-1}.K^{-1}$

Up till now no method for measuring the thermal conductivy is standardized. In Europe the hot wire method is often used for insulating materials. (A review on different testing methods is given by Schwiete et al [2-7].)

The hot wire method is used at Hoogovens for measuring the conductivity of insulating materials ($\lambda < 3$ $W.m^{-1}.K^{-1}$). The method is unsuitable for materials which can conduct electric current, because the heating wire is in direct contact with the test piece. Therefore at Hoogovens another measuring method was developed. The principle is that the temperature difference over a cylindrical test piece is measured when a known constant heat flow is generated along the cylinder axis of the test piece. The test piece is placed in a cylindrical furnace in an air tight tube in which a chosen atmosphere can be maintained. Figure 2.4 shows the arrangement of the apparatus. The central heating element (1) is placed along the axis of the test cylinder, the thermocouples (2), 1.5 mm in diameter, are placed in holes (diameter 2 mm) parallel to the heating element. The thermocouple junctions are situated in the center of the test piece.

The thermal conductivity is calculated from the equation:

$$\lambda = \frac{V \cdot I \cdot \ln (R_2/R_1)}{2 \cdot l \cdot (T_1 - T_2)} \qquad (2.5)$$

where: V = voltage drop over length l of the heating element V

I = current through the heating element A

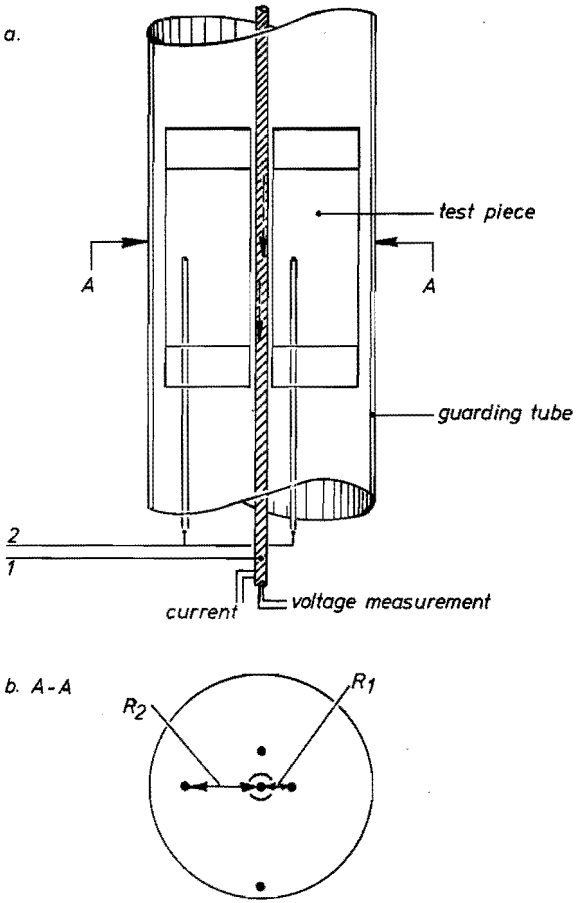

FIGURE 2.4 - The thermal conductivity apparatus as built at Hoogovens:
a. Vertical cross-section of the arrangement.
b. The position of the thermocouple holes in the test piece.

R_1	= radius on which the inner thermocouple is placed	m
R_2	= radius on which the outer thermocouple is placed	m
T_1	= temperature of the inner thermocouple	K
T_2	= temperature of the outer thermocouple	K

A detailed description of the apparatus and its use is given in Tonindustrie Zeitung (Van Konijnenburg [2-8]). Comparative tests carried

out at other laboratories with other measuring systems gave good agreement.

2.3.3 - Thermal shock resistance

As was indicated in Chapter 1 thermal shock is one of the main reasons for refractory failure. In the literature different tests are proposed ([2-3]; [2-9]; [2-10]; [2-11]). Most of them give a cycling test between a certain temperature and room temperature. After a number of tests the test piece is examined. The observed cracks are given in a sketch, which represents the test report. In our opinion these tests are not very selective. Winkelmann and Schott [2-12] tried to work out a theoretical relation for the thermal shock resistance, but they did not fully succeed. If the circumstances at the *hot-face* of a furnace wall are studied, one can define the thermal shock resistance as the maximum temperature difference given in a short time on a surface-area, which a refractory brick can withstand without cracking.

This definition gives the situation for the macroscopic structure, but in principle also the microscopic behaviour of the material is included. The thermal shock resistance (R) can be expressed as the ratio of the temperature difference ΔT upon a surface-area A to the period of time Δt and the cracking energy γ:

$$R = \frac{\Delta T \cdot A}{\gamma \cdot \Delta t} \qquad (2.6)$$

where: R = thermal shock resistance (dimension: $t.m^{-1}$)

ΔT = temperature difference

Δt = period of time in which the temperature difference occurs (dimension: t)

γ = cracking energy (dimension: $m.t^{-2}$)

A = surface-area (dimension: l^2)

γ can be represented by $M.\Delta d$ which is the modulus of rupture (M) multiplied by the bending through (Δd).

M = modulus of rupture (dimension: $m.l^{-1}.t^{-2}$)

Δd = bending through (dimension: 1).

The thermal shock resistance will depend upon the following properties:

- bulk density d_s
- heat capacity c_p
- heat conductivity λ

} or $a = \frac{\lambda}{c_p \cdot d_s}$ (dimension: $l^2.t^{-1}$)

- thermal expansion $\Delta l = \alpha.l$ (dimension: l)
- Young's modulus E (dimension: $m.l^{-1}.t^{-2}$).

Dimensional analyses will give the relation between the different properties. In principle:

$$R = \frac{\Delta T \cdot A}{M \cdot \Delta d \cdot \Delta t} = f\ (a, E, \alpha l) \tag{2.7}$$

Or in dimensions:

$$l^2.(m^{-1}.l^2.t^2).(l^{-1}).(t^{-1}) = (l^{2a}.t^{-a}).(m^b.l^{-1b}.t^{-2b}).(l^c) \tag{2.8}$$

This gives: $a = +1$

$b = -1$

$c = -1$.

So the complete relation is:

$$R = \frac{\Delta T \cdot A}{M \cdot \Delta d \cdot \Delta t} = C \cdot \frac{a}{\alpha \cdot l \cdot E} \tag{2.9}$$

Or the temperature shock is given as:

$$\Delta T = C \cdot \frac{M \cdot a \cdot \Delta d}{\alpha \cdot E} \cdot \frac{\Delta t}{A \cdot l} \tag{2.10}$$

where C is a constant.

If we also define the ratio Δt to A and l as a constant, which is allowed because in our case Δt is always within a few minutes and A is known (A is the internal surface area of the blast furnace stack) and l is the preset length, then it is possible to classify different refractory products via the equation:

$$R_R = \frac{M \cdot a \cdot \Delta d}{\alpha \cdot E} \tag{2.11}$$

Equation (2.11) contains only measurable data or data known from tables. In Chapter 4 relation (2.11) will be used for chosing the optimal refractory brick for a blast furnace stack.

2.4 - Chemical Testing Methods

As was mentioned in the previous chapter the chemical behaviour of refractory bricks in the stack is very important. In literature ([2-3]); [2-13]; [2-14] and [2-15]) a variety of testing methods is described. None of them, however, gives a figure on which an adequate ranking can be based.

For our purpose we are interested in a method of testing a brick for its resistance against blast-furnace bosh and stack slag (see table 1.2) and especially against liquid potassium carbonate attack.

Slag attack is tested mainly with three types of tests. Firstly the crucible test, which is suggested by DIN 1069 [2-15], secondly the finger test [2-3], and thirdly the rotating furnace test. The latter will not be described here, as this test was not used in our investigations.

Potassium attack can be tested by means of a simple crucible test. For the studies presented here other methods were tried but they gave no better results. For example, a special furnace was built to test different brick types in a potassium vapour at 900°C. The results of this test gave, however, no agreement with practical experience. It was also tried to get a test which gives a ranking figure for the alkali resistance of a brick. Therefore test pieces for the hot modulus of rupture test were impregnated with potassium carbonate and tested at 1000°C. The figures obtained from this test gave no good agreement with the results in practice either.

2.4.1 - Crucible test

For this test half a *standard size brick* is used. A hole of 40 mm diameter and about 45 mm depth is drilled in the test piece. The hole is filled with material to react with the brick. In our case either slack slag or potassium carbonate is used. After filling the crucible is sealed with a cover of the same material as the brick under test. This crucible is heated in an electric furnace to the test temperature and held at that temperature for a preset time. Afterwards the crucible is cut into two halves so that the interior can be studied. At first the crucible half is photographed and the morphology described, and then

the attacked surface is studied under the microscope.
Our investigations showed that the method is most adequate for measuring the potassium carbonate attack. Therefore a crucible is filled with 30 grams of K_2CO_3 and heated up to 1100°C and kept at that temperature for 4 h. Microscopic and X-ray examination showed the reaction products being formed.

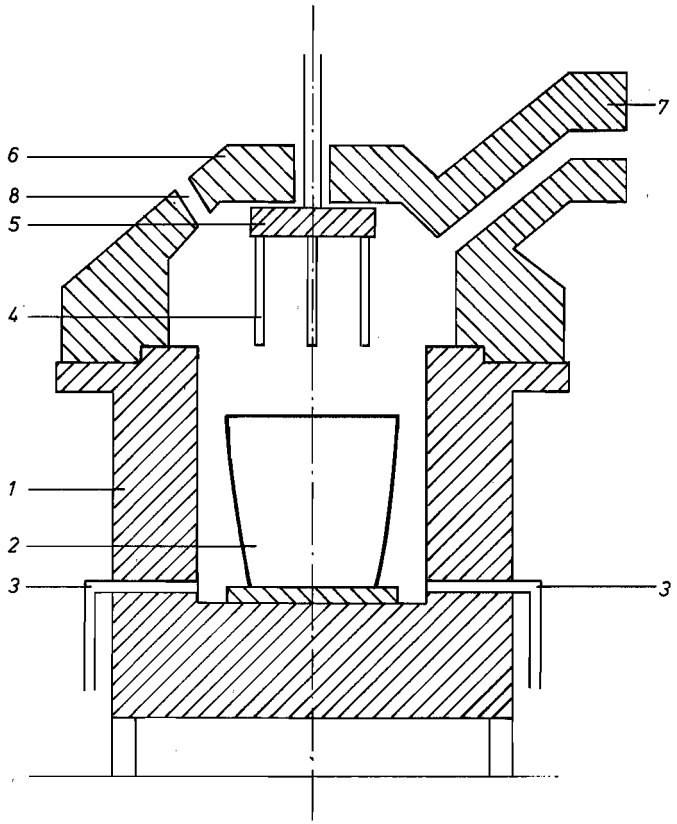

FIGURE 2.5 - The arrangement for a finger test in the gas fired furnace.
1 = furnace wall *5 = test piece holder*
2 = crucible *6 = furnace roof*
3 = 4 gas burners *7 = chimney connection*
4 = test pieces *8 = hole for temperature measurement.*

2,4.2 - Finger test

A clay-graphite crucible with an effective volume of about 5 dm^3 is filled with crushed blast furnace slag of a known composition. To the

slag 5 % (m/m) of K_2CO_3 is added to get a slag composition similar to the slag in the lower stack. In a gas fired furnace this slag is molten. In the furnace above the crucible a movable water cooled test piece holder is mounted (see figure 2.5). For this test, pieces are cut out of a brick in the form of a capital T. The shape is such that the test piece can be attached to the test piece holder. The test piece length has the length of a standard size brick (230 mm), while the bars of the T have a square cross section (15 x 15 mm^2).
In the crucible at maximum five different test pieces can be immersed into the slag.
After the slag is molten (at about 1500°C) the furnace is brought to the test temperature (1450°C). Then the test piece holder is lowered and the test pieces are immersed into the slag for a preset time (in our case 1 h). After this time the test pieces are drawn out of the slag and are allowed to drip off in about 10 minutes. After that time the furnace is switched off. The test pieces cool down in the furnace overnight. After the test the test pieces are photographed and the reduction of the cross-section is measured at one third of the test piece height. That cross-section is also studied under the microscope. The microscopic analyses give the actual attack taken place during the test. By means of preparing small samples out of this cross-section X-ray diffraction analyses can be made of the different phases present.

The methods appear to be a suitable test for slag attack on blast furnace bricks. The attack occurring in these tests are very similar to the attack observed in the bricks drilled out of a blast furnace wall during the campaign (see also Chapter 3).

L i t e r a t u r e

2- 1) *ISO/DIS 5017* — *Dense shaped refractory products - Determination of bulk density, apparent porosity and true porosity, 1975*

2- 2) *PRE Refractory Materials* — *Travaux et Recomandations de la Fédération Européenne de Fabricants de Produits Réfractaires, Zürich, 1972, p.45*

2- 3) *Chesters, J.H.* — *Refractories: Production and Properties. London, Iron and Steel Inst., 1973*

2- 4) *DIN 51067* — *Bestimmung der Druckfestigkeit bei Raumtemperatur (KDF) an feuerfeste Werkstoffen mit einer Gesamt Porosität bis Vol. 45 %*

2- 5) *ISO/R 1893* — *Dense shaped refractory products - Determination of refractoriness under load of refractory products, 1970*

2- 6) *NEN 3514* — *Bepaling van de vormverandering onder druk bij stijgende temperatuur, 1970*

2- 7) *Schwiete, H.E.; Westmark, H.* — *Die Wärmeleitfähigkeit feuerfeste Steine im Spiegel der Literatur. Köln, Westdeutscher Verlag, 1959*

2- 8) *Van Konijnenburg, J.T.* — *Ton.Ind.Ztg. 97 (1973) 89-94*

2- 9) *ASTM C 38* — *Basic Procedure in Panel Spalling. Test for Refractory Brick, 1973*

2-10) *DIN 51068* — *Bestimmung des Widerstandes gegen schroffen Temperatur Wechsel, 1969*

2-11) *Konopicky, K.* — *Feuerfeste Baustoffe. Düsseldorf, Verlag Stahleisen, 1957*

2-12) *Winkelmann, W.; Schott, O.* — *Ann. Phys. 51 (1894) 730-746*

2-13) *Harders, F.; Kienow, S.* — *Feuerfestkunde. Berlin, Springer Verlag, 1960*

2-14) *ASTM C 454* — *Disintegration of carbon Refractories by Alkali, 1971*

2-15) *DIN 1069* — *Prüfverfahren für feuerfeste Baustoffe A. Tiegelverfahren (VBT), 1931*

3.1 - Historical Review

Traditionally the wall of a blast furnace from the tuyeres upwards was built with fireclay bricks. Before World War II mostly bricks with an Al_2O_3 content of 32-37 % (m/m) were used. After World War II fireclay bricks with an Al_2O_3 content of 40-44 % (m/m) were more often used. These bricks had a slightly better refractoriness and were more abrasion resistant. The size tolerances of the bricks were very tight (0.75-1 %) and the bricks were built into the furnace without any expansion

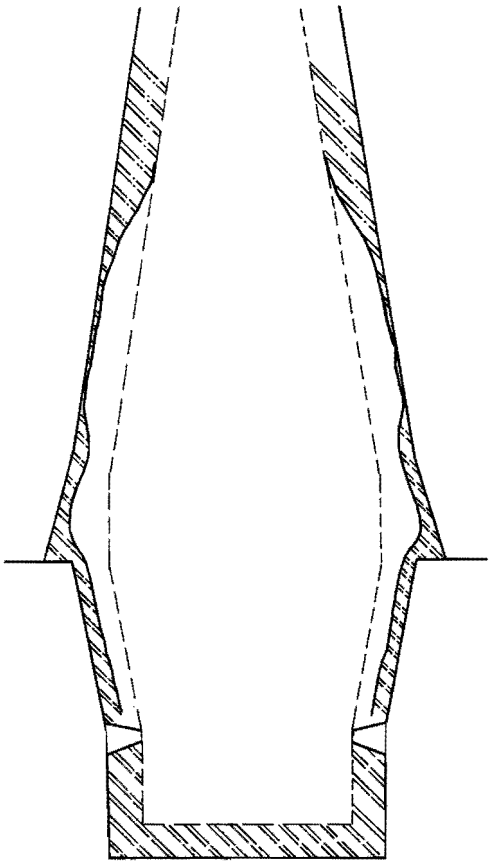

FIGURE 3.1 - A typical wear pattern of a worn out blast furnace as found at Hoogovens.

allowance. As was observed later from temperature readings *thermal spalling* occured already at the heating up of the furnace, as the thermal expansion was not compensated. Up to the sixties most of the blast furnaces were built as described above ([3-1], [3-2]). After each campaign the remaining *brickwork* was studied carefully. A typical wear pattern as often found in worn out blast furnaces is given in figure 3.1.

Willems et al [3-3]) showed that rather severe crusts of slag could be found against the blast furnace wall. In the remaining brickwork many potassium compounds were found (see also 1.4.1). Rigby et al [3-4]) and Jay et al [3-5]) both found independently leucite ($K_2O.Al_2O_3.4SiO_2$) in the remaining brickwork as Kahlhöfer et al [3-6]) did some years later in a German blast furnace. The leucite formation gives a volume expansion. According to calculations made by Jon [3-7]) the transition from $3Al_2O_3.2SiO_2$ into leucite brings a volume expansion of 10 % calculated upon the original volume of the mullite. The transition of mullite into kaliophilite ($K_2O.Al_2O_3.2SiO_2$) gives a volume expansion of 6 %. The expansion of the mullite crystals in the bricks due to the potassium compounds transitions causes rupture of the bricks. This phenomenon is known as *alkali bursting*.

In the sixties studies were started to avoid thermal spalling by means of building expansion allowances into the wall construction, and investigations were made to improve the alkali resistance of the fireclay bricks. The first step was to develop fireclay bricks of higher density. In the USA they became known as *high duty fireclay bricks*. They have an average Al_2O_3 content of 42 % (m/m) and a very low true porosity 14-18 % (V/V) whereas before over 18 % (V/V) was normal. In Europe those bricks were made out of a South African very dense fireclay *grog* (porosity < 6 % (V/V)). In dense fireclay bricks the alkali penetration will be retarded as Halm et al [3-8]) and Pitak et al [3-9]) have shown, but the alkali attack will still take place. Due to the very long period of exposure (4 years or more) even very slow penetration will destroy the bricks. König et al [3-10]) stated that for the potassium reactions a lowest reaction temperature can be given. They calculated a temperature of 400°C. Based upon studies made on samples taken out of the blast furnace wall by means of core drilling during the campaign, we conclude the lowest temperature to be about 700°C. The technique of core drilling

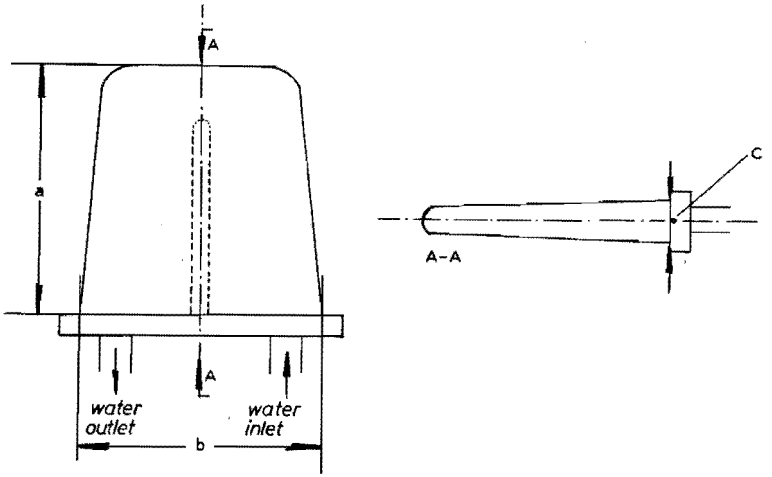

FIGURE 3.2a - The flat plate cooler. Typical dimensions are: a = 400-475 mm; b = 475 mm; c = 60 mm.

is described in [3-11]. The studies of König and of ourselves also showed, that good cooling of the refractory lining is of the utmost importance, since in that case the reactions will stop due to the low temperature. It is not the aim of this thesis to give a detailed description of the different cooling systems used. Only the most widely used system will be described here. This is the system where *flat plate coolers* (see figure 3.2a) are inserted into the refractory lining. The coolant of the plates is water. These coolers are placed in horizontal rows around the furnace and stick into the furnace wall upto ¾th of the total wall thickness (see figure 3.2b). It is obvious that the temperature distribution in the furnace wall is greatly influenced by the coolers. The main factors related with the temperature distribution are: the distance between the cooling plates, the hot face temperature of the wall, the wall thickness and heat conductivity of the refractory materials used. Van Laar and Maes [3-12] calculated the temperature distribution in the wall for different patterns. For their calculations they chose an area of the furnace where a wall temperature of 1100°C is expected. This will be the case in the upper bosh or the belly. They presumed that the brickwork was worn away upto the 1100°C isotherm. Their first calculation concerned the influence of the cooling plate distance upon a wall made of high duty fireclay bricks (λ = 0.9 $W.m^{-1}.K^{-1}$). For the thermal conductivity of the burden a value of 9 $W.m^{-1}.K^{-1}$

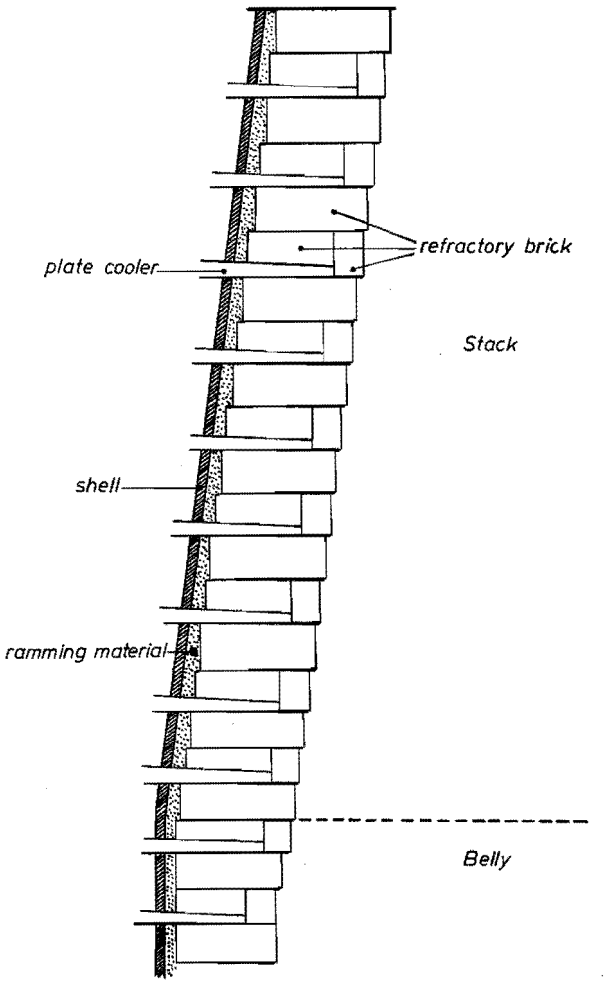

FIGURE 3.2b - The arrangement of the plate coolers in the furnace wall.

was used. The result of their calculations is shown in figure 3.3. The illustration shows that a relatively small difference in the position of the 1100°C isotherm is found. When the high duty fireclay is replaced by a high conductivity material as graphite, semi-graphite or silicon carbide, a more pronounced result is found, as is shown in figure 3.4. In this case the calculations were carried out with a conductivity value for the wall of 19 $W.m^{-1}.K^{-1}$ at 20°C and 6 $W.m^{-1}.K^{-1}$ at 1100°C, respec-

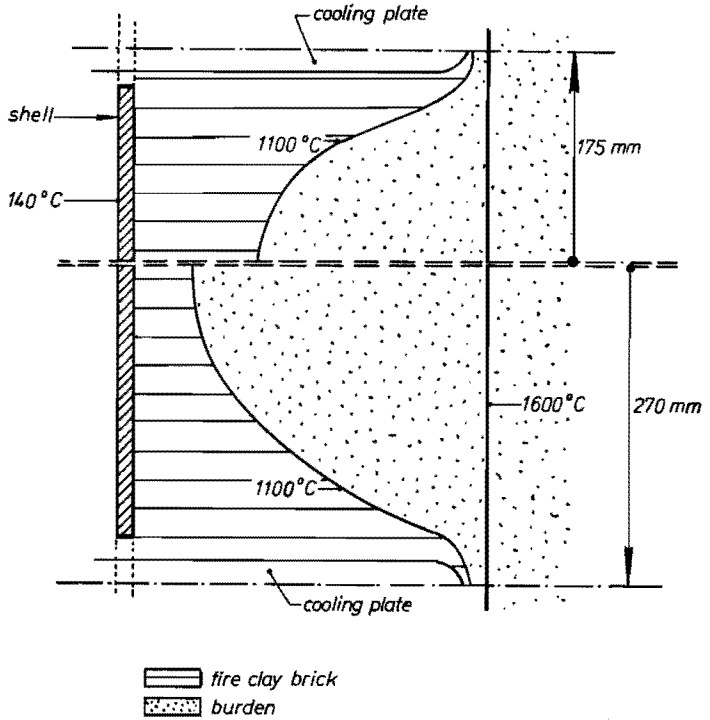

FIGURE 3.3 - The calculated temperature distribution between cooling plates for fireclay worn away upto the 1100°C isotherm. The upper part of the drawing is for a plate to plate distance of 350 mm, the lower part for 540 mm. The shift of the 1100°C isotherm is relatively small.

tively. The calculations show, that with the use of high conductivity material the isotherms in the refractory wall can be brought to the desired place by choosing the right plate to plate distance.

The work of König and of Van Laar shows, that it is difficult to freeze the potassium reaction parallel to the nozes of the cooling plates. A solution might be to prevent reactions to take place by coating the bricks externally and internally (in the pores as well). In that way direct contact between potassium and the brick is avoided. Such a protective coating was proposed by Visser [3-13], using mono-aluminium phosphate as a coating. Alkali tests showed a better behaviour of the fireclay bricks impregnated with mono-aluminium phosphate than of the unimpregnated ones. Panels of both types of bricks were built

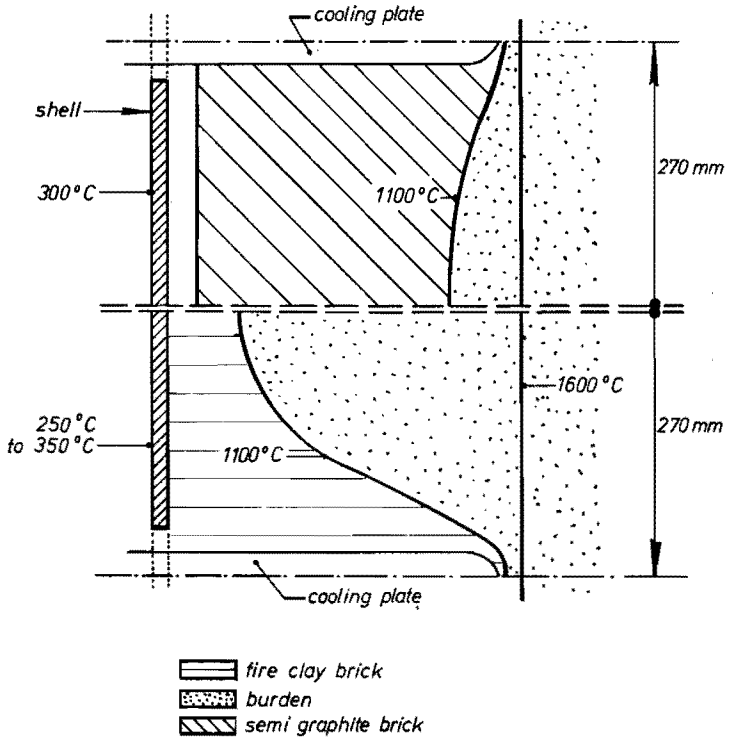

FIGURE 3.4 - The calculated temperature distribution between cooling plates for fireclay bricks and for semi-graphite bricks, for a lining worn away up to the 1100°C isotherm. Plate to plate distance = 540 mm.

in a blast furnace and during the campaign the wear was followed by means of cores drilled out of the wall. Chemical and mineralogical analyses of the cores showed less penetration of alkali into the impregnated bricks than into the unimpregnated ones. From measurements of panels in a blast furnace the difference in penetration is given in figure 3,5. A detailed review of this work is given by Doornenbal et al [3-14]. The studies showed, that penetration of alkali still takes place. Thus, the impregnation with mono-aluminium phosphate is of some help, but is no real solution in the long run, since rather rapid wear was still observed.

From the work described here, it can be concluded, that a good stack refractory lining should have the following properties:

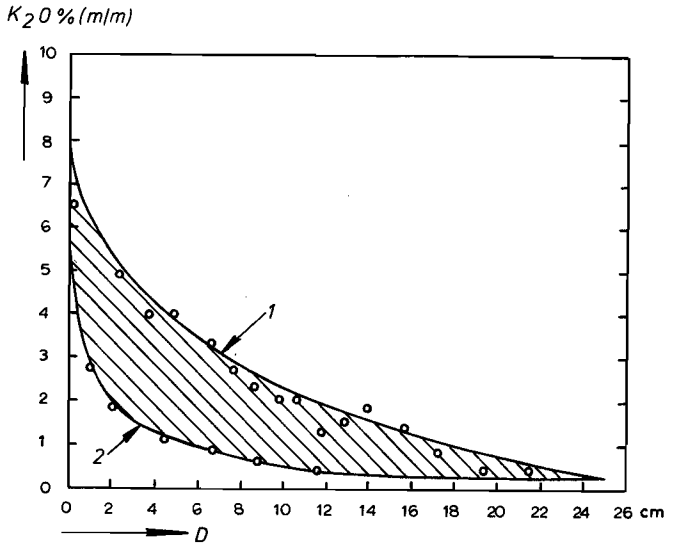

FIGURE 3.5 - The effect of mono-aluminium phosphate impregnation of fireclay bricks on the penetration of alkali. O = hot face; D = distance from the hot face; 1 = unimpregnated high duty fireclay brick; 2 = impregnated high duty fireclay brick.

- it should have excellent alkali resistance;
- it should be very abrasion resistant (see chapter 1);
- it should have a high thermal shock resistance (see also chapter 1);
- a high thermal conductivity is very helpful.

3.2 - Possible Refractory Materials

There are only a few, if any, refractory materials which meet all the specifications which are given in the last paragraph of section 3.1. To make a first selection it seems essential to consider alkali resistant materials. Good alkali resistant refractory materials are:

- graphite or semi-graphite (excellent resistance);
- magnesite, MgO (good resistance);
- silicon carbide, SiC (good resistance);
- corundum, Al_2O_3 (good resistance).

In the next section we will try to give a ranking for bricks made out

of these materials. When refractory bricks are investigated it is of importance to realize, that refractory bricks are inhomogeneous. A brick is made out of refractory grains and a suitable bond, or binding system. Such a brick is produced by means of mixing a refractory material, with a suitable distribution of the sizes of the grains, together with a binder. From this mixture bricks are pressed and fired. After firing a brick is formed which consists of the refractory grains bonded by the binder phase. Also voids (pores) will still be present. In most cases the binding phase is the weakest part of the brick. Most impurities are concentrated there and often the strength of the bond is less than the strength of the individual refractory grains. Therefore, good agreement with practice is found only, when data of commercially available bricks are used. In the ranking given in the next sections this is done. The refractory grains in the bricks considered consist of the materials given above with high duty fireclay as a reference.

3.3 - Ranking According to Laboratory Tests

3.3.1 - Abrasion resistance

The abrasion resistance of refractory bricks depends on the hardness of the refractory grains and the strength of the bond. The hardness of the grains is characterized by the Moh's scale, the strength of the bond can be characterized by the bending strength of a brick. Since the bending load applied to a brick will bring the brick partly under tensile stresses, fracture will occur in the bonding phase between the refractory grains, when the bonding strength is less than the strength of the individual refractory grains. In practice the burden in the furnace will scratch the refractory grains out of the brick structure. If the bond is strong this will be much more difficult.
The hardness of the refractory materials mentioned in 3.2 are according to the Moh's scale [3-15]:

graphite	- 1
magnesite	- 4.7
fireclay	- 5
corundum	- 9
silicon carbide	- 9.5

Only graphite is a really soft material. The abrasion resistance of an entire brick will depend to a great extend on the strength of the bond. As stated above this can be measured by means of the bending strength. Since we are interested in the abrasion resistance at high temperatures it is necessary to measure the hot modulus of rupture. It will be clear that at all temperatures concerned a high modulus of rupture is required at the hot face of the stack lining bricks. Table 3.1 shows the modulus of rupture data of different types of bricks with the modulus of rupture of the high duty fireclay brick as reference.

TABLE 3.1 - Hot modulus of rupture $MN.m^{-2}$ [1])

M / temp.	graphite	semi-graphite	high duty fireclay	magnesite *)	corundum **)	silicon carbide ***)
20°C	3.7	7.3	16	18.6	44	54
400	5.8	8.8	20	8.9	48	56
800	4.0	8.4	15	5.6	47	54
1000	4.2	8.8	13	9.5	48	44
1200	4.4	8.9	8	5.4	28	26
1400	3.8	8.6	4	3.2	18	18

*) Self bonded magnesite (MgO = 95 % (m/m)).
**) Mullite bonded corundum (Al_2O_3 = 95 % (m/m)).
***) Oxynitride bonded silicon carbide (SiC = 92 % (m/m)).

Most of the modulus of rupture data show a maximum value at higher temperatures; this is often due to elastic behaviour of the binding phase just before a reasonable amount of molten material appears in the bond. The data of table 3.1 show the following ranking in abrasion resistance for these materials (see table 3.2).

[1]) Since the characteristics of these bricks are more often used in this thesis they are summarized in Appendix II.

TABLE 3.2 - Abrasion Resistance

ranking	material	performance
1	silicon carbide	good
2	corundum	good
3	high duty fireclay	reasonable
4	magnesite	reasonable
5	semi-graphite	poor
6	graphite	very poor

Table 3.2 shows that the abrasion resistance of semi-graphite and graphite bricks is poor. Graphite and semi-graphite will last only in those places, where no abrasion occurs, where the burden movement is very low, or where the burden itself is soft. This will be the case in the bosh and hearth of the blast furnace. Therefore, graphite and semi-graphite will not be considered in the further work. The abrasion resistance of silicon carbide and corundum bricks is good, that of high duty fireclay and magnesite bricks is reasonable.

3.3.2 - Thermal shock resistance

In this section the ranking is given of the thermal shock resistance of magnesite, high duty fireclay, corundum and silicon carbide, using relation (2.12):

$$R_R = \frac{M \cdot a \cdot \Delta d}{\alpha \cdot E} \qquad (2.12)$$

When: $$a = \frac{\lambda}{d_s \cdot c_p}$$

relation (2.12) can be written as:

$$R_R = \frac{M \cdot \lambda \cdot \Delta d}{d_s \cdot \alpha \cdot c_p \cdot E} \qquad (3.1)$$

The calculations will be made for a hot face temperature of 1000°C, a temperature which will often occur in the lower stack. The values used are derived from Appendix II, table II-a. Table 3.3 shows the results of the calculations. The table shows that the thermal shock resistance of oxynitride-bonded silicon carbide is about 20 times as good as that of fired magnesite bricks and about 4 times as good as those of corundum

TABLE 3.3 - Thermal shock resistance

ranking	material	R_R $m^3.s^{-1}.K^{-1}$
1	silicon carbide	$15.0 \cdot 10^{-9}$
2	corundum	$3.4 \cdot 10^{-9}$
3	high duty fireclay	$3.0 \cdot 10^{-9}$
4	magnesite	$0.7 \cdot 10^{-9}$

and high duty fireclay bricks. Due to these results no further study was made of magnesite bricks.

3.3.3 - Chemical resistance

The alkali and slag resistance of the three remaining types of brick were studied. The crucible test (chapter 2.4.1) was carried out on the high duty fireclay, the corundum and the silicon carbide brick as characterized in Appendix II, table II-a.
The crucibles were filled with 30 grams of K_2CO_3 and sealed with a lid of the material to be tested. The crucibles were heated up and held at

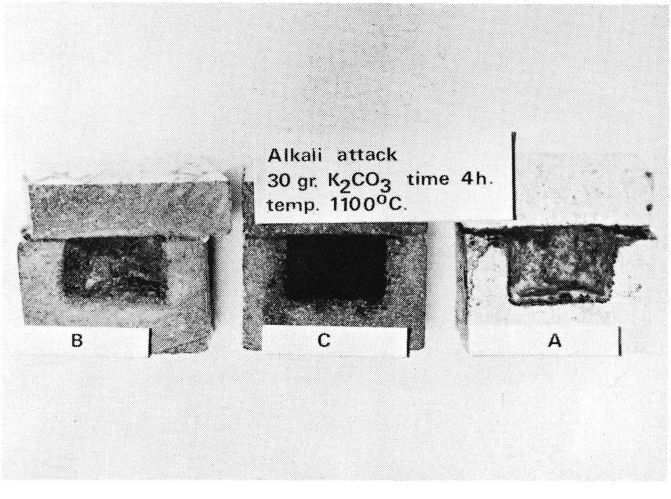

FIGURE 3.6a - Results of the crucible test shows the high duty fireclay brick (A) and the oxynitride-bonded silicon carbide brick (B), (C) is the type of brick discussed in chapter 7.

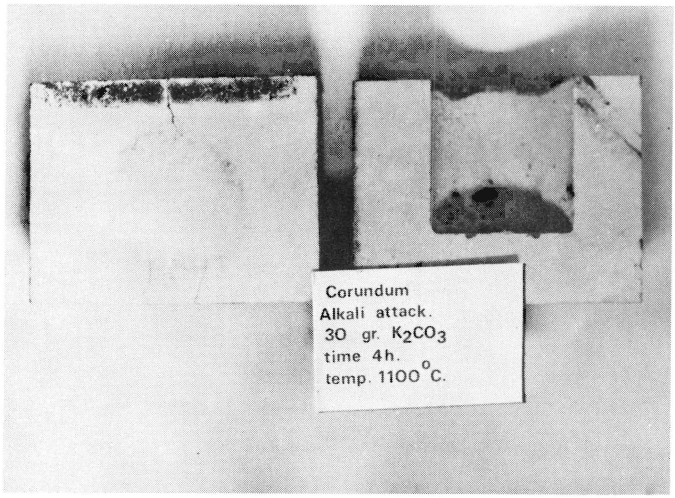

FIGURE 3.6b - Results of the crucible test shows a corundum brick. The cracks in the exterior of the crucible are due to alkali bursting.

a temperature of 1100°C for 4 h. The results of the tests are shown in figures 3.6 a en b. In figure 3.6a it is clearly seen, that the impregnated high duty fireclay brick (A) is heavily attacked by potassium carbonate. No visible attack can be observed at the silicon carbide brick (B). The corundum brick (figure 3.6b) shows some cracks due to alkali bursting. X-ray diffraction studies indicated the formation of $K_2O.Al_2O_3$. This compound causes a volume expansion of 20 %. Even formation of $K_2O.11Al_2O_3$ would have given an expansion of 17 %. Microscopic examination of the silicon carbide crucible showed that the potassium carbonate had attacked the bond. The oxynitride bond had disappeared over a depth of about 2 mm. Figure 3.7 shows the exposed brick surface on the left side. The bond can be seen on the far left of the picture. Between the silicon carbide grains a potassium silicate phase is formed.

The slag resistance of the bricks was tested by means of the slag dip test as described in 2.4.2. T shaped test pieces were cut out of the three bricks. The slag used for the test was a normal blast furnace slag with an addition of 5 % (m/m) K_2CO_3. By mixing this amount of potassium carbonate to the slag, a slag composition very similar

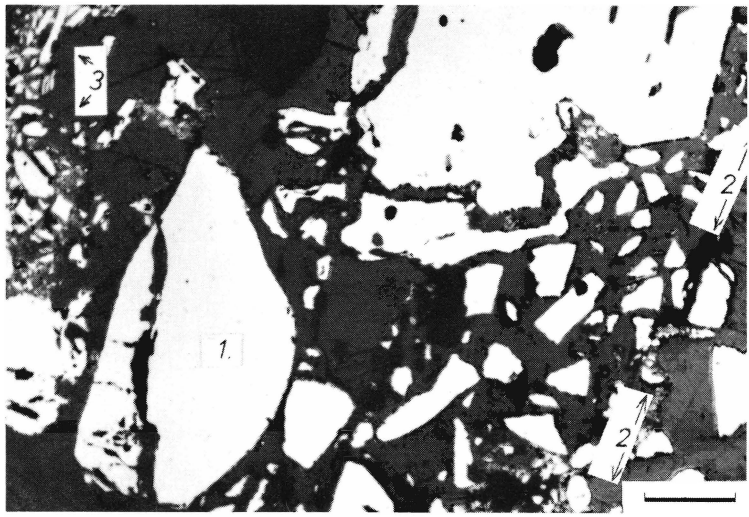

FIGURE 3.7 - Part of the oxynitride bond between the silicon carbide grains (1) has been dissolved in the potassium carbonate. The exposed surface is indicated as (2) in the picture. The remaining bond (3) is visible at the left side of the picture. Bar = 266 μm.

to the probable composition of the lower blast furnace stack slag as given in table 1.2 was attained. The test pieces were soaked for 1 h at 1450°C. The high temperature was chosen for having a slag with low viscosity and to measure slag attack in a relatively short time of exposure. In figure 3.8 the results of the finger test are given. The reduction of cross-section caused by the slag attack is given in table 3.4.

TABLE 3.4 - Reduction of cross-section after Slag Attack

type of brick	attack *)
high duty fireclay	60 % (A/A)
corundum	30
silicon carbide	nihil

*) The given data result from measurements of the cross-section of the specimen before and after the test. The cross-section was measured at one quarter of the length measured from the specimen basis.

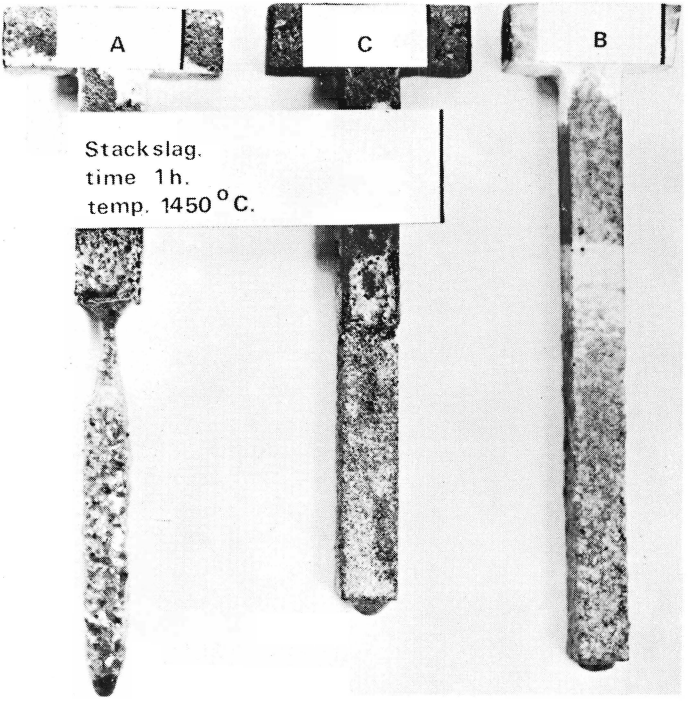

FIGURE 3.8 - The results of a slag finger test with slag of a composition as expected in the blast furnace (see also table 1.2). A) high duty fireclay - B) corundum - C) oxynitride bonded silicon carbide

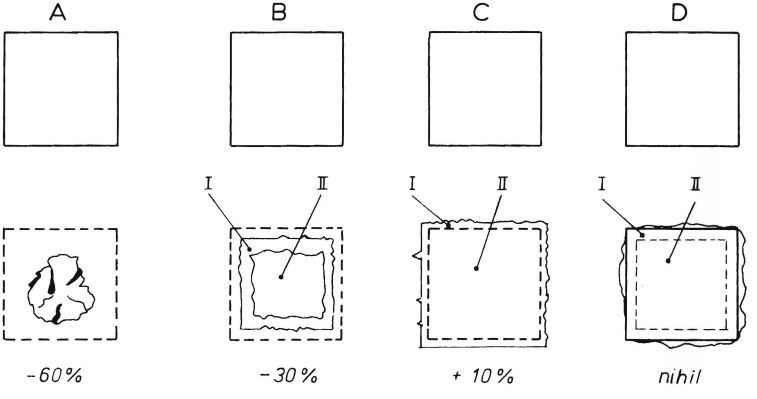

FIGURE 3.9 - A drawing of the cross-sections of the test pieces before and after testing
A) The cross-section loss of the high duty fireclay brick
B) The cross-section loss of 95 % (m/m) corundum brick
C) The cross-section growth of 99 % (m/m) corundum brick
D) The cross-section of the silicon carbide brick.

The same test carried out with a corundum brick with 99 % (m/m) Al_2O_3 *) gave other results. Now a cross-section growth of 10 % (A/A) was found instead of a cross-section loss. A schematic drawing of the cross-sections of the test pieces is given in figure 3.9. I indicates the reacted zone, II the unchanged zone. Mineralogical analyses of the corundum and silicon carbide test pieces are shown in table 3.5.

TABLE 3.5 - Mineralogical Examination

brick type	zone	Al_2O_3	$3Al_2O_3.2SiO_2$	$K_2O.Al_2O_3$	$FeAl_2O_4$	SiC	Si_2ON_2
corundum (95 % (m/m))	I	+	▭	-	+		
	II	++	+				
corundum (99 % (m/m)	I *	nd	nd	nd	nd		
	II	++		-	▭		
silicon carbide	I **					nd	nd
	II					++	▭

* Zone too small (about 2 mm) to prepare test material for X-ray diffraction.
** Microscopic examinations showed a loss of bond over 2 mm from the surface.

++ lot of the phase present
\+ reasonable amount of the phase present
▭ a little of the phase present
\- phase just to be indicated
nd no data available.

The table shows an appreciable impregnation of Fe in the corundum bricks. This is not very likely to occur in practice, since the temperature is then about 200 to 300°C lower than used in the test.

Of the bricks tested the silicon carbide brick appears to offer the best combination of abrasion resistance, thermal shock resistance and chemical resistance. The only disadvantage of the brick seems to be the bonding system. The chemical tests show clearly, that the oxynitride bond is affected by potassium. Extensive studies of silicon carbide bricks with other bonding systems seemed to be of importance in the light of the experimental results described.
In the last section of this chapter we will discuss the results of experiments in practice with silicon carbide bricks with various bonding systems.

*) The characterization of the brick is given in Appendix II, table II-a.

3.4 - Experiments in Practice

In the small experimental blast furnace in Ougrée - Belgium series of experiments were carried out to find the best material for the bosh and stack lining. Those experiments were carried out as a part of a research program of the European Community of Carbon and Steel. The results were published in a report of "Centrum voor Research in de Metallurgie" [3-16]) and was summarized by Konopicky [3-17]). The experiments showed, as was found in the laboratory studies described above, that magnesite bricks fail due to thermal spalling. In the experimental furnace experiments were carried out with the 99 % (m/m) Al_2O_3 (3.3.3 and Appendix II). The experiments showed alkali bursting and penetration of alkali into the bricks. Also a test panel of oxynitride bonded silicon carbide bricks was built in the lower stack of the furnace. After the test period a loss of bond over a length of 20 mm from the hot face was found (total brick length was 230 mm). From about 60 mm behind the hot face the brick was unchanged. In the zone directly behind the hot face penetration of alkali was observed.

At Hoogovens experiments were carried out in the middle stack of blast furnace No 6 (hearth diameter 10 m; average hot metal production 4000 ton a day). Figure 3.10 shows the position of the test panels in the middle stack. The characteristics of the five brick types used are summarized in Appendix II, table II-b. A short description is given in table 3.6.

TABLE 3.6 - The bricks tested in blast furnace No 6

code	SiC content	bonding system
I	92 % (m/m)	Si_2ON_2
II	67	Al_2O_3-SiO_2
III	90	TiO_2-Al_2O_3
IV	85	Al_2O_3-SiO_2
V	45	pitch
	(45 % (m/m) graphite)	

The wear of the silicon carbide bricks was studied using a mono-aluminium phosphate impregnated high duty fireclay brick as the reference. The test panels form the hot face layer of bricks in the furnace

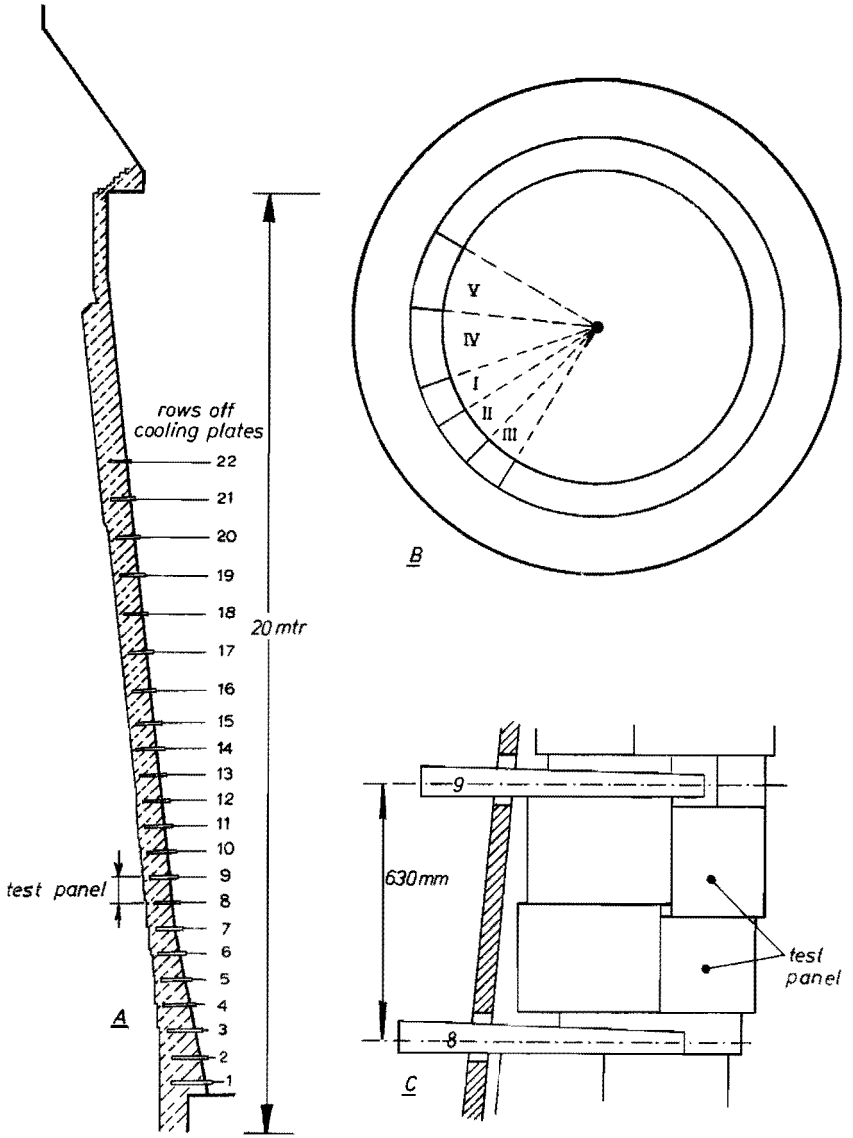

FIGURE 3.10 - The place of the five test panels in the stack of blast furnace No 6. The thickness of the refractory wall was 630 mm. The thickness of the hot face brick layer was 230 mm. A - Situation seen in a vertical cross-section of the furnace; B - The horizontal cross-section at the height of the test panels; C - Test panels between two rows of cooling plates.

as can be seen in figure 3.10. The wear of the lining during the campaign was measured by means of core drilling. The results of these experiments are given in figure 3.11. The wear curves show a rapid wear

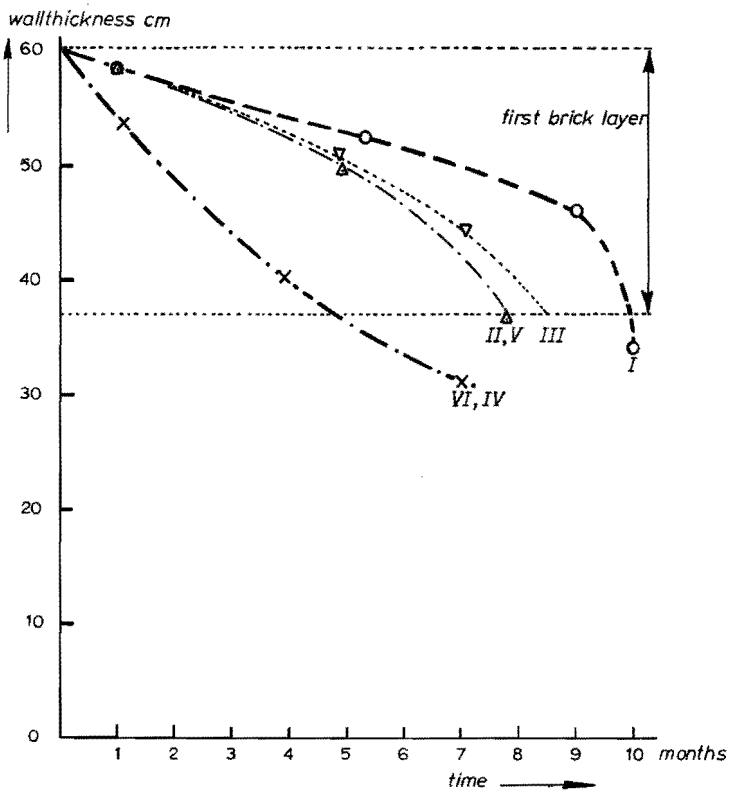

FIGURE 3.11 - The wear of five different types of bricks in the stack of blast furnace No 6. (VI) impregnated high duty fireclay; (II),(IV) ceramic bonded SiC; (III) TiO_2 bonded SiC; (V) SiC/graphite; (I) oxynitride bonded SiC.

of the high duty fireclay bricks and the ceramic bonded silicon carbide bricks. The latter wore away, as the alkali penetration in the bond caused alkali bursting. The TiO_2 and the carbon bonded bricks had a slightly better performance. The best results were, again, obtained with the oxynitride bonded silicon carbide. Microscopic analyses of the hot face of the latter bricks showed a loss of bond over a few millimeters as was found in the bricks of the experimental furnace and as was also found in the laboratory tests (see figure 3.12).

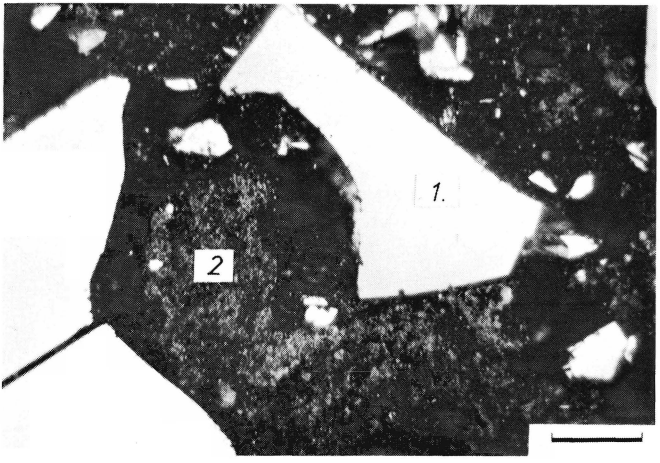

FIGURE 3.12 - The hot face area of a oxynitride bonded SiC brick after 9 month of service in practice. The picture is very similar to figure 3.7. Bar = 30 µm.

Summarizing it can be stated, that there is good agreement between the results of the laboratory tests and the results of the experiments in practice. From the laboratory studies and the experiments in practice it can be seen, that silicon carbide is a promising material for the lining of a blast furnace stack, provided a suitable bonding system can be found.
In the following chapters of this thesis a method will be described and analysed to produce a direct-bonded silicon carbide brick.

L i t e r a t u r e

3- [1]) *Konopicky, K.* — *Feuerfestbaustoffe, Düsseldorf, Verlag Stahleisen, 1957*

3- [2]) *Harders, F.; Kienow, S.* — *Feuerfestkunde, Berlin, Springer Verlag, 1960*

[3- 3] Willems, J.; Heynert, G.; Quade, G.; Zischkale, W. — Stahl und Eisen 84 (1964) 57-62

[3- 4] Rigby, R.G.; Richardson, H.M. — Min.Mag., London, 27 (1947) 75-89

[3- 5] Jay, A.H.; Andrews, K.W. — Min.Mag., London, 28 (1948) 88-89

[3- 6] Kahlhöfer, G.; Overkott, E.; Konopicky, K.; Patzak, I. — Stahl und Eisen 85 (1965) 189-194

[3- 7] Jon, M.; Halm, L. — SIPRE meeting June 1976

[3- 8] Halm, L.; Schoendorfer, M.J. — Blast Furnace Refractories, London, Iron and Steel Inst., 1968. Publ. 116; p. 83

[3- 9] Pitak, N.V.; Ain'yar, E.A.; Levitanskii, V.J.; Rutkoskii, A.J. — Ogneupory 7/8 (1968) 426 (Eng. Transl.: Refractories)

[3-10] König, G.; Weidemüller, C.; Pietzke, G. — Stahl und Eisen 91 (1971) 63-69

[3-11] Steele, G.; Lister, R.R. — Refract.J. 44 (1968) 396-408

[3-12] Van Laar, J.; Maes, J. — Stahl und Eisen 91 (1971) 1098-1101

[3-13] Visser, R.; Van Laar, J. — GB Patent 1,226,949

[3-14] Doornenbal, W.; Van Konijnenburg, J.T.; Visser, R.; Waasdorp, A. — CNRM Metallurgical Repts. (1970) 25, 11-20

[3-15] Weast, R.C. (ed) — Handbook of chemistry and physics 54th edition, 1973-74, Cleveland Ohio, CRC Press, 1974

[3-16] Konopicky, K.; Routschka, G.; Van Laar, J.; Visser, R.; Waasdorp, A.; Halm, L. — Rapport de synthese sur les essais de produits refractaires dans le haut fourneau expérimental d'Ougrée, nr S 9/72, C.R.M. report 1972

[3-17] Konopicky, K. — Stahl und Eisen 92 (1972) 481-487

PART TWO

Study of Silicon Carbide Refractory Bricks

Chapter 4 - THE FORMATION OF SILICON CARBIDE BRICKS

4.1 - Introduction

In part two of this thesis a study will be made of the production possibilities of pure silicon carbide bricks. Chapter 4 gives a general outline, chapters 5 and 6 give the study of the bonding system and in chapter 7 the experimental production and the experiments in the blast furnace are discussed.

In this chapter a short description of the Acheson process is given. Nearly all the commercially available silicon carbide is produced by the Acheson process. The main characteristics of the material so produced are given. The major steps in producing refractory bricks are described and a model is given for correlating the final brick properties with the production characteristics.
The possibilities for normal refractory production are the basis for our further study, since it is the aim of this thesis to describe a production method which can be carried out in a normal refractory production plant. In the last part of this chapter various production methods for silicon carbide bricks are described and some initial experiments carried out in our laboratory are discussed.

4.2 - The Refractory Material Silicon Carbide

Silicon carbide (SiC) was first observed in laboratory experiments by a number of investigators in the period between 1824 and 1881 [4-1], [4-2]. By analysing a meteorite silicon carbide was found by Moissan in 1905 [4-3].
Silicon carbide proved to be a very hard and stable compound. It could be used for cutting and grinding purposes. Cowless [4-4] and Acheson [4-5] realized that production on a large scale of this material was profitable.

The method mostly used for the production of technical silicon carbide is based on the Acheson process. In this process a mixture of silica (SiO_2 ≈ 50 % (m/m)) and carbon (coke ≈ 40 % (m/m)) with some additions to obtain a smooth process, is heated in a trough type furnace. Figure 4.1 shows schematically the Acheson furnace.

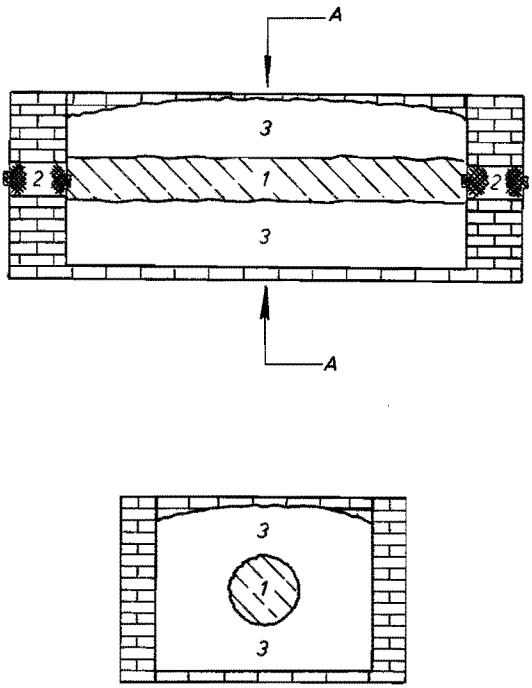

FIGURE 4.1 - Cross-sections of the Acheson furnace
1 - carbon core heater; 2 - electrodes; 3 - the mixture of silica and carbon.

The central core in the furnace consists of graphite and coke. This core is the heating element for the furnace. Both core ends are connected with electrodes for the power supply. The furnace has a bottom and four side walls and no roof. The reaction mixture is filled in around the core.

The process is based upon the following reactions:

$$SiO_2 + 2\,C = Si + 2\,CO \qquad [4.1]$$

$$Si + C = SiC + 2\,CO \qquad [4.2]$$

$$+ \quad SiO_2 + 3\,C = SiC + 2\,CO \qquad [4.3]$$

according to Ruff [4-6].

The reaction temperature is about 2200°C, and the reaction time about 30 h.

As is shown in figure 4.2 different zones of reaction products will be

found after firing. Directly around the carbon core a layer of pure graphite is found. (N.B.: for the production of graphite in principle the same firing method is used.) Around that layer a mass of large SiC crystals is found with voids. At the outer parts of the furnace "amorphous SiC" and remnants of the starting mixture are found.

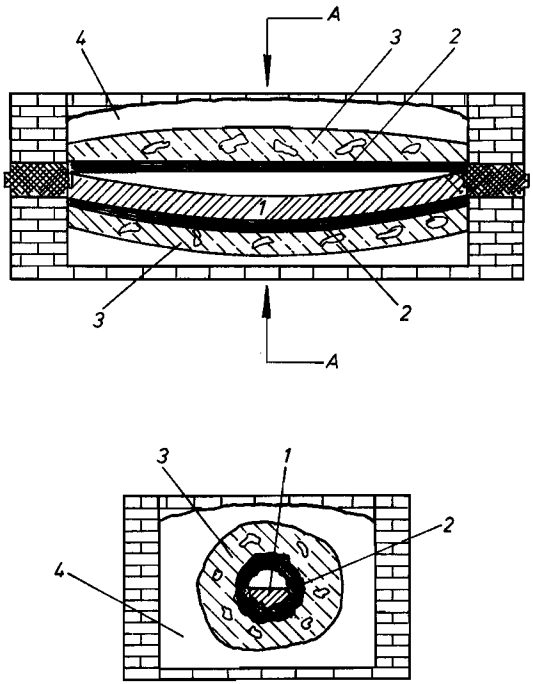

FIGURE 4.2 - The contents of an Acheson furnace after firing
1 - core; 2 - graphite; 3 - massive SiC with voids;
4 - amorphous SiC with remnants of the starting mixture.

The bulk of the SiC thus formed is of the α-type SiC structure. The α-type SiC consists of two groups of crystal classes: the hexagonal-pyramidal (international symbol: 6 mm) and the ditrigonal-pyramidal (international symbol: 3 m) class, as Thibault [4-7], [4-8] has shown. In principle the crystal structure is either hexagonal of rhombic. Over 40 polytypes have been found. The basic building block is a C atom tetrahedrally bound to 4 Si atoms [4-9].

A small part of the silicon carbide used for refractory purposes consists of so called β-type SiC, which has a cubic structure (spacing

$a = 4.36$ Å [4-10], [4-11]).

Table 4.1 gives the main properties of technical silicon carbide, which is produced with the Acheson method.

TABLE 4.1 - Characteristics of silicon carbide

CHEMICAL ANALYSES		
SiC		97 - 99 % (m/m)
main impurities		SiO_2, Si, Fe
crystal structure		α-SiC (hexagonal, rhombic)
		β-SiC (cubic)
color		dark green to black
PHYSICAL PROPERTIES		
ρ	g/cm^3	3.2
c_p < 100°C	$kcal.m^{-1}.h^{-1}.°C^{-1}$	0.18
1000°C	"	0.27
λ 20°C	$W.m^{-1}.K^{-1}$	> 40
1000°C	"	≈ 15
α 0 - 1000°C		$4.8.10^{-6}$
MECHANICAL PROPERTIES		
hardness scale of Mohs		9.5
Young's modulus	$MN.m^{-2}$	$3.5 - 4.0.10^3$ up to 1500°C

The values given in this table were taken from Gugel [4-12]) and are in good agreement with values used by other authors [4-11]), [4-13]). The lumps of SiC found after the Acheson process are rather large, more than 10 mm diameter. They mainly consist of elongated irregularly shaped crystallites and polycristalline agglomerates. The porosity is extremely low, between 1,5 and 2 % (V/V) [4-14]).
For refractory purposes, the lumps are crushed to a maximum grain size of about 3-4 mm.

From the phase diagram (figure 4.3) it can be seen, that SiC is stable up to about 2760°C. The strength of the material is high up to a very high temperature. The modulus of rupture of α- and β-SiC has a constant value up to 1500°C [4-12]). The chemical resistance of the material is also rather good. Oxidation of silicon carbide is observed even

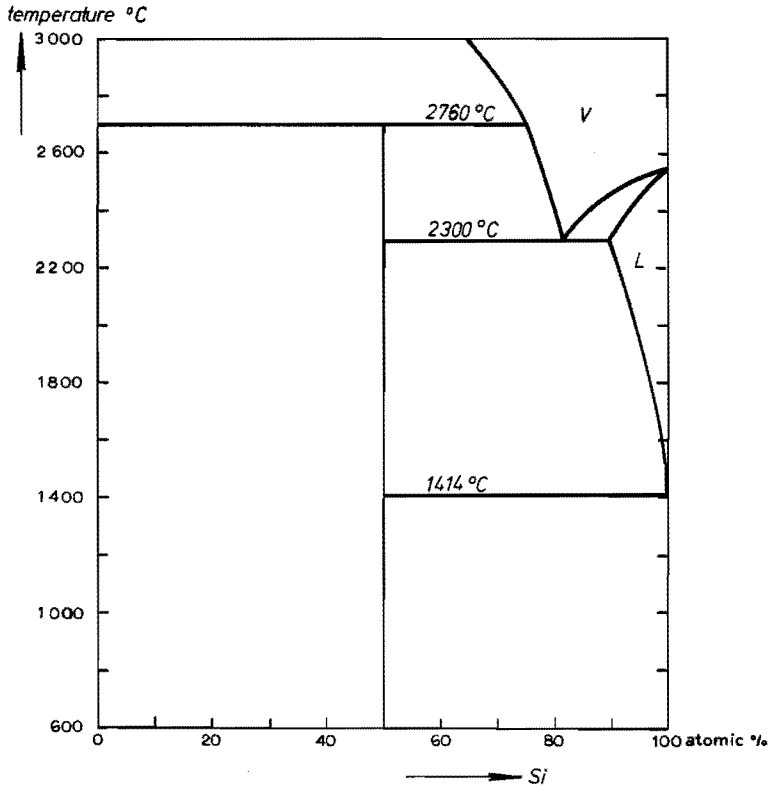

FIGURE 4.3 - Phase diagram of Si and C at 1 atm [4-15]).

at rather low temperatures, but below 900°C this reaction is very slow [4-12]). Our own experiments with silicon carbide powder with a maximum grain size of 60 µm showed, that no oxidation was measured after heating it in a constant air flow up to 1200°C with a heating rate of 1 $K.min^{-1}$. After this test no sealing SiO_2 layer was found either.
Silicon carbide is resistant against molten Al, Cu, Pb, Zn, Sn and Cd, but in contact with molten Fe, Ni, Co, Cr and Mn it will form silicon alloys, such as FeSi.
Silicon carbide is resistant against most oxides up to 1000°C. It is not attacked by alkali compounds as was shown in the previous chapter.

4.3 - Brick Manufacture

The production of refractory bricks can be separated in different steps. The steps are schematically shown in figure 4.4. In manufacturing bricks, special care has to be taken in the production steps before the shaping of the bricks. This is related to the physical and chemical properties which the brick should have in the final stage.

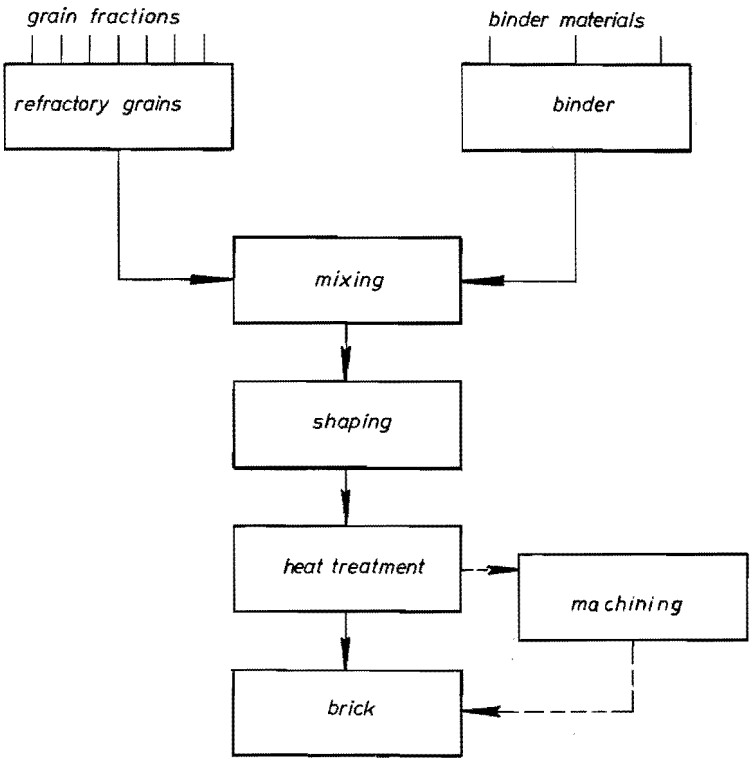

FIGURE 4.4 - The production scheme of a refractory brick. Machining after firing is only carried out when the firing causes deformation of the bricks. By means of machining the brick dimensions can be corrected.

A brick consists of refractory grains and binding material. For a good characterization of a brick, however, it is of use to define it in more detail. Using the *topo-ceramic model* as introduced by Van Haeften [4-16] it is possible to give a rough description of the brick properties and the correlation between these properties and the brick structure. Refrac-

tory bricks are known to be composed of various crystalline and amorphous phases and pores. The properties and behaviour of these inhomogeneous bricks do not only depend on the mean chemical and mineralogical composition or porosity, but essentially on the way in which the composing phases occur, distributed to nature, form and size. Such a distribution can be called the *topology*. The behaviour and the properties of the brick will be determined primarily by its topology. The main items for correlation of the brick structure with the brick properties are:

- type and shape of the refractory grains
- distributive function regarding the size of the grains
- bonding system
- matrix.

The *matrix* consists of a high percentage of a glassy phase, very fine crystalline particles (mostly fines of the refractory grains) and pores. The microstructure is schematically shown in figure 4.5.

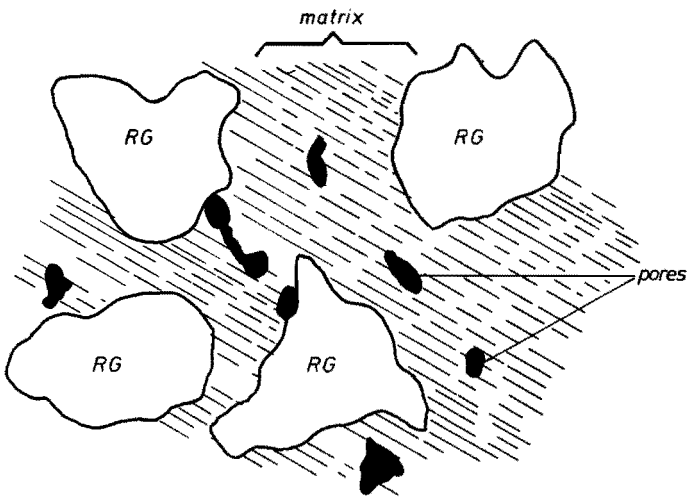

FIGURE 4.5 - The matrix of a brick is the space between the refractory grains (R.G.) > 150 μm in diameter.

It is of importance that a matrix is formed which completely surrounds the larger grains. The matrix, which is very important for the final strength of the brick, is formed by all the material and the pores in

the brick which are smaller than 150 μm. This value is arbitrarily chosen, but the work of Van Haeften [4-16] showed that this value is suitable for characterizing the brick. In a well-fired brick often crystallites of about 100-200 μm are formed during firing, therefore it is of use to choose a value in that same order.

The grain size distribution determines the best possible packing density of the refractory grains used. This subject has been studied extensively by a great number of authors, for instance Fuller et al [4-17], Litzow [4-18] and Andreasen [4-19]. Andreasen defined a distribution of spheres of different sizes for optimal density. The equation for such a packing is:

$$\frac{dm}{m} = n \cdot \frac{dD}{D} \qquad (4.1)$$

where: m - mass of the grains

D - grain diameter

n - constant (for optimal packing density of spheres n = 0.5).

The integration of (4.1) gives the actual relation of the grain size distribution. This is:

$$m_D = \left(\frac{D}{D_{max}}\right)^n \qquad (4.2)$$

where: m_D - mass fraction with diameter D

D_{max} - maximum diameter of the grains used.

Fuller et al [4-17] showed that the most suitable grain size distribution for practice is found for $1/3 < n < 2/3$. Fuller proposed a special distribution for brick making purposes which lies within the given range, but which does not fully obey relation (4.2). In figure 4.6 the different grain size distributions are shown.

The specific shape of the refractory grains of a certain composition makes it impossible to give exact rules for the grain size distribution to be used. The ideal distribution of the size for irregular grains like refractory grains, has to be found by trial and error.

In practice usually a smaller amount of fine grains is added to the mixture, than prescribed by the distribution function. The remaining gap in the distribution is filled in with binder material. In that way the total mixture has the "ideal" grain size distribution. The effect of shrinkage of the binder must be taken into account as well.

The shaping of a brick is usually done in a steel mould by means

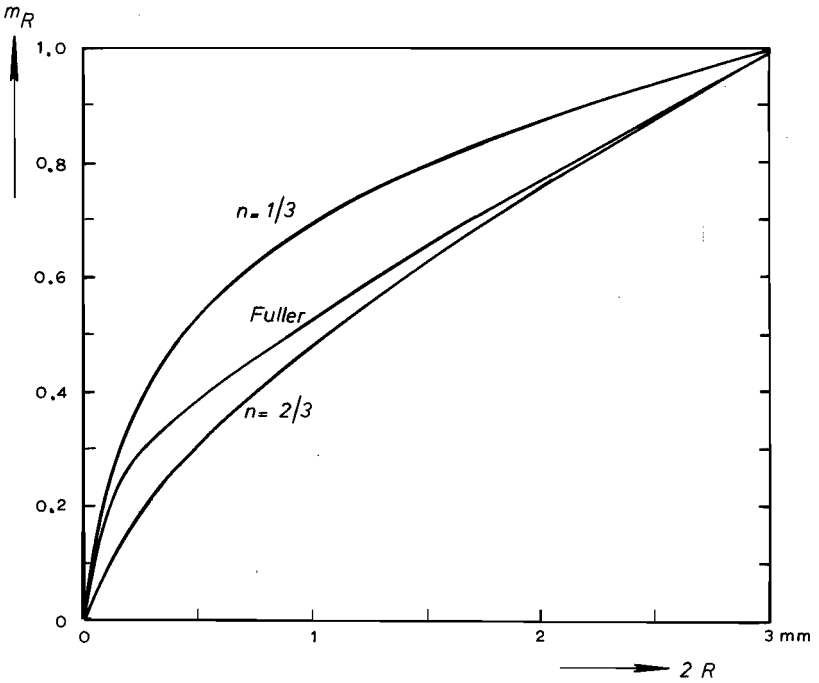

FIGURE 4.6 - Different grain size distributions according to relation (4.2). The example is chosen for D_{max} = 3 mm. The distribution proposed by Fuller for refractory grains is shown as well.

of a hydraulic press. The pressure to be used has to be established for each mixture. The aim is to press to an optimal *green* density and so far that the *green brick* does not show any shrinkage or swelling when it is demoulded. The way of mixing and shaping of the green brick also influences the final properties of the brick.

While firing the brick a ceramic bond is formed between the refractory grains. Firing temperature and time are chosen such, that the matrix formed fully surrounds the refractory grains.
The firing must be carried out in such a way, that the brick is volume stable at the temperature of application. In some cases small deformations of the brick take place during firing. When the deformations are small, it is possible to bring them back into the dimensional tolerance range by means of machining. This expensive method should be avoided as much as possible.

4.4 - Production Methods for Silicon Carbide Bricks

The main problem in producing silicon carbide bricks is to find a suitable bonding system. As was shown in 4.1 the SiC grains do not react with most of the classical bonding materials. For refractory brick purposes up till 1974 no direct-bonded brick has been produced commercially. In table 4.2 the major bonding types for silicon carbide are given with the binder materials used.

TABLE 4.2 - Binder systems for silicon carbide

bond	binder
ceramic	Al_2O_3, SiO_2, glass phase
non-ceramic	C, Si_3N_4, Si_2ON_2
direct *	SiC via: sintering, hot pressing, reaction sintering

* Methods used for special materials like heating elements, electrical and engineering ceramics.

The ceramic bond is the oldest and most important one for most of the SiC refractory bricks used. Ceramic bonded bricks have a span in the SiC used in the different qualities of this type of brick. The major part has a SiC content between 50 % (m/m) and 85 % (m/m). Characteristic data of three of those brick qualities are given in Appendix II, table II-b (II, III, IV).
The production of ceramic bonded bricks is characterized as follows. A certain grain size distribution of silicon carbide grains is made by mixing fractions of different sizes together with a suitable amount of refractory clay. Mostly technical silicon carbide grains have a maximum size of 3 to 4 mm. Grains below 1 mm are more expensive and contain more impurities (e.g. Fe). Therefore, the use of fines is limited in practice. After pressing and firing in an oxidizing atmosphere a silicon carbide brick with a matrix consisting out of silicate and glass phase is formed. Often a direct-bond between the SiO_2 layer on the silicon carbide grains, resulting from the oxidizing firing procedure, and the silicate in the matrix is found.

Due to the high strength and the high thermal conductivity the importance of Si_3N_4 and Si_2ON_2 as a binder for silicon carbide becomes

greater. In the sixties studies carried out throughout Europe ([4-20], [4-21], [4-22]) showed that it is possible to produce Si_3N_4 bonded bricks by using silicon powder in the matrix and firing the bricks at about 1400°C in a nitrogen atmosphere with some carbon powder present. The studies showed that even at high N_2 pressures (up to 30 atm) no nitridation of the silicon carbide grains occured, although theoretically nitridation is possible. In production furnaces it is difficult to fire the bricks in a pure nitrogen atmosphere, hence a bonding phase is formed which consists of a mixture of Si_3N_4 and Si_2ON_2. In the USA a similar process has been developed. No silicon powder is used, but a SiO_2 powder which is fired in an atmosphere of at least 80 % (V/V) of nitrogen and temperatures above 1400°C [4-23]. In this way a very strong brick was made with a matrix consisting primarily out of Si_3N_4 and Si_2ON_2.

As is shown above the production of nitride bonded silicon carbide bricks is relatively simple. Karay et al [4-24] reviewed the different ways of producing nitride bonded bricks in more detail. The characteristics of bricks made with silicon in the matrix, are given in Appendix II, table II-a. Gugel et al [4-25] gave a report on the slag resistance of these bricks.

In the sixties in Japan a brick was developed for blast furnace purposes consisting of a mixture of silicon carbide and graphite. The brick was mentioned already in the previous chapter. We have investigated the bricks and according to this study we suppose that the following production method has been used: SiC grains (about 45 % (m/m) of the total mixture) and graphite grains (about 45 % (m/m) of the total mixture) are mixed with pitch at elevated temperatures. The bricks are pressed and fired in a reducing atmosphere. The firing temperature is sufficiently high to form a good carbon bond by coking the pitch. Our investigations showed that the coking temperature must have been about 1400°C, since a good secundary coke skeleton has been formed out of the pitch, but no graphitization was found. Bricks made in that way appear to have a good chemical resistance and a high thermal conductivity. The strength and the abrasion resistance are not very good as can be seen from Appendix II, table II-b.

In the next section the possibilities for direct-bonded silicon carbide bricks will be discussed.

4.5 - Direct-bonded Silicon Carbide Bricks

Table 4.2 shows three methods for producing direct-bonded silicon carbide. Sintering and hot pressing are methods used for special ceramics. Both methods work at very high temperatures, mostly above 1900°C. The materials formed with those methods are very dense and rather brittle. An example of sintered silicon carbide materials are heating elements used for electric heating of laboratory furnaces up to 1600°C. The rod shaped elements are very dense, hard and brittle. For use as a refractory brick high strength under compression and under bending conditions is required, as was shown in chapter 3. Sintered and hot pressed SiC products are hard and brittle and therefore of no interest for brick making.

Therefore the reaction firing method is the only one left. The requirements which are needed for a successful production of commercial direct-bonded SiC bricks can be summarized as follows:

- the production should be possible in a normal refractories producing plant;
- normal mixing and shaping must be possible;
- the firing should be possible in a standard gas or oil fired furnaces, which usually work in a temperature range between 1200 and 1600°C. Only small alterations are allowed for the firing conditions in such furnaces.

In order to satisfy these requirements it is impossible to think of a modified Acheson process, since in that case a temperature above 2000°C is required. One has to think of a direct reaction between silicon and carbon according to:

$$Si + C = SiC \qquad [4.4]$$

Thermodynamic data from literature [4-26], [4-27] show that the reaction in principle is possible in the temperature range concerned, as the Gibbs standard free energy of formation $\Delta G^{\circ}(T)$ is negative. $\Delta G^{\circ}(T)$ can be calculated as:

$$\Delta G^{\circ}(T) = \mu^{\circ}(SiC,s) - \mu^{\circ}(Si,s) - \mu^{\circ}(C,s) \qquad (4.3)$$

The values of ΔG° and μ° are given in literature kcal.mol^{-1}. In order to stay as close as possible to the original values these old dimensions are used for the thermodynamical calculations in this thesis.

In figure 4.7 ΔG^{o} is given as function of temperature for the temperature range of interest.

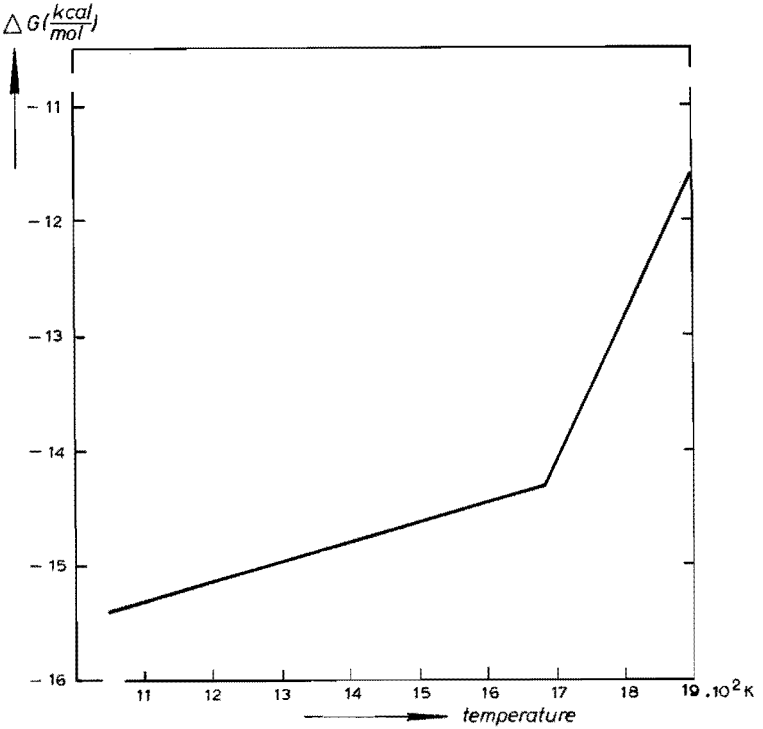

FIGURE 4.7 - The total Gibbs free energy of formation $\Delta G^{o}(T)$ for the reaction Si + C = SiC in the temperature range from 1100 K up to 1900 K. Data used are derived from [4-27]. The break in the curve is due to the melting of Si.

From personal communications with Dr. Schuster [4-28]) it was learned that some experiments were carried out to bind SiC grains with SiC by *reaction firing*. As reactants silicon powder and graphite powder were used. The results were not encouraging, hence the experiments were stopped in the laboratory of Dr. Schuster. In our laboratory we started experiments in the same way to get an idea about the reaction rate and the possible reaction temperatures. In the first experiments carried out, a stoichiometric mixture of silicon powder (70 % (m/m), with grains < 60 µm) and graphite (30 % (m/m) with flakes < 500 µm) was made and pressed with a little tar - for initial bond - into a cylindrical test piece. The tar addition caused an excess of about 11 % (m/m) of

carbon in the total mixture. This test piece was heated up to a temperature of about 1450°C and was held at that temperature for 12 hours. In the furnace a reducing atmosphere was maintained. This temperature was chosen, to make sure that if SiC formation takes place it will be of the α-SiC structure, which corresponds with the structure of the SiC used as a refractory grain. After firing a cold crushing strength of 6.3 $MN.m^{-2}$ was measured. X-ray diffraction analysis of the test piece showed the following constituents:

- α-SiC (hexagonal)
- graphite
- Si
- Si_2ON_2
- Si_3N_4 (small amounts).

Microscopic analysis showed that graphite flakes were surrounded by a layer of SiC (see 1 in figure 4.8). Si_2ON_2 whiskers were visible as cloud-like formations (2), and some Si droplets were present. (N.B.: the firing temperature was above the melting point of Si, which is 1414°C.)

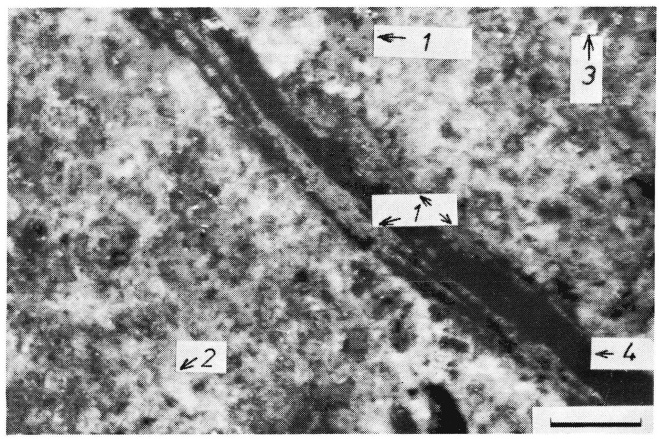

FIGURE 4.8 - The formation of silicon carbide in a test piece made out of a mixture of Si powder and graphite flakes bonded with a little tar. 1 - SiC; 2 - Si_2ON_2; 3 - Si; 4 - graphite flakes. Bar = 150 μm.

A firing temperature above the melting point of silicon will be a disadvantage, as in that case it is possible for the Si to migrate to the bottom of the test piece (or brick). For this reason it is of interest to know whether the reaction rate is high enough at lower temperatures. From the different values found for the reaction enthalpies for the SiC reaction it is seen, that the reaction is slightly exothermic. According to data from Barin and Knacke [4-27] the values are for the temperature range of interest:

$$\Delta H^{\circ}_{1500K} = -4.5 \text{ kcal.mol}^{-1}$$
$$\Delta H^{\circ}_{1700K} = -2.0 \text{ kcal.mol}^{-1}.$$

When a stoichiometric mixture of silicon and carbon is heated in an inert atmosphere (argon for instance), the exothermic behaviour of the mixture can be measured in a Differential Thermal Analysis (DTA) apparatus. In our laboratory we carried out this experiment with a Dupont 990 Thermoanalyser with a 1600°C DTA-cell. In the DTA-cell 5 mg of the silicon-carbon mixture (a tar residu was used to obtain a very reactive carbon with a large surface area; see also next chapter) was introduced; in the reference crucible 5 mg of inert Al_2O_3 powder was introduced. The DTA-cell was heated up with a heating rate of 0.33 $K.s^{-1}$. During the heating the temperature difference between the two thermocouples under the crucibles was recorded. A slight difference was observed due to initial sintering of the Si powder. The sintering causes a slight modification of the thermal conductivity of the test material. At about 1250°C a break in the ΔT-curve is observed as can be seen in figure 4.9.
The experiment in the DTA-cell shows, that the SiC reaction has a marked reaction rate above 1250°C. The DTA-curve shows also, that the reaction rate is rather slow. If the reaction rate would have been high a sharp peak would have been visible on the ΔT-curve.

4.6 - Summary

In this chapter a short description has been given of the production of silicon carbide grains as well as of the production methods used for producing silicon carbide refractory bricks. In the last section it is indicated, that formation of a SiC bond is, in principle, possible.

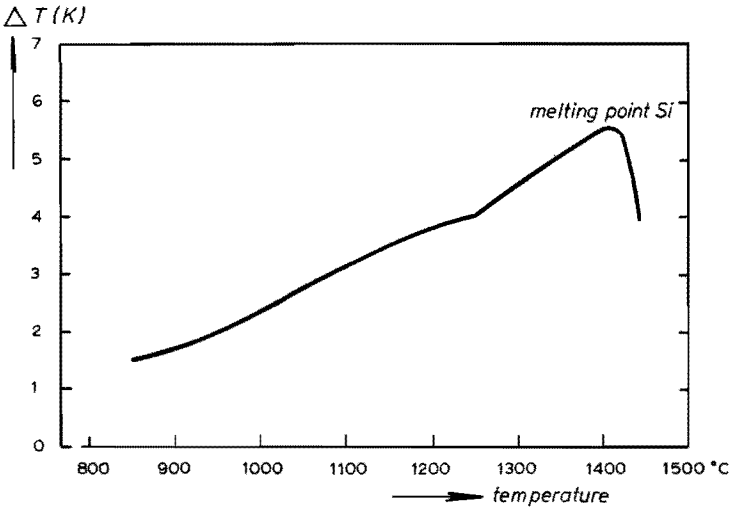

FIGURE 4.9 - The result of the experiment carried out in the DTA-cell with a stoichiometric mixture of Si and C. The heating rate was 0.33 K.s^{-1}, the mass of the mixture was 5 mg. The experiment was carried out in an argon atmosphere.

In the next chapters this possibility will be studied in more detail. In chapter 5 the reactions possible under different circumstances will be studied for the temperature range of a normal factory furnace for firing refractories. In chapter 6 the results of experiments concerning the reaction mechanisms are discussed. In the last chapter results of experiments in practice with the production of self-bonded bricks and their behaviour in the blast furnace are discussed.

The study discussed in this chapter shows, that for the further investigation the following points are of importance:

- The bond should consist out of almost pure SiC, and formation of nitride and oxynitride should be suppressed as far as possible.
- The initial experiments (DTA and firing of the C and Si mixture) show, that the best firing temperature is somewhere between 1250^{o} and 1400^{o}C.

L i t e r a t u r e

4- 1)	*Berzelius, J.J.*	*Ann.Phys.Lpz. 1 (1824) 169*
4- 2)	*Schuetzenberger, P.*	*C.r.hebd.Séanc.Acad.Sci.Paris 92 (1881) 1508*
4- 3)	*Moissan, H.*	*C.r.hebd.Séanc.Acad.Sci.Paris 140 (1905) 405*
4- 4)	*Cowless, A.H.; Cowless, E.H.*	*US Patent 319945 (1885)*
4- 5)	*Acheson, A.G.*	*GB Patent 17911 (1892)*
4- 6)	*Ruff, O.*	*Trans.Electrochem.Soc. 68 (1935) 87-110*
4- 7)	*Thibault, N.W.*	*Am.Miner. 29 (1944) 250-278*
4- 8)	*Thibault, N.W.*	*Am.Miner. 29 (1944) 328-362*
4- 9)	*Harris, R.C.A.*	*J.Am.Ceram.Soc. 58 (1975) 7-8*
4-10)	*ASTM*	*X-ray diffraction card No 1-1119*
4-11)	*Appendix II*	*Silicon carbide 1973. Proc. 3rd Int.Conf. Miami Beach. Sept. 1973. ed. Marshall e.a. Columbia Univ. of South Carolina Press. 1974*
4-12)	*Gugel, E.*	*Keramische Sonderwerkstoffe in der Industrie. Essen. Hrsg. K. Giesen 206 (1969) 29-38*
4-13)	*Bilaine, J.*	*Circul.Infs.Techn.Cent.Docum. Sidérurg. 25 (1968) No 9, 1965-1971*
4-14)	*George, W.*	*Proc.Brit.Ceram.Soc. 40 (1973) 147-167*
4-15)	*Nowotny, H.; Parthe, E.; Kieffer, R.; Benesovsky, F.*	*Monatsch.Chem. 85 (1954) 255*

[4-16] *Van Haeften, A.W.* — *Topological Considerations on some properties of refractory products. Delft, Waltman, 1960.*

[4-17] *Fuller, W.B.; Thompson, S.E.* — *Proc.Am.Soc.Civ.Engrs. 33 (1907) 22*

[4-18] *Litzow, K.* — *Glastechn.Ber. 8 (1930) 149-153*

[4-19] *Andreasen, A.H.M.* — *Kolloid.Z. 50 (1930) 217*

[4-20] *Gugel, E.; Ettmayer, P.; Schmidt, A.* — *Ber.D.K.G. 45 (1968) 395-402*

[4-21] *Voronin, I.I.; Krasotkina, I.I.; Stavorko, A.P.; Milsenko, R.C.* — *Ogneupory (1961) 157 (Engs.Trans. Refractories)*

[4-22] *Popper, P.; Ruddlesden, S.N.* — *Trans.Brit.Ceram.Soc. 60 (1961) 603*

[4-23] *Taylor, K.M.* — *NL Patent 150089*

[4-24] *Karay, E.; Ivanova, M.Ya.; Fraifeyd, M.S.; Guzman, I.Ya.* — *Ogneupory (1975) 6-9 (Engs.Trans. Refractories)*

[4-25] *Gugel, E.; Schuster, P.; Senftleben, G.* — *Stahl und Eisen 92 (1972) 3-8*

[4-26] *Elliot, J.F.; Gleiser, M.* — *Thermochemistry for steelmaking Vol. II. London, Addison-Wesley, 1963*

[4-27] *Barin, J.; Knacke, O.* — *Thermochemical properties of inorganic substances. Berlin, Springer, 1973*

[4-28] *Schuster, P.* — *Privat communication, 1972. "Former leader of refractory research of the Cremergruppe"*

5.1 - Introduction

In this chapter a theoretical study of the reaction mechanisms will be described. The chosen conditions are related with the expected circumstances occuring in industrial furnaces. The formation of different reaction products in various atmospheres will be discussed.

For the theoretical considerations we will study the behaviour of a number of elements in a nearly closed chamber, e.g. a pore in a refractory brick. The wall of such a chamber is prepared from an inert material; in our case it might be SiC. In the chamber Si and C are found in nearly stoichiometric proportions. The Si and C are either mixed or located in separate heaps (see figure 5.1 a and b, respectively).

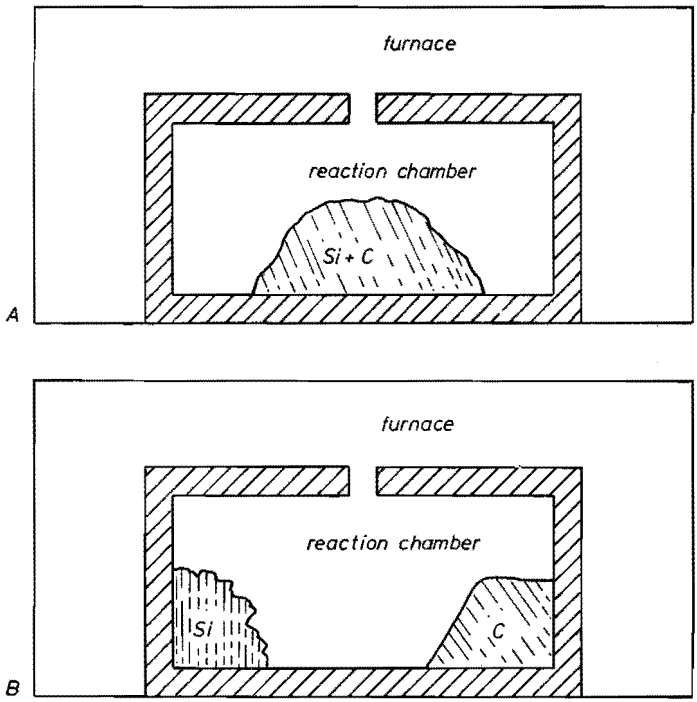

FIGURE 5.1 - The reaction chamber in which the reactions for the theoretical study take place.

In practice only the mixture will be used. For better understanding of the reaction mechanism, however, it is of use to consider the behaviour of separate heaps as well. The chamber is in contact with the outer furnace atmosphere by means of a small channel.
In the next sections the reactions proceeding in different atmospheres will be studied. The atmospheres considered are:

- inert (argon);
- argon with addition of oxygen;
- pure nitrogen;
- mixture of nitrogen and oxygen.

In all cases the total pressure of the gas mixture in the reaction chamber is 1 atm.

5.2 - Reactions Proceeding in an Inert Atmosphere

It is assumed that the atmosphere in the chamber of figure 5.1 at room temperature consists of pure argon with a pressure of 1 atm. The chamber is heated up to a temperature in the range found with the DTA experiment described in chapter 4. The two possibilities drawn in figure 5.1 a and b will be studied. In figure 5.1a a mixture of Si and C particles is present in the reaction chamber. In this case a direct solid-solid reaction may occur at the contact surfaces of silicon and carbon. In figure 5.1b the Si and C are separated; if in this case any reaction will occur, this must be due to either Si or C vapour. The pressure for carbon is found to be negligible ($p_C = 3.3 \cdot 10^{-19}$ atm and $p_C = 2.2 \cdot 10^{-14}$ atm at 1400 K and at 1700 K, respectively [5-1]), which data are in good agreement with data given by [5-2]). Therefore only the pressure of Si is of importance. In figure 5.2 the equilibrium vapour pressure of Si is given as a function of temperature according to data from Hultgren et al [5-1].
The given vapour pressures of Si in the temperature range of interest show, that a reasonable number of Si atoms (somewhere between 3.10^{11} and 4.10^{12} atoms.cm^{-3}) is available in the atmosphere of the reaction chamber.

The possible reactions will be studied now by calculating the Gibbs free energies of formation for the reactions concerned as a function of temperature. If the Gibbs free energy of formation for the

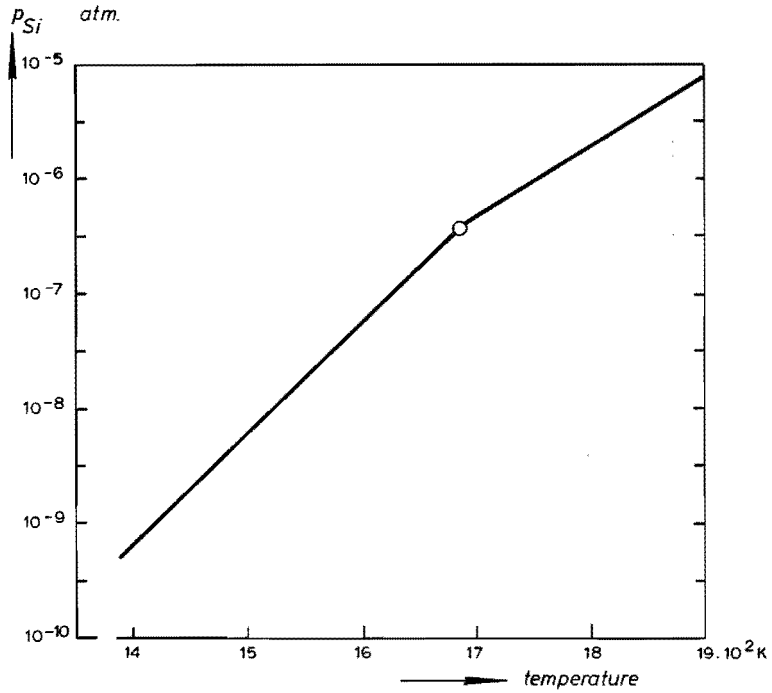

FIGURE 5.2 - The equilibrium vapour pressure of Si as function of temperature according to Hultgren et al [5-1].

SiC reaction is negative the reaction may take place. With the data available nothing can be said about the reaction rate under different circumstances.

Firstly the reaction:

$$Si_s + C_s = SiC_s \qquad [5.1]$$

will be considered. At a pressure of 1 atm the Gibbs free energy of formation ($\Delta G^{\circ}(T)$) can be written as:

$$\Delta G^{\circ}(T)_{SiC,s} = \mu^{\circ}(SiC,s) - \mu^{\circ}(Si,s) - \mu^{\circ}(C,s) \qquad (5.1)$$

where: μ° - standard free energy.

In table 5.1 the Gibbs free energy of formation is given in kcal.mol^{-1}. The values for μ° have been taken from [5-3]. Due to the fact, that all the values found for the temperature range concerned are negative, it

will be clear, that the reaction in principle is possible for the solids Si and C. $\Delta G^{o}(T)_{SiC,s}$ will have the same value in the second case, when the reaction does not take place through the solid-solid reaction, but through the solid(C)-gas(Si) reaction. The Gibbs free energy of formation in that case can be calculated with the following relation:

$$\Delta G^{o}(T)_{SiC,s} = \mu^{o}(SiC,s) - \mu^{o}(C,s) - \mu^{o}(Si,g) - R.T.\ln(p_{Si}) \qquad (5.2)$$

This relation is valid when it is assumed, that the solid phases of carbon and silicon carbide are pure (see also [5-4], [5-5]). The data given in table 5.1 are calculated with relation (5.1) and verified with the data for Si gas at 1 atm pressure given in [5-3] and the pressure values given in [5-1] with relation (5.2). Only small differences were observed.

TABLE 5.1 - The Gibbs free energy of formation $\Delta G^{o}(T)_{SiC,s}$

temperature K	$\Delta G^{o}(T)_{SiC,s}$ kcal.mol^{-1}
1000	- 15.60
1200	- 15.24
1400	- 14.88
1600	- 14.52
1800	- 13.34
2000	- 11.56

With these thermodynamic data it is still impossible to say something of the reaction rate. The reaction rate will be different for the solid-solid reaction and for the solid-gas reaction. The first reaction will be influenced by the diffusion rate of the Si and C atoms and the number of contact surfaces present in the mixture. The reaction rate of the solid-gas reaction will be limited by the silicon partial pressure and by the reactive surface areas of silicon and carbon.

The study given above shows, that the SiC formed will grow either on the interfaces between the silicon and carbon particles - for the solid-solid reaction - or on the carbon particles - for the solid-gas reaction -, since the partial pressure of Si is much larger than that of carbon. This conclusion indicates that in both chambers of figure 5.1 a reaction will take place. For both cases it is of importance, that for a good growth a very large Si and carbon surface is available.

The large surface area of Si can be formed by using very fine Si powder. For carbon fine carbon powder, or residual carbon of a coking process of tar and pitch can be used. As Hüttinger [5-6]) showed, coke-oven tar and pitch give very fine carbon particles after calcination. The particle diameter is only a few μm. Moreover for the solid-solid reaction a very close contact between carbon and silicon is of importance. In practice this can be achieved by a good mixing and pressing procedure.

5.3 - Reactions Proceeding in an Atmosphere with Oxygen

We assume, that the mixture of Si and C in the reaction chamber of figure 5.1 has an excess of carbon. The atmosphere consists of argon with a small amount of oxygen. At the temperature used this oxygen will react instantaneously with the carbon present and form CO according to:

$$C + \tfrac{1}{2} O_2 = CO \qquad [5.2]$$

This causes a partial pressure of CO in the chamber. Depending on the partial pressure of CO different reactions may take place. They are:

$$2\ Si + CO = SiO + SiC \qquad [5.3]$$

and

$$Si + 2\ CO = SiO_2 + 2\ C \qquad [5.4]$$

or

$$CO + SiO = SiO_2 + C \qquad [5.5]$$

Since we wish to form SiC and not SiO_2 the reactions [5.4] and [5.5] are undesirable. Therefore it is of importance to calculate the maximum partial pressures of CO and SiO which are allowed so that no SiO_2 will be formed.

In principle we are looking for the conditions which correspond to the simultaneous existence of the equilibria:

$$Si_s + \tfrac{1}{2} O_{2,g} = SiO_g \qquad [5.6]$$

$$Si_s + O_{2,g} = SiO_{2,s} \qquad [5.7]$$

$$C_s + \tfrac{1}{2} O_{2,g} = CO_g \qquad [5.2]$$

In that case the Gibbs free energy of formation is zero for these three reactions. Three equations can be formulated with the three partial pressures (p_{O_2}, p_{CO}, and p_{SiO}) being the unknowns. The pressures can be found by elimination. The enthalpies for the reactions can be written,

for [5.6] as:

$$\mu^{o}(Si,s) + \tfrac{1}{2}\,\mu^{o}(O_2,g) + \tfrac{1}{2}\,R.T.\ln(p_{O_2}) - \mu^{o}(SiO,g) - R.T.\ln(p_{SiO}) = 0$$

or: (5.3)

$$\Delta G^{o}(SiO) = R.T.\ln \frac{\left(p_{O_2}\right)^{\frac{1}{2}}}{(p_{SiO})} \qquad (5.4)$$

where: $\Delta G^{o}(SiO) = \mu^{o}(SiO,g) - \mu^{o}(Si,s) - \tfrac{1}{2}\,\mu^{o}(O_2,g)$.

For [5.7] as:

$$\mu^{o}(Si,s) + \mu^{o}(O_2,g) + R.T.\ln(p_{O_2}) - \mu^{o}(SiO_2,s) = 0 \qquad (5.5)$$

or:

$$\Delta G^{o}(SiO_2) = R.T.\ln(p_{O_2}) \qquad (5.6)$$

where: $\Delta G^{o}(SiO_2) = \mu^{o}(SiO_2,s) - \mu^{o}(Si,s) - \mu^{o}(O_2,g)$.

For [5.2] as:

$$\mu^{o}(C,s) + \tfrac{1}{2}\,\mu^{o}(O_2,g) + \tfrac{1}{2}\,R.T.\ln(p_{O_2}) - \mu^{o}(CO,g) - R.T.\ln(p_{CO}) = 0 \qquad (5.7)$$

or

$$\Delta G^{o}(C) = R.T.\ln \frac{\left(p_{O_2}\right)^{\frac{1}{2}}}{(p_{CO})} \qquad (5.8)$$

where: $\Delta G^{o}(CO) = \mu^{o}(CO,g) - \mu^{o}(C,s) - \tfrac{1}{2}\,\mu^{o}(O_2,g)$.

The relations (5.4), (5.6) and (5.8) are the three equations from which the pressures can be calculated.
Eliminating p_{O_2} from the relations (5.4) and (5.8) with (5.6) results in the following relations for the equilibrium partial pressures of CO and SiO:

$$p_{CO} = \exp\left\{\frac{\Delta G^{o}(SiO_2) - 2\,\Delta G^{o}(CO)}{2\ R.T}\right\} \qquad (5.9)$$

and

$$p_{SiO} = \exp\left\{\frac{\Delta G^{o}(SiO_2) - 2\,\Delta G^{o}(SiO)}{2\ R.T}\right\} \qquad (5.10)$$

These relations are valid under the assumption, that the solids occuring in the reactions are pure. The $\Delta G^{o}(SiO_2)$, $\Delta G^{o}(SiO)$ and $\Delta G^{o}(CO)$ can be derived from tables from literature. For the calculations data from Barin and Knacke [5-3]) and Elliot and Gleiser [5-7]) are used. The pressures found in both cases were in good agreement. In table 5.2 the pressures found are given as a function of temperature.

TABLE 5.2 - Maximum partial pressures of CO and SiO at which no SiO_2 will be formed

temperature K	p_{CO} atm		p_{SiO} atm	
	ref. [5-3]	ref. [5-7]	ref. [5-3]	ref. [5-7]
1400	$2.5 \cdot 10^{-4}$	$3.0 \cdot 10^{-4}$	$6.8 \cdot 10^{-5}$	$3.3 \cdot 10^{-5}$
1600	$9.1 \cdot 10^{-3}$	$1.0 \cdot 10^{-2}$	$2.6 \cdot 10^{-3}$	$1.4 \cdot 10^{-3}$
1800	$1.8 \cdot 10^{-1}$	$1.8 \cdot 10^{-1}$	$3.2 \cdot 10^{-2}$	$2.3 \cdot 10^{-2}$
2000	2.0	2.0	$3.3 \cdot 10^{-1}$	$3.0 \cdot 10^{-1}$

In figure 5.3 the pressure of CO and SiO are given as a function of temperature for the data calculated with [5-3]. The shaded area gives the pressure range in which SiO_2 can be formed.
The partial pressures of CO for the calculated points are indicated in the drawing. From the data it can be seen, that for our temperature range CO partial pressures of $2.5 \cdot 10^{-4}$ atm at 1200°C up to $5 \cdot 10^{-2}$ atm at 1350°C are allowed without formation of SiO_2. From this it is clear that for normal air entering the reaction chamber, SiO_2 will be formed, since in that case a p_{CO} of about 0.3 atm will occur.
When in the reaction chamber a partial pressure of CO is kept lower than indicated above, no SiO_2 will be formed. Reaction [5.3], however, will be possible. The reaction introduces SiO gas in the chamber, which gives a fourth possibility for SiC formation according to:

$$SiO_g + 2\ C_s = SiC_s + CO_g \qquad [5.8]$$

In [5.3] as well as in [5.8] oxygen acts like a catalyst.

Summarizing, for the formation of silicon carbide four reaction mechanisms are proposed due to the thermodynamic considerations given:

1) The direct silicon-carbon (solid-solid) reaction, when silicon and carbon are mixed and pressed together.
2) Silicon carbide will be formed on the carbon surfaces due to the reaction between carbon and the Si gas.
3) Silicon carbide will be formed in an atmosphere with a low partial pressure of CO (< 10^{-4} atm) by a reaction via SiO.
4) Silicon carbide can be formed out of the gas-gas reaction between SiO and CO.

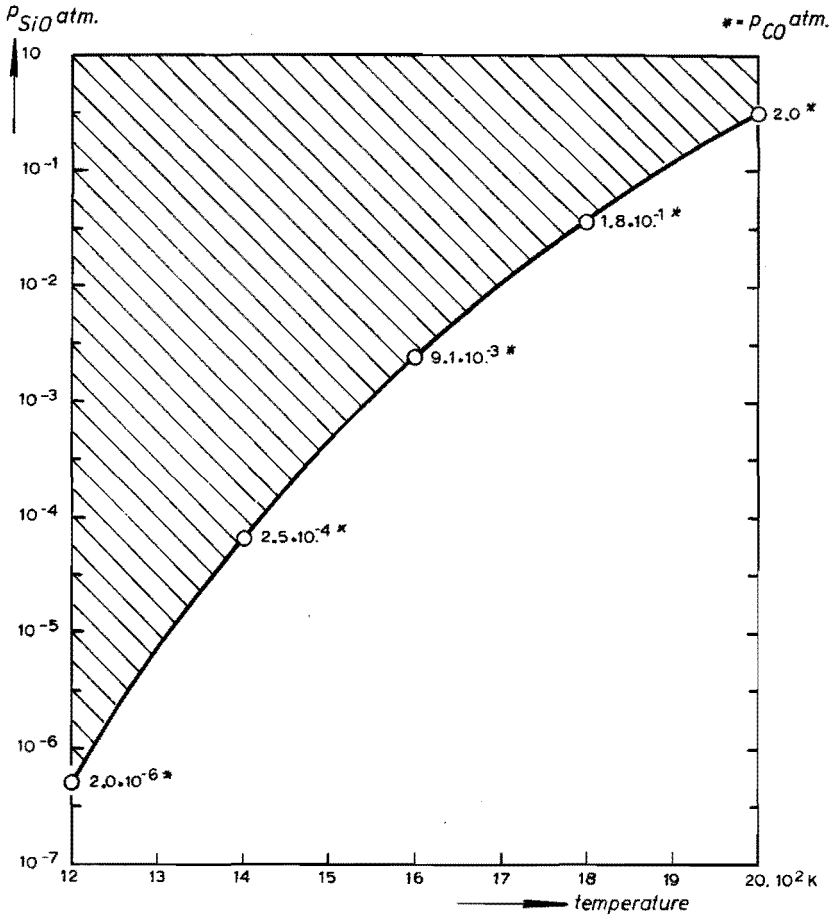

FIGURE 5.3 - The minimum SiO or CO partial pressure at which SiO_2 can be formed. The shaded area indicates the SiO or CO pressure range in which SiO_2 formation is possible.

Part of the experimental work was done to find out which of the four given mechanisms is the most important one. In chapter 6 the experiments and the results will be treated.

5.4 - Reactions Proceeding in an Atmosphere with Nitrogen

The atmosphere in the reaction chamber of figure 5.1 consists in this case of a mixture of nitrogen and an inert gas. Again the chamber is heated up to the temperatures mentioned. In that case it will be possible to form silicon nitride according to:

$$3\ Si_s + 2\ N_{2,g} = Si_3N_{4,s} \qquad [5.9]$$

As was done in the previous section for the SiO_2 formation, it is also possible in this case to calculate a minimum partial pressure of N_2 at which reaction [5.9] will take place. This can be calculated according to relation:

$$\Delta G(T)_{Si_3N_4,s} = \mu^o(Si_3N_4,s) - 3\ \mu^o(Si,s) - 2\ \mu^o(N_2,g) - 2\ R.T.\ln(p_{N_2}) \qquad (5.11)$$

It is assumed again that the solids Si and Si_3N_4 are pure, otherwise the used equations are not valid. For equilibrium, equation (5.11) will be zero. When for the enthalpies is written:
$\Delta G^o(Si_3N_4) = \mu^o(Si_3N_4,s) - 3\ \mu^o(Si,s) - 2\ \mu^o(N_2,g)$ the minimum partial pressure at which silicon nitride will be formed, is calculated as:

$$p_{N_2} = \exp\left\{\frac{\Delta G^o(Si_3N_4)}{2\ R.T}\right\} \qquad (5.12)$$

Table 5.3 gives the calculated values of $\Delta G^o(Si_3N_4)$ according to data of Barin and Knacke [5-3]. The calculations of the partial pressure of N_2 were verified with data from Elliot and Gleiser [5-7] and again good agreement was found. Figure 5.4 shows the minimum partial pressure of N_2 at which Si_3N_4 formation can occur as a function of temperature.

TABLE 5.3 - The Gibbs free energy of formation for silicon nitride

temperature K	$\Delta G^o(Si_3N_4)$ kcal.mol^{-1}
1000	- 98.7
1200	- 86.0
1400	- 67.4
1600	- 52.0
1800	- 34.1
2000	- 14.6

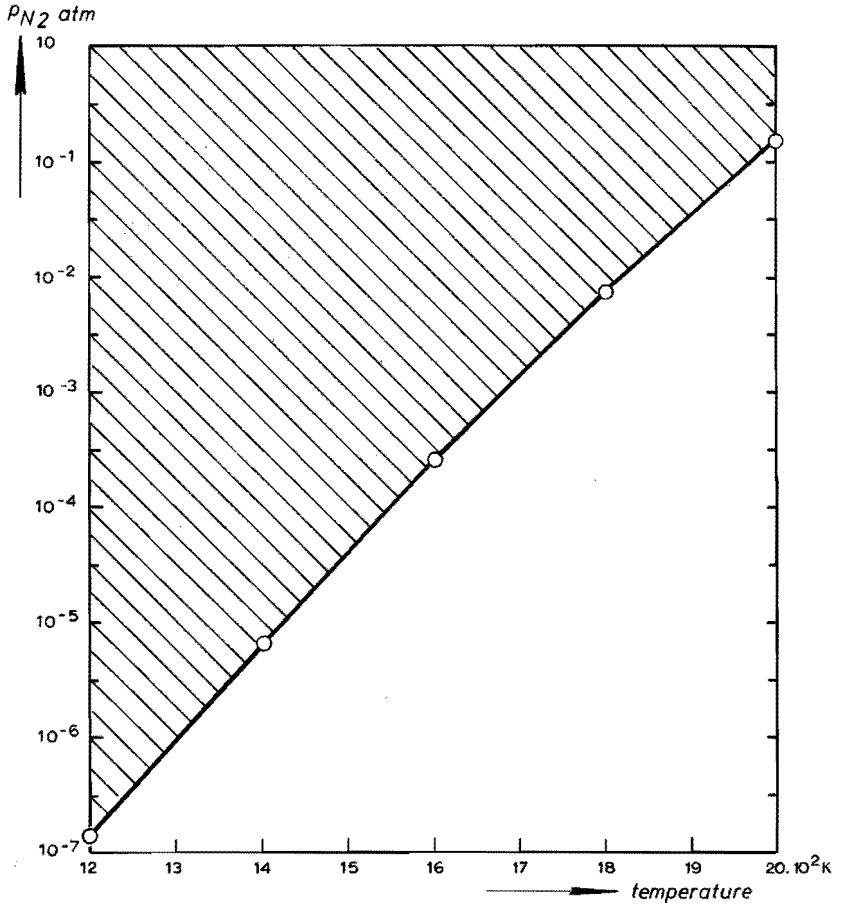

FIGURE 5.4 - The minimum N_2 partial pressure at which Si_3N_4 formation can occur. The shaded area indicates the N_2 pressure range in which Si_3N_4 formation is possible.

For the temperature range of interest the minimum N_2 pressure at which silicon nitride can be formed lies between 10^{-5} and 10^{-3} atm. For our experiments with a direct SiC bond in a silicon carbide brick the N_2 pressure in the reaction furnace should be below the pressures indicated. If not, Si_3N_4 formation may take place and can possibly hinder the formation of SiC.

Gugel et al [5-8]) stated that silicon carbide is unaffected by nitrogen.

From the thermodynamic data it is possible to calculate if in principle a reaction between SiC and N_2 is possible. The reaction should be:

$$3\ SiC + 2\ N_2 = Si_3N_4 + 3\ C \qquad [5.10]$$

In table 5.4 the change in Gibbs free energy for this reaction is calculated for an atmosphere of pure nitrogen with a pressure of 1 atm. The calculations are carried out according to:

$$\Delta G^{\circ}(T)'_{Si_3N_4} = \mu^{\circ}(Si_3N_4,s) + 3\ \mu^{\circ}(C,s) - 3\ \mu^{\circ}(SiC,s) - 2\ \mu^{\circ}(N_2,g) - 2\ R.T\ \ln(p_{N_2}) \qquad (5.13)$$

The calculated values are derived from tables of Barin and Knacke [5-3].

TABLE 5.4 - The change in Gibbs free energy for Si_3N_4 and the minimum P_{N_2}

temperature K	$\Delta G^{\circ}(Si_3N_4)'$ kcal.mol^{-1}	p_{N_2} atm
1000	- 51.9	$2.1 \cdot 10^{-6}$
1200	- 37.1	$4.1 \cdot 10^{-4}$
1400	- 22.7	$1.7 \cdot 10^{-2}$
1600	- 8.5	$2.6 \cdot 10^{-1}$
1800	+ 6.1	2.3
2000	+ 19.9	$1.2 \cdot 10^{1}$

Also for this reaction the minimum partial pressure of N_2 can be calculated for which it is possible, that SiC is transformed into Si_3N_4. The calculation can be made with the following relation:

$$p_{N_2} = \exp\left\{\frac{\Delta G^{\circ}(Si_3N_4)'}{2\ R.T}\right\} \qquad (5.14)$$

The minimum partial pressures of N_2 at which the reaction will take place are given in table 5.4. The data given show that the reaction is only possible for rather high partial pressures of N_2. In our case we aimed at avoiding high partial pressures of N_2, as was stated before. Therefore, it is very unlikely that reaction [5.10] will take place. The thermodynamical calculations made in this section show on the other side, that up to rather low nitrogen partial pressures Si_3N_4 formation is possible directly out of silicon. Crystals will grow from the silicon surface and will hinder the silicon carbide formation in a mixture of silicon and carbon. The minimum partial pressure for nitrogen

to cause formation of Si_3N_4 in the considered temperature range is much lower, than the partial pressure of nitrogen in air (about 0.6 atm). By introducing air in the reaction chamber of figure 5.1 silicon carbide, silicon nitride, silicon monoxyde and silica may be formed simultaneously. In section 5.5 we will study this possibility in more detail.

5.5 - Reactions Proceeding in an Atmosphere with Oxygen and Nitrogen

Through the hole in the roof of the reaction chamber shown in figure 5.1 a mixture of O_2 and N_2 enters the reaction chamber. At temperature oxygen will react instantaneously with the carbon present to form CO. According to Guzmann [5-9] the following reaction may take place:

$$3\ Si_s + CO_g + N_{2,g} = SiC_s + Si_2ON_{2,s} \qquad [5.11]$$

For further thermodynamic investigation this reaction can be simplified by writing the 3 partial reactions which form [5.11]. They are:

$$C_s + \tfrac{1}{2}\ O_{2,g} = CO_g \qquad [5.2]$$

$$Si_s + C_s = SiC_s \qquad [5.1]$$

$$2\ Si_s + \tfrac{1}{2}\ O_{2,g} + N_{2,g} = Si_2ON_{2,s} \qquad [5.12]$$

In literature other reactions than [5.12] are suggested as well. Colquhoun et al [5-10] suggest the existence of a slightly oxydized version of silicon nitride. In this study we will only discuss stoichiometric reaction products, therefore only reaction [5.12] will be considered.

Different investigators have tried to find the change in Gibbs free energy for the reaction [5.12]. Values with rather big differences have been found [5-11]; [5-12]. The newest data found are given by Colquhoun et al [5-10]. Their data for $\Delta G^o(T)_{Si_2ON_2}$ are given in table 5.5.

Along the same lines as given before, Colquhoun et al have calculated the minimum p_{O_2} and p_{N_2} for the reaction at different temperatures. They show that Si_2ON_2 may be formed already at very low pressures, for instance $p_{O_2} \approx 10^{-23}$ atm and $p_{N_2} \approx 10^{-4}$ atm. Other investigators, for instance Mitomo [5-13], state that at low partial pressures of O_2 and N_2 only little nitridation and oxidation of silicon is observed in

TABLE 5.5 - The change in Gibbs free energy for the formation of Si_2ON_2

temperature K	$\Delta G^{\circ}(T)_{Si_2ON_2}$ kcal.mol^{-1}
1473	- 225.6
1523	- 212.0
1573	- 199.8
1623	- 190.2

the temperature range concerned. According to Mitomo only some nitrogen or oxygen is dissolved into the α or β phase of the silicon.

For the present study it is of importance that Si_2ON_2 may be formed when silicon is brought into contact with a gas mixture containing N_2 and CO or O_2, which is the case when air is brought into the chamber.

5.6 - The influence of a SiO_2 Layer on the Si Particles

In literature often the presence of a thin layer of SiO_2 on the surface of silicon grains is indicated. Layer thicknesses of 1-3 μm have been observed ([5-14]), [5-15]), [5-16]), [5-17])). The presence of such a layer is of importance for the work presented here, since it will influence the reactions described in the previous sections. Atkinson and Moulson [5-17]) observed no nitridation of silicon after firing the silicon particles for 2 h in air at 1000°C.

For our work we have to know, whether the SiO_2 layer will react with the elements present in our reaction chamber in the used temperature range or not. Different reactions will be possible. The two principal reactions are:

$$SiO_2 + 3\ C = SiC + 2\ CO \qquad [5.13]$$

and

$$2\ SiO_2 + N_2 = Si_2ON_2 + O_2 \qquad [5.14]$$

Under standard conditions the change in Gibbs free energy for reaction [5.13] is positive up to 1800 K, therefore up to that temperature no reaction will take place. At 1800 K the $\Delta G^{\circ}(T)$ for this reaction is only - 1.0 kcal.mol^{-1}, which is a very low value; thus it is unlikely

that the reaction will occur. In practice also reaction [5.14] is very unlikely to occur, since the N_2 partial pressure will be lower than 1 atm. In that case the $\Delta G^{\circ}(T)$ value will become even less negative. This means, that a SiO_2 layer on the surfaces of the silicon particles will not be removed and therefore will hinder the reactions described in the previous sections.

5.7 - Conclusions

The thermodynamic studies carried out in this chapter show that:

- silicon carbide may be formed in an inert atmosphere in the temperature range (1250-1410°C), either by direct reaction between solid silicon and solid carbon, or by reaction of silicon gas and solid carbon.
- When a small amount of oxygen ($p < 10^{-4}$ atm) is added to the inert atmosphere additional reactions can take place. Due to the presence of carbon the oxygen will react to CO. This may react with Si under formation of SiO. The SiO may react with carbon under formation of SiC releasing O_2.
- Addition of nitrogen to the reaction chamber atmosphere can introduce other reactions as well. Even at rather low partial pressures of N_2 (10^{-4} up to 10^{-2} atm) Si_3N_4 formation must be expected. The Si_3N_4 crystals will grow on the Si particle surfaces and will hinder the SiC formation. At temperatures concerned it is impossible that Si_3N_4 and carbon will react and form SiC.
- Addition of nitrogen and oxygen to the chamber atmosphere gives the possibility for formation of Si_2ON_2. The thermodynamic data for this reaction given by different investigators show rather big discrepancies.

From the summing up given here it can be seen, that quite a variety of reactions may take place in different atmospheres. Good control of the atmosphere in the reaction chamber is indispensable to make sure, that only the SiC reaction will take place.

From the thermodynamical data it is not possible to predict a reaction rate. In order to achieve the best possible reaction rate, care has to be taken, that the silicon particle surfaces are free of SiO_2,

the surface area of the silicon and the carbon is as large as possible (very fine particles) and that an excess of carbon is present. The excess carbon is necessary to make sure that O_2 impurities originating from either leakage or dissociation of SiO_2 will find C to react with under formation of CO.

L i t e r a t u r e

5- 1)	*Hultgren, R.; Desay, P.D.; Hawkins, D.T.; Gleiser, M.; Kelley, K.K.; Wagman, D.D.*	*Selected values of the thermodynamic properties of the elements. Metals Park, Am.Soc. for Metals, 1973*
5- 2)	*Drowart, J.; Burns, R.D.; De Maria, G.; Inghram, M.G.*	*J.Chem.Phys. 31 (1959) 1131*
5- 3)	*Barin, J.; Knacke, O.*	*Thermochemical properties of inorganic substances. Berlin, Springer Verlag, 1973*
5- 4)	*Hennicke, W.*	*Thermodynamisches Rechnen in die Keramik. Handbuch der Keramik. Freiburg, Verlag Schmid, 1973*
5- 5)	*Duffey, G.H.*	*Physical Chemistry. New York. McGraw-Hill, 1962*
5- 6)	*Hüttinger, K.J.*	*Chem.Ing.Tech. 43 (1971) 1145-1188*
5- 7)	*Elliot, J.F.; Gleiser, M.*	*Thermochemistry for Steelmaking Vol. II. London, Addison-Wesley, 1963*
5- 8)	*Gugel, E.; Ettmayer, P.; Schmidt, A.*	*Ber.Dt.Keram.Ges. 45 (1968) 395-402*
5- 9)	*Guzmann, I.Ya.*	*Ogneupory (1970) 41-46*
5-10)	*Colquhoun, I.; Wild, S.; Grieveson, P.; Jack, K.H.*	*Proc.Brit.Ceram.Soc. 10 (1973) 207-227*

[5-11] *Wild, S.; Grieveson, P.; Jack, K.H.* — *Special Ceramics No 5 (1972) 385*

[5-12] *Pehlke, R.D.; Elliot, J.F.* — *Trans.Metall.Soc. AIME 215 (1959) 781-785*

[5-13] *Mitomo, M.* — *J.Am.Ceram.Soc. 58 (1975) 527*

[5-14] *Reves, A.G.; Evans, R.J.* — *J.Mat.Sci. 10 (1973) 1242-1243*

[5-15] *Locker, L.D.; Capio, C.D.* — *J.Appl.Phys. 44 (1973) 4366*

[5-16] *Phillips, H.R.* — *J.Appl.Phys. 43 (1972) 2835*

[5-17] *Atkinson, A.; Moulson, A.J.* — *Science of Ceramics No 8 (1976) 111-121*

6.1 - Experimental Procedures

To study the reaction mechanisms of the different reactions discussed in chapter 5 a special furnace was built. The furnace is an electrically heated horizontal furnace. The heating elements are silicon carbide rods and the furnace can reach a temperature of 1450°C. The tube in the furnace is a gas tight alumina tube. The ends of the tube protrude from the furnace at a length of 100 mm at each side. The furnace construction is schematically shown in figure 6.1a, the actual experimental set up in figure 6.1b. At the right side a gas inlet and a gas tight thermocouple lead-through is mounted on the tube. At the opposite side the test piece holder is clamped onto the furnace tube. The principle of the clamping system is drawn in figure 6.2.
The gas flows out of the furnace through a labyrinth. The labyrinth is a 135 mm long cylinder with a diameter of 35 mm in which 5 partitions are placed. The gas is led through a pinhole in each partition. The labyrinth prevents back diffusion of gases into the furnace tube.

For measuring the reaction rate of the different possible reactions a test piece was made by ramming a mixture of the material to be tested into an alumina tube. The tube is 40 mm long, with an internal diameter of 6 mm. By ramming the mixture into the tube, a test piece with a length of 27 mm is formed. In the open ends of the tube small graphite rods (4 mm diameter) are placed. This test piece assembly is placed in the test piece holder (see figure 6.2), which consists of two concentric alumina tubes. The outer tube has one closed end. At that side of the holder, a part of the upper surface of the outer tube and the inner tube are removed over a length of 60 mm, as is indicated in figure 6.2. The graphite rods of the assembly are pressed between two vertical carbon disks. The carbon disk at the left of the test piece assembly is pressed against the specimen by means of the inner tube. The pressure on this tube is obtained by means of a spring, which is built into the clamping system (part 8 of fig. 6.2). In this way it is possible to keep the test piece itself as dense as possible during the whole firing procedure.

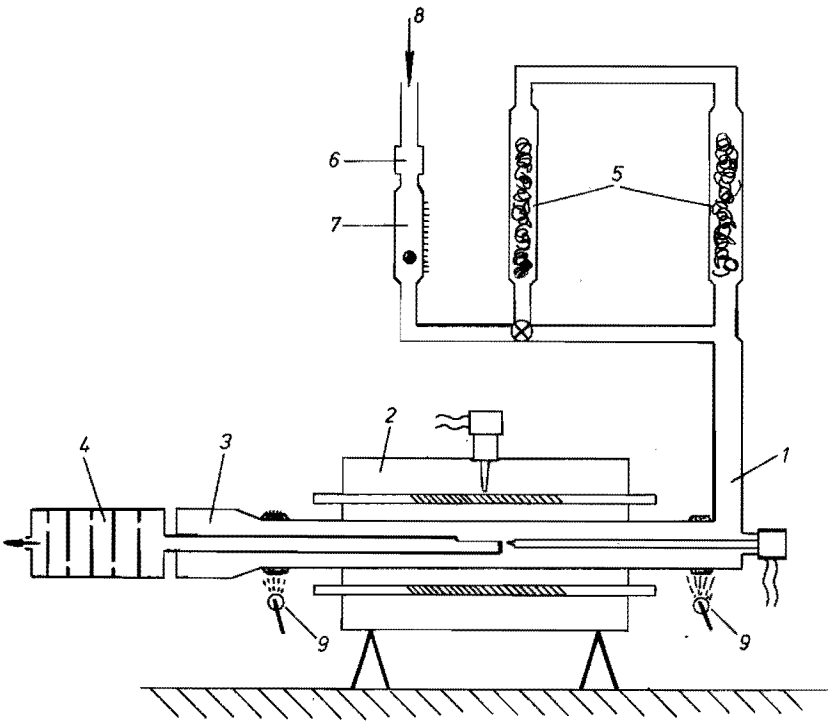

FIGURE 6.1a - A schematic drawing of the experimental set up.

1 - gas inlet with the gas tight thermocouple lead-through
2 - furnace with control thermocouple
3 - test piece holder
4 - gas outlet (labyrinth)
5 - BTS-cell (O_2 and N_2 trap)
6 - constant flow valve
7 - rotameter
8 - gas inlet via gas bottle and reduction valve
9 - air cooling

For studying the reaction mechanisms another type of test piece is used. In this case a plate (10 x 6 x 3 mm) of a silicon single crystal is used together with a plate of carbon (8 x 4 x 3 mm). These are placed on top of each other and brought into a small crucible made out of glassy-carbon. The position of the crucible and the test piece is shown in figure 6.3.

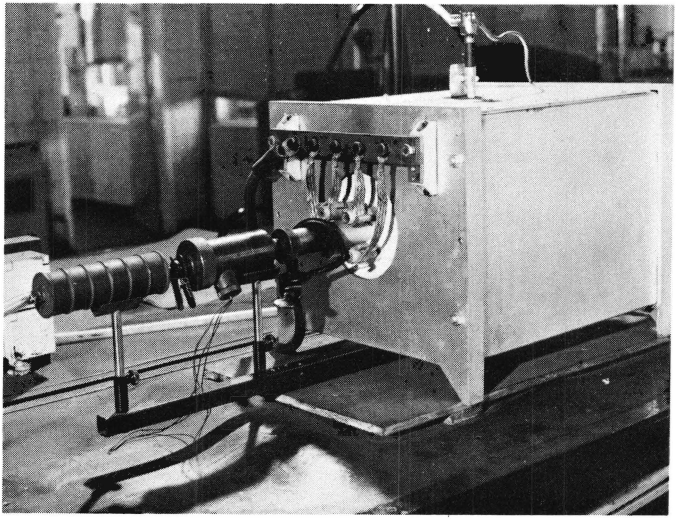

FIGURE 6.1b - The experimental furnace.

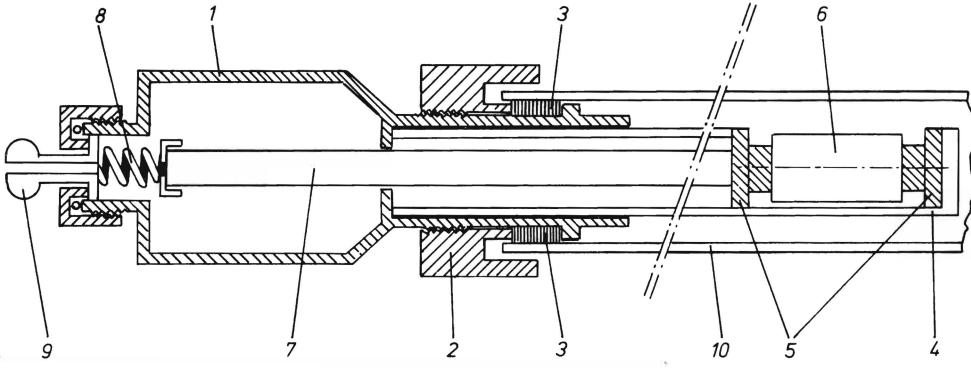

FIGURE 6.2 - The clamping system and the test piece holder in the furnace tube.

1 - test piece holder; 2 - adjusting screw; 3 - clamping and sealing ring (made out of silicon rubber); 4 - outer tube of the sample holder; 5 - carbon disks; 6 - test piece assembly; 7 - inner tube; 8 - adjustable spring pressing the inner tube against the test piece assembly; 9 - gas connection to the labyrinth; 10 - furnace tube.

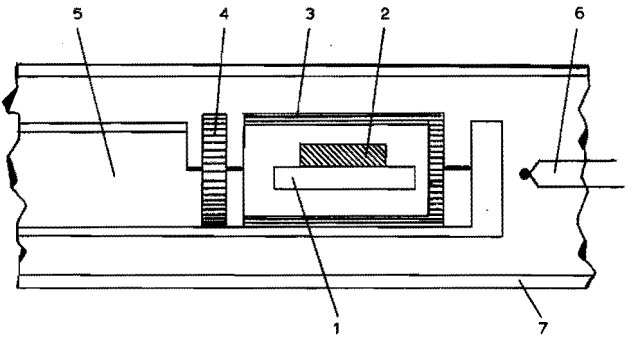

FIGURE 6.3 - The test piece assembly for studying the reaction mechanisms.

1 - silicon single crystal; 2 - carbon plate; 3 - crucible; 4 - lid; 5 - test piece holder; 6 - thermocouple; 7 - furnace tube.

The experimental procedure in the furnace was as follows:

- For measuring the reaction rates of the different reactions considered, a mixture was made. From that mixture different test pieces were made. For one series of tests each test piece was fired at 1300°C for a preset time in a well defined gas atmosphere, the temperature being well within the range indicated by the DTA experiment (see 4.4). It is high enough to expect a reasonable reaction rate and low enough to avoid the melting of the silicon (melting point of Si is 1414°C). The reaction temperature will be higher than the furnace temperature, since the reactions are exothermic.
- For studying the reaction mechanisms the test piece assembly was also fired at 1300°C for a preset time in a well defined gas atmosphere. After firing the test piece was cut in such a way, that the contact surfaces between silicon and carbon could be studied under the microscope. Microscope specimens were also made out of the test piece of the mixtures described above. The test pieces were embedded in araldite and polished. These specimens were studied in a reflection microscope with oil between the specimen and the objective.

Table 6.1 shows the characteristics of the materials used for the experiments. The tests are carried out in three different gas atmospheres given in table 6.2.

TABLE 6.1 - Characteristics of the materials used in the experiments

experiment	material	composition % (m/m)	size
reaction rate	silicon	Si - 97 Fe - 0.4 Mn - 0.8 Al - 1.3 Ca - 0.5	< 100 µm
	carbon (residual C from tar)	C - 99	< 100 µm
	tar	C - 39	
reaction mechanism	silicon	Si - 99.9	single crystal plate 10 x 6 x 3 mm
	carbon	C - 99.5 ash - 0.5	plate of semi-graphite brick, π_s = 22.0 % (V/V) 8 x 4 x 3 mm

TABLE 6.2 - Gas atmospheres used for the experiments

experimental series	composition
I	argon
II	nitrogen
III	argon + 200 ppm of oxygen

The mixture of argon and 200 ppm of oxygen was chosen in accordance with section 5.3. Figure 5.3 shows the maximum amount of CO in the mixture which may be present without formation of SiO_2. To find the maximum possible influence of oxygen on the silicon carbide formation the chosen amount of oxygen was used.

6.2 - The Experiments in an Inert Atmosphere

To obtain an inert atmosphere in the furnace tube (fig. 6.1) pure argon (maximum amount of impurities about 30 ppm $N_2 + O_2$) was used. Via a constant-flow valve a flow of 6 $l.h^{-1}$ passed through the furnace. The small amounts of oxygen and nitrogen in the argon were trapped by a

so called BTS-cell* which was placed at the entrance of the furnace tube (part 5 in fig. 6.1). The cell contains a silica carrier with activated copper oxide. Measurement of oxygen and nitrogen after the furnace tube showed that only 2 ppm O_2 was present in the gas at the experimental temperature of 1300°C. No nitrogen was found and later experiments showed no nitridation of the silicon.

6.2.1 - Experiments on the reaction rate

For the experiments on the reaction rate a mixture of silicon grains and carbon, produced as a residue from coking tar, was mixed with 10 % (m/m) of tar. In this way a mixture was produced with 51.5 % (m/m) of silicon and 48.5 % (m/m) of carbon after coking the tar. The mixture had an excess of 10 % (m/m) of carbon. Eight test pieces were made with this mixture. Each test piece was fired at 1300°C for a preset time. After firing the test piece was analysed by means of X-ray diffraction. By using CaF_2 as an internal standard and preparing standard mixtures with β-SiC formed after the longest firing period (140 h), it was possible to carry out a quantitative analysis of silicon carbide on each test piece. It is allowed to use the 140 h test piece as an absolute standard, because only 10 % (m/m) of free carbon was found and no free silicon or other impurities. X-ray diffraction indicated the presence of β-SiC only. To verify this the true density (ρ) of the test piece was measured. The value found was: $\rho = 2.93\ g.cm^{-3}$. The theoretical density to be expected is:

$$\rho = 0.9 \cdot \rho_{SiC} + 0.1 \cdot \rho_{res.C} = 2.92^5\ g.cm^{-3}$$

The theoretical density of β-SiC is 3.21 $g.cm^{-3}$. The density of residual carbon from coked tar is $\rho_{res.C} = 1.35\ g.cm^{-3}$ according to values given by Hüttinger [6-1]). The calculation shows that the density found is in good agreement with the theoretical value.
In figure 6.4 the silicon carbide content of the test pieces is shown as a function of time. The standard deviation of the measurements is found to be about ± 2 % (m/m).

---

* BTS is the designation of the supplier.

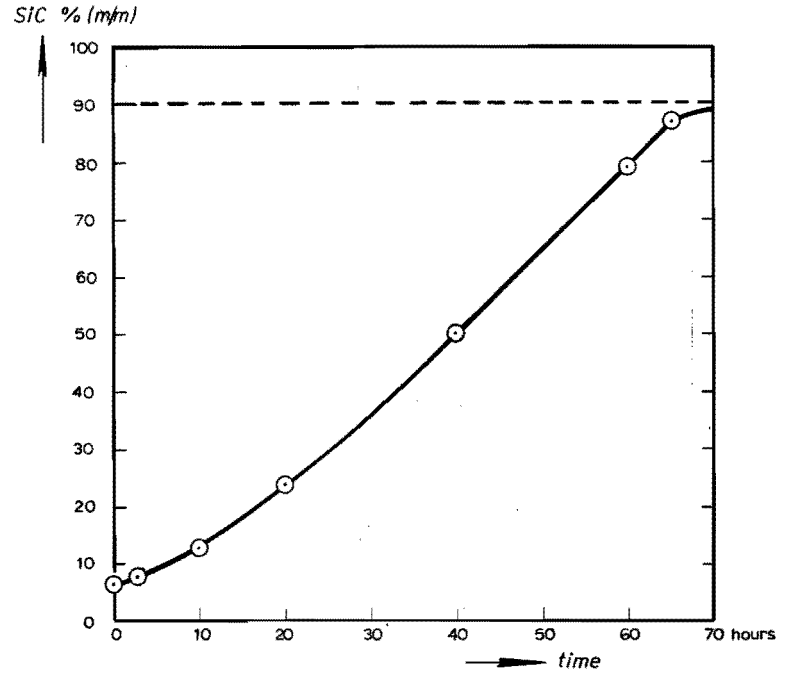

FIGURE 6.4 - The reaction rate of the reaction between silicon and carbon in an inert atmosphere at 1300°C. The value of 90 % (m/m) of silicon carbide was found after 140 h of firing.

Using the first 8 measuring points it is possible to calculate a relation for the best fitting line through these points. Using a third order equation a correlation coefficient of 0.9997 is found with σ_{rest} is 0.85. The relation is:

$$SiC = 6.6 + 0.29 \cdot t + 0.02 \cdot t^2 - 1.6 \cdot 10^{-4} \cdot t^3 \qquad (6.1)$$

Other investigators [6-2], [6-3] have indicated that the reaction rate will be influenced by the presence of metallic impurities. In our case such impurities are present as table 6.2 shows; therefore it is possible that the reaction rate found is slightly higher than one would measure when using pure silicon. The relation found, therefore, is valid only for the experimental circumstances described.

From different test pieces microscopic analyses were made. Figure 6.5 shows a test piece after heating up to 1300°C and cooling down again (firing time 0 h). The white grains (1) are silicon grains.

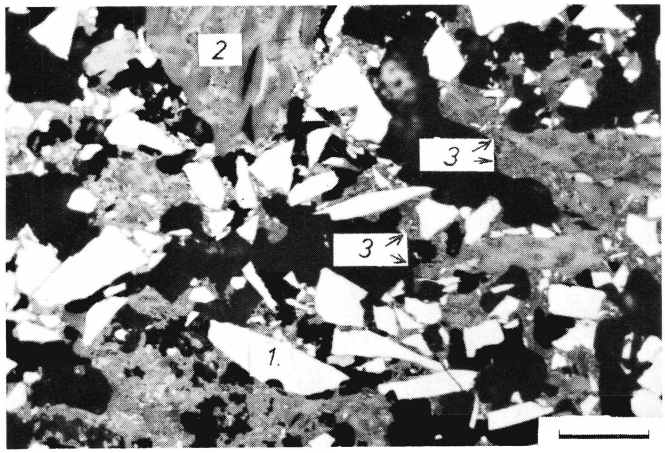

FIGURE 6.5 - The mixture of Si + C and SiC after heating up to 1300°C and cooling down again. 1 - Silicon; 2 - Carbon; 3 - Silicon carbide. Bar = 30 μm.

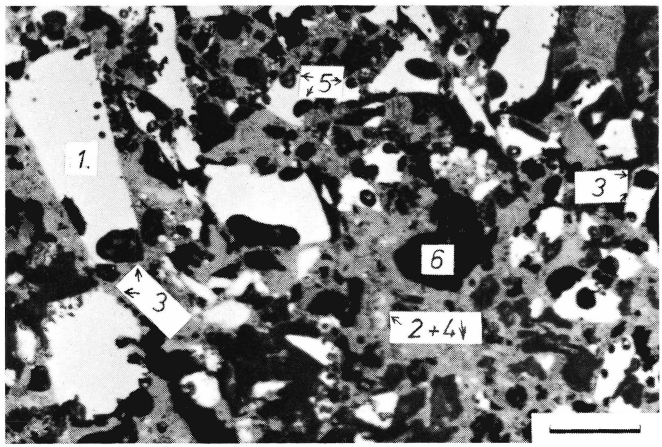

FIGURE 6.6 - A test piece after 40 h of firing in argon at 1300°C. 1 - Silicon; 2 - Carbon; 3 - Silicon carbide layer around silicon grains; 4 - Silicon carbide in carbon; 5 - Globular pore in Si; 6 - Pore. Bar = 30 μm.

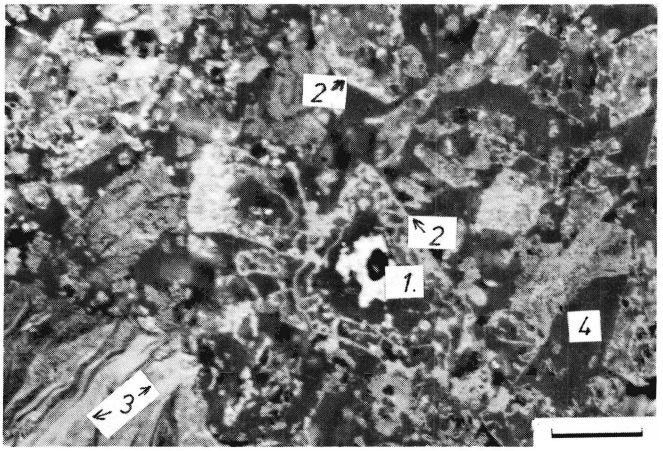

FIGURE 6.7 - A test piece after 60 h of firing in argon at 1300°C. 1 - Silicon; 2 - Ring shaped silicon carbide layers; 3 - Graphite; 4 - Pore. Bar = 30 μm.

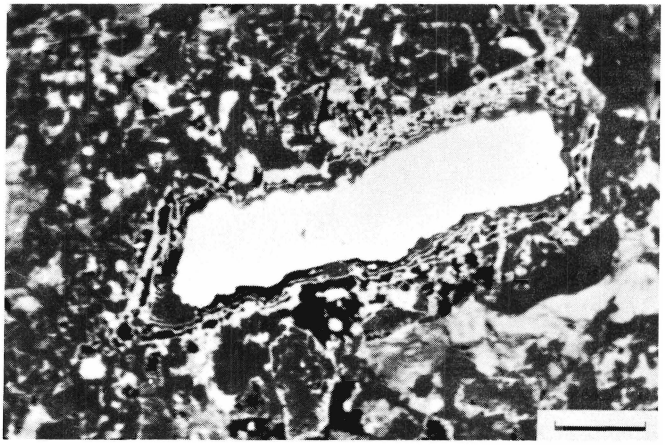

FIGURE 6.8 - A test piece after 60 h of firing in argon at 1300°C. Detail of silicon carbide layers surrounding a silicon grain. Bar = 40 μm.

Between the silicon, the grains with varying grey tints (2) are carbon grains. Very small SiC particles (3) can be seen as well. The black areas are pores in the test piece.
Figure 6.6 shows a test piece after a firing time of 40 h. In this case it is clearly visible, that the silicon grains (1) are changing their shape. Most of them are surrounded by a grey layer of silicon carbide (3), and show globular cavities (5). The residual carbon from the tar (2) is mixed now with silicon carbide (4). Again the black areas (6) are pores in the test piece.
Figure 6.7 shows a test piece after 60 h of firing. Only a few larger silicon grains (1) are left. The grains are surrounded by layers of silicon carbide (2). When all the silicon has reacted the shape of the original silicon grain is still recognizable, because of the presence of silicon carbide layers which surrounded the silicon grains.
Figure 6.8 shows a very large (over 200 µm in length) silicon grain surrounded by layers of silicon carbide. The thickness of the layers is about 3 µm, their spacing being about 10 µm. Some connections between the layers can be observed. It points to an uneven growth of silicon carbide, which stops and only can start again at certain places, for instance places where dislocations occur.
Figure 6.9 shows some details of siliconized carbon areas. The light grey parts (1) are remaining carbon. The dark grey parts (2) are the siliconized areas (see also section 6.2.2). Precise observation of the areas shows a dotted appearance which points to a mixture of carbon and silicon carbide. On the other hand the silicon carbide formed around the silicon grains is even in colour.

6.2.2 - Experiment with a silicon single crystal and carbon

A diffusion couple was made by means of placing a carbon plate on top of a silicon single crystal plate. Such couples were fired for 20 h and 95 h in an argon atmosphere at 1300°C. Figure 6.10 shows schematically the appearance of the couples after firing.
Microscopic analysis of the 20 h fired couple showed a very thin layer of silicon carbide on the surface of the silicon single crystal.
Figure 6.11 shows the polished cross-section of the couple which was fired for 95 h in argon at 1300°C. The white part (1) is the silicon single crystal; on the contact surfaces between silicon and carbon

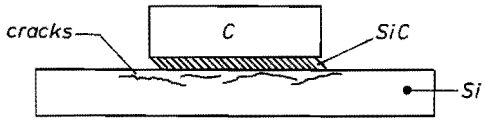

FIGURE 6.10 - A schematic drawing of the appearance of the diffusion couple after firing in argon at 1300°C.

layers of silicon carbide (2) were formed. These bands are similar to those found surrounding the silicon grains in the mixture. The thickness of the bands and the spacing of the bands are about the same as shown in figure 6.8. On removing the diffusion couple from the crucible the carbon on top of the silicon broke off. This is due to the band shaped silicon carbide formation. Only very little connections are present between the different bands.
Figure 6.12a shows the carbon plate in more detail. The last band of silicon carbide (1) is in direct contact with the carbon. The areas (2) show a dotted appearance as was found in figure 6.9. The grains (3) and (4) are unchanged carbon grains. In figure 6.12b a microprobe analysis of the silicon distribution is shown for the same area as shown in figure 6.12a. Corresponding spots are indicated by the same numbers. The microprobe analysis confirms the formation of silicon carbide in the carbon even at places where no direct contact between silicon and carbon is present.

6.2.3 - Discussion of the results

The results of the experiments described in 6.2.1 and in 6.2.2 are in good agreement with the given theory in 5.2. Both the experiments with the mixture and the diffusion couple show that the formation mechanisms proposed actually do occur.
The measurement of the reaction rate (6.2.1) shows a total transition of the silicon present into silicon carbide in about 100 h at 1300°C. With the analysing techniques used it was impossible to trace minor impurities in the test pieces.
Microscopic investigations of the silicon and carbon mixture after different periods of firing, showed two zones of silicon carbide formation. The reaction zone discussed first concerns the silicon carbide

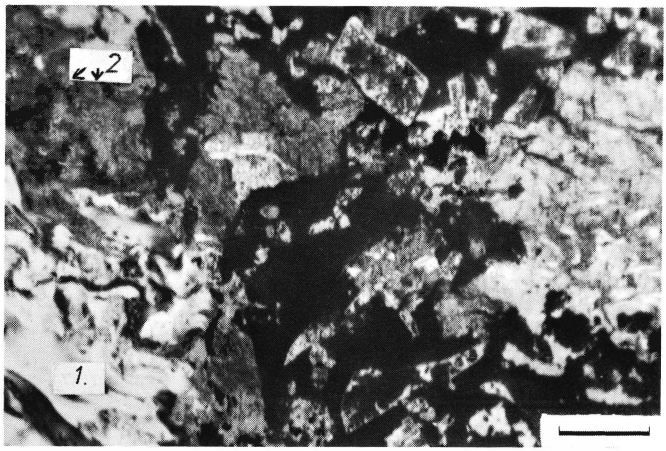

FIGURE 6.9 - Siliconized areas in a carbon grain. 1 - Carbon; 2 - Silicon carbide. Bar = 19 μm.

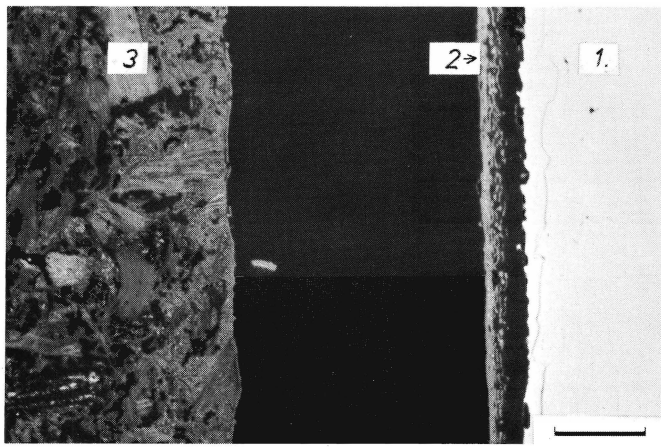

FIGURE 6.11 - The reaction between a silicon single crystal and carbon in an inert atmosphere. 1 - Silicon; 2 - Silicon carbide primary bands; 3 - Carbon. Bar = 75 μm.

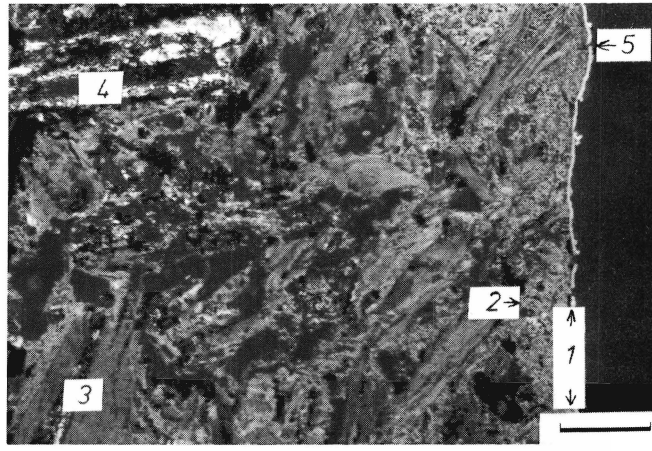

FIGURE 6.12a - The formation of SiC in a carbon grain in an inert atmosphere at 1300°C.
1 - Silicon carbide band; 2 - Silicon carbide particles; 3,4 - Carbon grains. Bar = 30 μm.

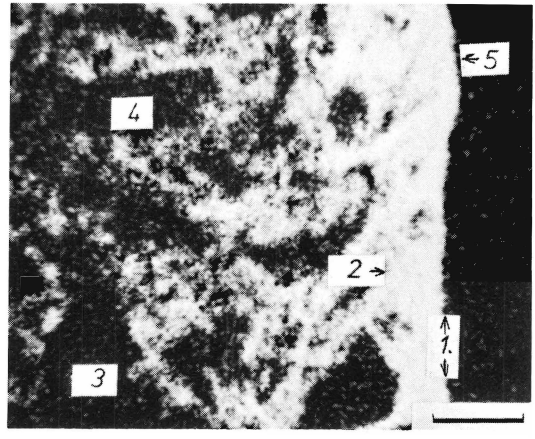

FIGURE 6.12b - Microprobe analyses of Si-Kα radiation of the area shown in fig. 6.12a.

Numbers show corresponding spot in figure 6.12a and b. Bar = 34 μm.

layers around the silicon grains. After 40 h of firing a dense silicon carbide layer is observed in direct contact with the silicon grains. Interesting is the appearance of globular pores at the interface between the silicon and the silicon carbide layer. Comparison between figure 6.5 and 6.6 shows the difference in appearance of the silicon grains. Atkinson et al [6-4]) found similar formation of pores in silicon grains during the formation of silicon nitride. They proposed the following reaction mechanism: the initial stage involves the growth of a layer of the reaction product on the silicon grain (fig. 6.13a). When all the silicon surfaces are covered, the reaction must continue by the outward transport of silicon through the reaction layer (fig. 6.13b). The outward transport of silicon from the grains results in the formation of an excess of vacancies, which condense as pores at the reaction interface (fig. 6.13b). In the case of nitridation a two way diffusion will occur, therefore Si_3N_4 may be formed in the newly formed pores as well (fig. 6.13c).

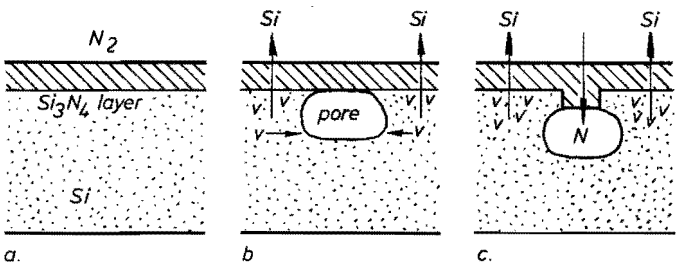

FIGURE 6.13 - Schematic illustration of formation of silicon nitride (after Atkinson et al [6-4]).
a. Silicon is first covered with a layer of nitride.
b. Silicon migrates out of the grains leaving vacancies which condense as pores.
c. Nitride growth into a pore.

In the case of silicon carbide formation only silicon diffusion through the reaction layer will be possible, since the vapour pressure of carbon is extremely low. The reaction mechanism for silicon carbide will be similar to that for nitride in the initial stage. The only difference being that the initial formation is due to a solid-solid reaction (fig. 6.14a). After that, outward transport of silicon from the grains

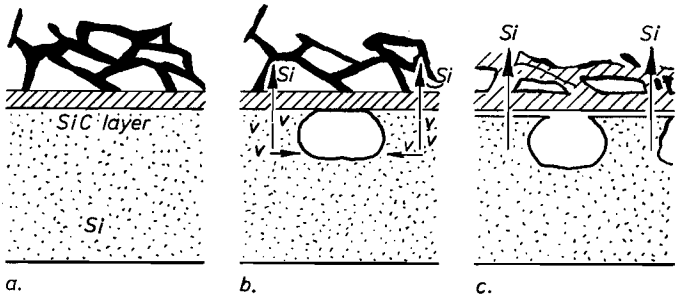

FIGURE 6.14 - Schematic illustration of formation of silicon carbide.
a. Silicon is first covered with a layer of silicon carbide.
b. Silicon migrates out of the grains leaving vacancies which condense as pores.
c. The carbon network is reformed into silicon carbide; the gap between the initial layer and the silicon grain is due to the one way diffusion which occurs (only Si out).

will occur and the globular pores are formed. The silicon leaving the initial reaction layer will find a very fine network of residual carbon surrounding the grain. Our experiments concerning mixtures of tar and refractory grains showed that the residual carbon after coking tends to form a fine network around the refractory grains. The micrographs of figure 6.8 and 6.11 show clearly the formation of almost parallel layers of silicon carbide around the silicon grains. Walker [6-3]) suggested that these "bands" are due to crystal misfits. He called similar layers "primary bands" because they are separate layers and are visible in unetched microscopic sections. Walker only gives a restricted explanation for the occurrence of those primary bands. In our opinion the formation of primary bands may be initiated by the direct contact of carbon and silicon and, after the formation of the initial layer, the direct contact between carbon and the silicon carbide layer. Those places of contact will form nuclei for further growth of silicon carbide (see fig. 6.14b). Silicon may diffuse into such contact areas and will penetrate the carbon network from the outside. This will result in a first formation of silicon carbide on the surfaces of the network. Conglomeration of those silicon carbide nuclei may be the driving force for bringing about parallel layers (see also fig. 6.14c). Due to the outward diffusion

of the silicon a gap will be formed after a certain time between the initial layer and the silicon grain, as is shown in figure 6.14c. This can clearly be seen in the photo-micrograph of figure 6.11. At the end of the reaction all silicon has gone and a hollow shell of silicon carbide remains (see also the upper number 2 in figure 6.7).

The second reaction zone to be discussed in the silicon carbide within carbon grains (see fig. 6.9). The appearance of these siliconized areas in carbon is similar to the siliconized areas found by Walker [6-3]). He found silicon carbide layers interspersed by carbon. He made silicon carbide by the fluid bed method. Because of the inhomogeneous bulk material found by him, he called these carbon-silicon carbide layers "non stoichiometric bands". With the fluid bed method carbon is deposited upon a silicon layer. Walker indicates that the "non stoichiometric bands" are due to fluctuations in the process. For the process described in this chapter silicon is deposited on the carbon. The presence of silicon vapour (see section 5.2) will bring silicon to the carbon grains. As figure 6.12b shows, silicon diffusion into the carbon grains occurs. This diffusion is only possible in highly porous carbon and is not possible in the dense highly graphitized zones as figure 6.8 and 6.12 show. From the microscopic observations we suppose that the silicon reacts with the carbon along the tiny pores in the carbon, forming thin layers of silicon carbide at the surfaces of the pores. This process can explain the dotted appearance of these carbon zones under the microscope (see also figure 6.15).

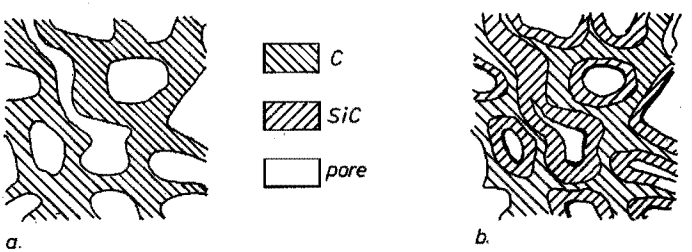

FIGURE 6.15 - Schematic illustration of the formation of silicon carbide in porous carbon.
a. The original carbon.
b. Carbon with silicon carbide at the surfaces of the pores.

6.3 - Experiments in a Pure Nitrogen Atmosphere

As a start for experiments in a pure nitrogen atmosphere an experiment with silicon powder was carried out on a thermogravimetric balance. The aim was to find the temperature at which the Si_3N_4 reaction starts having a measurable reaction rate. In a Stanton thermobalance, 86 mg of Si powder was heated up at a rate of 5 $K.min^{-1}$ in a pure N_2 atmosphere. The increase in mass of the powder was measured as a function of the temperature. Figure 6.16 shows the result of the test.

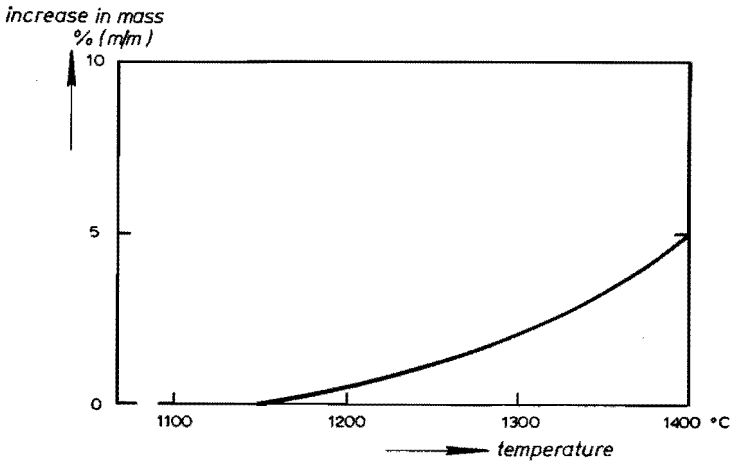

FIGURE 6.16 - The reaction 3 Si + N_2 = Si_3N_4 measured as a function of temperature by means of the increase of mass of the specimen. Heating rate 5 $K.min^{-1}$.

The curve in figure 6.16 shows that the reaction starts somewhat below 1200°C. The reaction has a good measurable rate at a temperature of 1300°C. X-ray diffraction analysis showed besides silicon only the presence of silicon nitride in the specimen. The result is in agreement with that of Brokhin et al [6-5], who indicated nitridation to start even at somewhat lower temperatures than found by us. They measured the nitride content of a specimen after firing it at a certain temperature for 1 h. The experiments carried out by Brokhin et al and those described above show, that nitridation must be expected when nitrogen is brought in a reaction chamber as described in chapter 5. The influence

of nitrogen on the silicon carbide formation will be studied in the following sections.

6.3.1 - The rate of nitridation of silicon powder at 1300°C

For the experiments to measure the reaction rate, fine silicon powder (< 100 µm) was brought in the test piece tube (see 6.1). The ends were sealed with graphite rods. Five test pieces were made. Each test piece was fired in pure nitrogen at 1300°C for a preset time. After firing the test piece was analysed by means of X-ray diffraction, the nitrogen content was measured chemically, and on some of the test pieces microscopic examinations were carried out.
The X-ray analyses were carried out with a goniometer (Rigaku, vertical 2Θ goniometer). In the specimens silicon, α-Si_3N_4 and β-Si_3N_4 were found. In our case it was impossible to measure the amounts of both types of nitrides, but the peak heights of the strongest lines were measured. The results are given in table 6.3. Also other investigators [6-6]) have found the parallel appearance of α- and β-Si_3N_4 (see also 6.3.4).

TABLE 6.3 - X-ray diffraction peak height in mm

firing time h	α-Si_3N_4	β-Si_3N_4
0	20	0
15	99	17
40	200	50
140	>200	70

The chemically measured amount of nitrogen in the specimen was used to calculate the total amount of Si_3N_4. The results had an accuracy of about $\pm$ 1 % (m/m) of Si_3N_4 and are shown graphically in figure 6.17a. In figure 6.17b a semi-logarithmic plot is shown of the Si_3N_4 formation. From figure 6.17b it can be seen, that the formation can be written as:

$$Si_3N_4 = 0.8 \cdot \exp(- c.t^{-1}) \qquad (6.2)$$

In this equation c is a temperature dependent value (13.8 in our case). The given relation suggests and the curve of figure 6.17b shows that at $t = \infty$ the Si_3N_4 content of the test piece will be about 80 % (m/m). So no total nitridation seems to be possible under the given circum-

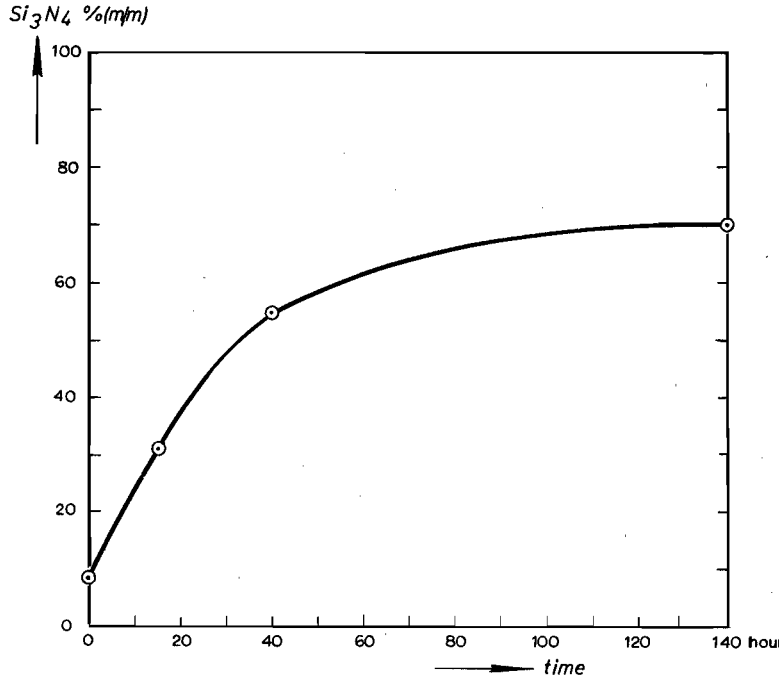

FIGURE 6.17a - The formation of Si_3N_4 at 1300°C in a pure nitrogen atmosphere.

stances. Atkinson et al [6-6]) have observed a similar effect. This will be discussed in section 6.3.4.

Our microscopic analysis showed only very little formation of Si_3N_4 after heating up and cooling down again. As can be seen in figure 6.18 nearly unchanged silicon grains are present with some growth of Si_3N_4 in between. Figure 6.19 shows the results of nitridation after 15 h at 1300°C. A gap between the silicon grains and the dense Si_3N_4 formed can be observed (3). In some places a direct contact between the silicon grains and the silicon nitride can also be seen (4). The appearance of the silicon grains is nearly unchanged. After 40 h of firing more Si_3N_4 is formed; microscopic analyses show very few pores left in the test piece. The test piece after 140 h of firing is even more dense, as is shown in figure 6.20. The Si_3N_4 formed between the silicon grains has a very dense and "glassy" appearance. The picture shows that the Si_3N_4 is not often in direct contact with the silicon grains. In the picture no pores or channels in the silicon nitride are visible, so it

FIGURE 6.18 - The microscopic picture of a test piece with silicon grains after heating up to 1300°C in a nitrogen atmosphere and cooling down again. 1 - silicon; 2 - silicon nitride. Bar = 30 μm.

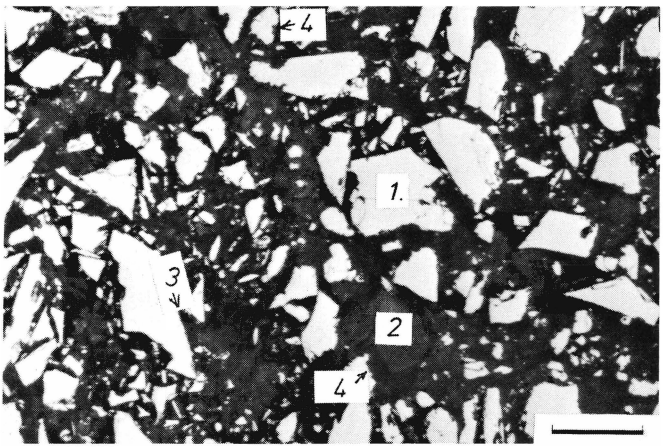

FIGURE 6.19 - Silicon grains after 15 h of firing at 1300°C in a nitrogen atmosphere. 1 - silicon; 2 - silicon nitride; 3 - gap; 4 - direct contact of silicon and silicon nitride. Bar = 30 μm.

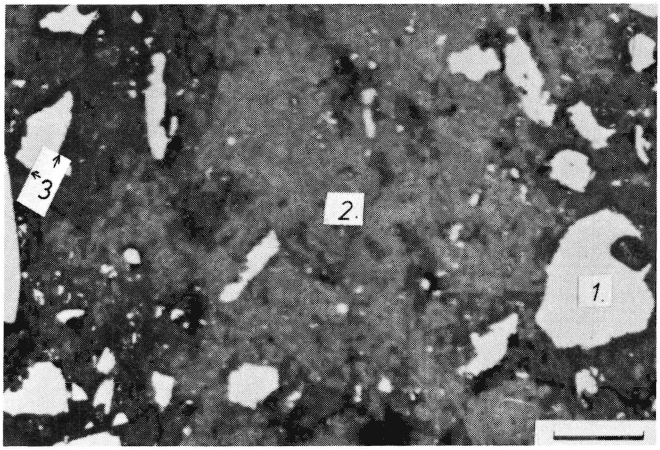

FIGURE 6.20 - Silicon grains after 140 h of firing at 1300°C in a nitrogen atmosphere. 1 - silicon; 2 - silicon nitride; 3 - gap between silicon and silicon nitride. Bar = 30 μm.

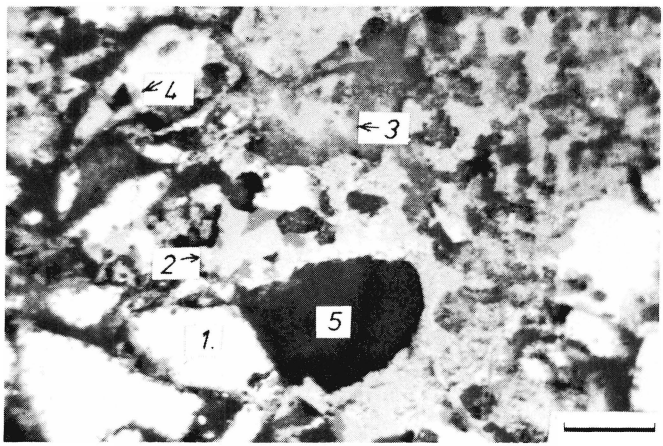

FIGURE 6.22 - The mixture silicon and carbon after 60 h of firing in a nitrogen atmosphere at 1300°C. 1 - silicon; 2 - silicon carbide; 3 - silicon nitride; 4 - pore filled with silicon carbide and silicon nitride; 5 - pore. Bar = 30 μm.

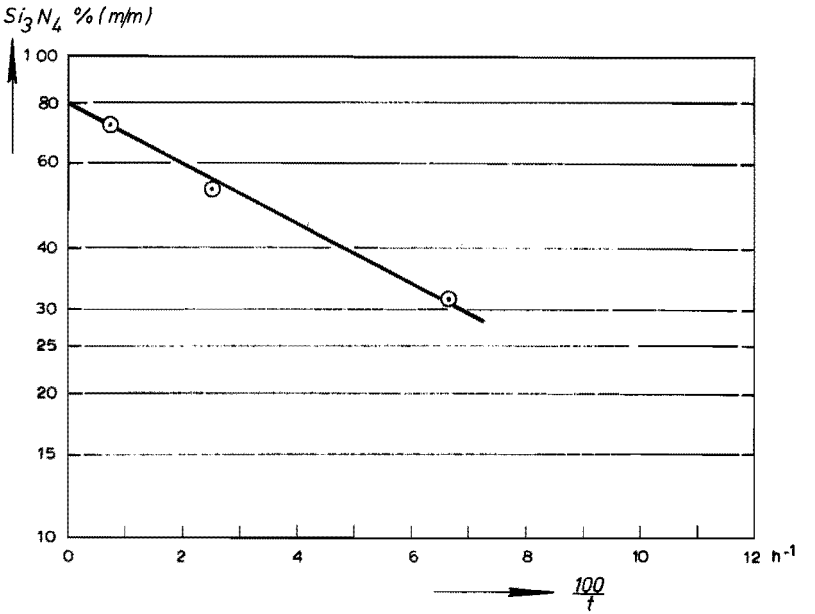

FIGURE 6.17b - A semi-logarithmic plot of the Si_3N_4 formation.

may be assumed, that gas transport through the specimen is difficult.

6.3.2 - Experiments with a silicon and carbon mixture at 1300°C in a nitrogen atmosphere

Material of the same mixture as used for the experiments described in 6.2.1 was used for experiments in a nitrogen atmosphere. Test pieces were fired respectively for 0, 2, 24, 48, and 72 h at 1300°C. The results of the experiments are summarized in figure 6.21. Curve I shows a great difference with the reaction rate for SiC in pure argon as given in figure 6.4. Curve II, Si_3N_4, also gives a different reaction rate than found in figure 6.17.

Even after 70 h of firing very little Si_3N_4 (31 % (m/m)) and SiC (17,0 % (m/m)) are formed. From figure 6.21 it can be seen, that the nitridation even ceased in the end (the last two points of the curve have the same value). The SiC formation continues, since silicon and carbon are in direct contact, provided an efficient mixing procedure was applied.

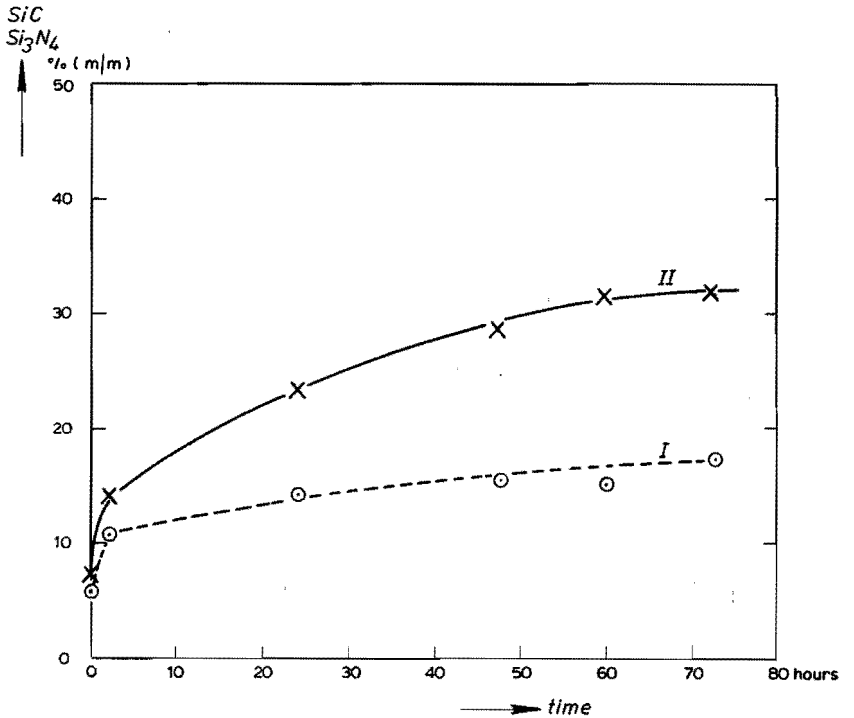

FIGURE 6.21 - The reaction rates of the reactions:
$Si + C = SiC$ (curve I) and $3\ Si + 2\ N_2 = Si_3N_4$ (curve II).

In figure 6.22 the test piece fired for 60 h is shown. Silicon is still present in rather large amounts, compared with the test piece fired for 60 h in an inert atmosphere (figure 6.7). Further, a rather dense mixture of silicon carbide and silicon nitride is formed. Similar pores as observed in figure 6.6 (No 5) seem to appear in this case as well. They are now partly filled with silicon carbide and partly with silicon nitride (see No 4 in fig. 6.22). Hollow silicon carbide shells have not been found.

6.3.3 - Experiment with a silicon single crystal and carbon

A test piece made as described in 6.2.2 was fired at 1300°C for 80 h in a pure nitrogen atmosphere. In figure 6.23 a photo-micrograph of the diffusion couple is shown. Again it is observed that the silicon single

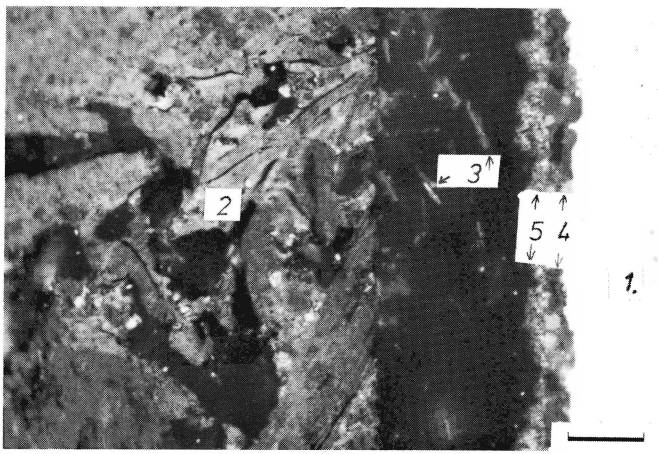

FIGURE 6.23 - The reaction between silicon, carbon and nitrogen after firing at 1300°C. 1 - silicon; 2 - carbon; 3 - silicon nitride whiskers; 4 - homogeneous layer; 5 - inhomogeneous layer. Bar = 10 μm.

crystal is severly cracked. On the silicon surface a small layer of about 5 μm in thickness has grown. In the gap between the carbon and the silicon different whiskers with lengths between 1 and 10 μm (3) are observed. From figure 6.23 it can be seen, that the reaction zone on the silicon surface consists of two layers, namely an even grey (4) and a less homogeneous coloured layer (5). A line scan with a microprobe was made on silicon and carbon across the reaction layers. Figure 6.24a shows the line chosen and figure 6.24b the result of the scan. The scan was started in a crack in the silicon single crystal (A). At point B the even grey layer was reached. It can be seen from the microprobe analysis that the Si content in that area is slightly lower. The scan also shows that no carbon is present, except in small amounts in the cracks. Therefore it is concluded that a layer of Si_3N_4 is formed. The microscopic appearance of the layer is very similar to Si_3N_4 layers found by Atkinson et al [6-6]). Between the points C and D the second, less homogeneous layer is found. In this layer the silicon content is lower and carbon is measured in relatively large amounts as well. There-

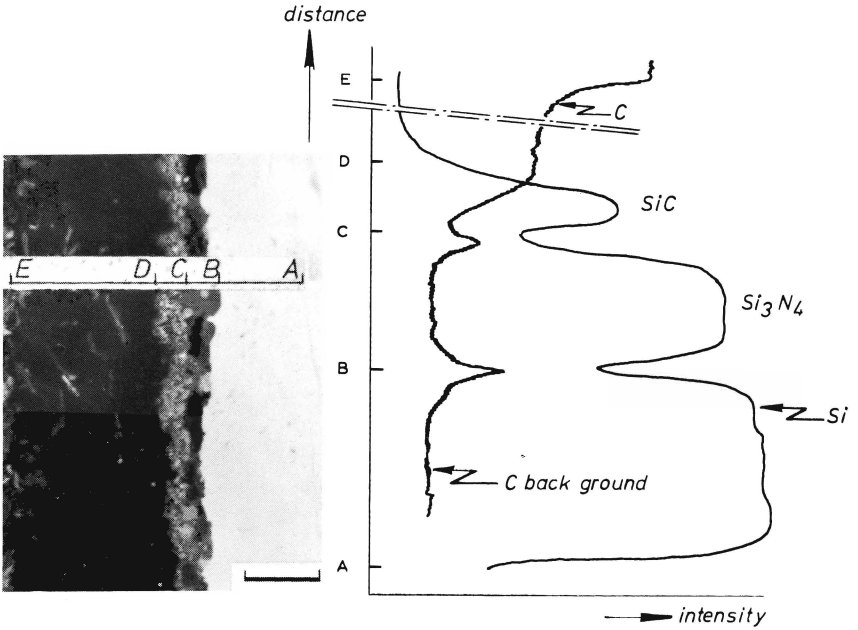

a b

FIGURE 6.24 - The reaction zone between silicon and carbon.
a. Micrograph of the scanned area. Bar = 10 μm.
b. Microscan. A - starting point; A-B - silicon; B-C - silicon nitride; C-D - inhomogeneous layer; D-E - gap; E - carbon.

fore, it is concluded that some silicon carbide may be formed. From the microprobe analyses it is impossible to conclude whether silicon nitride is formed in this layer or not. A surface scan on silicon in the carbon plate showed no marked silicon carbide formation in the carbon.

6.3.4 - Discussion of the results

The results of the experiments described in 6.3.1, 6.3.2 and 6.3.3 show the formation of silicon nitride under different circumstances. In principle two forms of silicon nitride have been observed, namely as dense layers in direct contact with the silicon grains and as whiskers. In figure 6.13 the growth of silicon nitride on a silicon surface has been drawn schematically after the theory proposed by Atkinson et al [6-4].

The grains found in our reaction rate studies (section 6.3.1) showed nearly unchanged silicon with only a very few pores. At the surface of some silicon grains the formation of the initial layer is observed (fig. 6.19, No 4). On the other hand, also free laying silicon grains surrounded by silicon nitride are found (fig. 6.19, No 3). In the latter case a gap between the silicon grain and the silicon nitride is found. Atkinson and Moulson [6-7]) showed that metallic impurities will greatly influence the formation process. Table 6.1 shows that the silicon used for the experiments described contains such impurities. This might explain the difference of our results with those of other investigators and this view is supported by the results obtained with the diffusion couple (6.3.3). The experiments with the diffusion couple showed formation of Si_3N_4 at the silicon surface in a very similar way as was found by Atkinson [6-6]) (zone 4 in fig. 6.23).
From table 6.3 it can be seen that in the initial stage the major silicon nitride structure found is the α-Si_3N_4 structure. In a later stage β-Si_3N_4 is found as well. This is in good agreement with experiments carried out by Jennings and Richman [6-8]), who propose different reaction mechanisms for the Si_3N_4 formation: In the initial stage the mechanism described by Atkinson et al [6-4]) and reviewed in 6.2.3, is most important. Jennings and Richman indicate, that the initial layer on the silicon surface contains pure α-Si_3N_4. After this layer is formed, β-Si_3N_4 will grow into the pores in the silicon grains (see fig. 6.13c). The silicon diffusion through the initial layer will tend to form α-Si_3N_4 whiskers, growing from the initial layer into the pores between the grains. Veldkamp [6-9]) discussed the forming mechanisms of whiskers and showed the gas-gas reaction to be the easiest for whisker formation. Jennings and Richman found the α-Si_3N_4 formation to be in favour of the β-Si_3N_4 formation below 1410°C, which is confirmed by our experiments.

From the model concerning the reaction mechanism described above it will be clear, that the reaction rate is influenced by several conditions, as diffusion rate of the silicon and nitrogen, temperature, grain size of the silicon grains, impurities etc. Each mechanism will have its own rate controlling condition. This explains the differences in reaction rate found by different investigators [6-5]), [6-7]), [6-10]), [6-11]). Most investigators show curves indicating a total transition of silicon into silicon nitride at $t = \infty$. Most of those experiments, however, are carried out at higher temperatures than 1300°C. Amato [6-10])

and Popper et al [6-11]) did experiments at that temperature as well. From the curves given it can, however, not be concluded whether a total transition takes place or not.
Brokhin et al [6-5]) showed that the first nitridation takes place at temperatures even lower than those found in the work presented here (about 1000°C). The explanation for this is the difference in the experimental method used. Brokhin measured the N_2 content of silicon after heating up to a certain temperature and firing it at that temperature for 1 h in a nitrogen atmosphere. With our method silicon is heated in a nitrogen atmosphere with a certain heating rate. During this heating up the gain in test piece weight is measured. Therefore, an effect will only be measured at temperatures where a marked reaction rate is present. The curve given by Brokhin shows a noticeable increase in reaction rate over 1100°C, which temperature coincidences with the start of weight gain measured in our thermobalance.

As found in 6.3.2 the formation of SiC in a mixture of silicon and carbon fired in nitrogen is hindered by the growth of silicon nitride. The silicon will partly be covered by a silicon nitride layer. This layer will be the first one to be formed, as can be seen from the curves concerning the reaction rate of silicon carbide (fig. 6.4) and silicon nitride (fig. 6.17). This first layer of silicon nitride will hinder the silicon carbide growth at the surfaces of the silicon grains. The silicon vapour will either react with nitrogen or with the carbon present in the mixture. The silicon carbide formation in a carbon-silicon mixture fired in a nitrogen atmosphere will be the result of either a direct solid-solid reaction at the contact zones between silicon and carbon, or a solid (carbon)-gas (silicon) reaction in the carbon grains.

6.4 - The Experiments in Argon with Addition of 200 ppm of Oxygen

6.4.1 - Experiments on the reaction rate

Material of the same mixture as used for the experiments in an inert atmosphere (section 6.2.1) was used for the experiments in an atmosphere of argon with an addition of 200 ppm of oxygen.
For the experiments 200 ppm of oxygen were added to a bottle of pure argon. The gas flow was in this case led directly via the constant flow

valve to the rotameter and into the furnace tube (see also section 6.1). The BTS-cell was not used, since copper oxide in the cell would have removed the oxygen from the gas flow. Due to this procedure it could not be avoided that the small amount of nitrogen present in the argon was introduced into the furnace tube.

The amount of 200 ppm of oxygen was chosen to create an oxygen partial pressure which gives a SiO and CO pressure lower than the minimum SiO and CO pressure for SiO_2 formation, as was calculated in section 5.3 (see fig. 5.3). In figure 6.25 curve I shows the silicon carbide formation. Curve II, at another scale, shows the silicon nitride formation as calculated from the chemical analysis of the nitrogen content of the test pieces. This was allowed, since with X-ray diffraction no Si_2ON_2 was found.

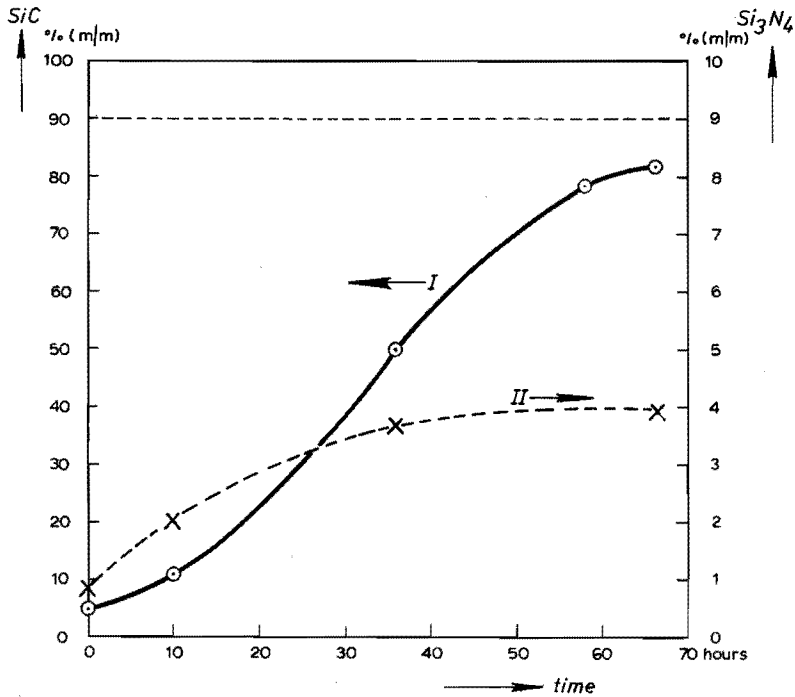

FIGURE 6.25 - The silicon carbide formation after firing at 1300°C in an inert atmosphere to which 200 ppm O_2 was added and containing traces of nitrogen. Curve I - silicon carbide formation; curve II - silicon nitride formation.

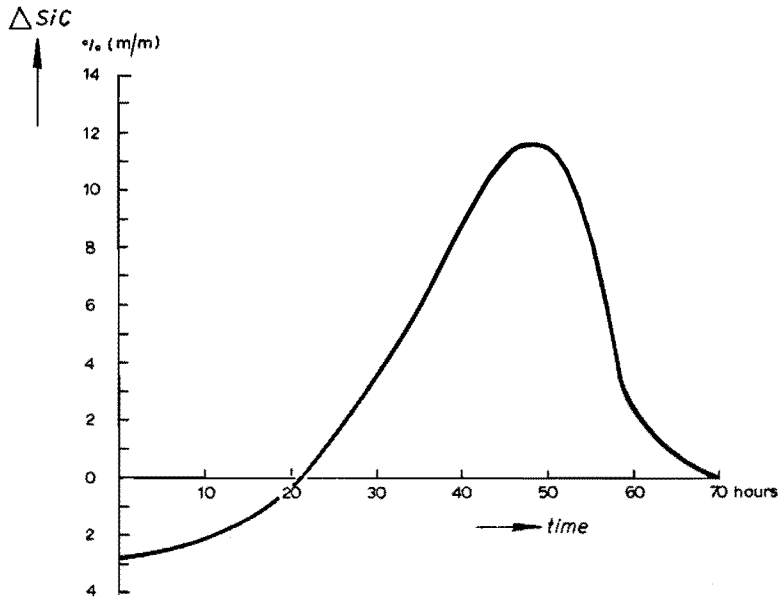

FIGURE 6.26 - The difference in reaction rate for the SiC formation in argon and in argon + 200 ppm of oxygen.

To investigate, whether the reaction rate of the silicon carbide was influenced by addition of oxygen to the gas mixture or not, the difference in amount of silicon carbide, formed after a certain time, was derived from figure 6.4 and curve I in figure 6.25. The difference was calculated according to:

$$\Delta SiC = \%\ (m/m)\ SiC_{Ar+O_2} - \%\ (m/m)\ SiC_{Ar} \qquad (6.3)$$

The difference is plotted in figure 6.26. The curve will be discussed in section 6.4.3.

The microscopic study of the test pieces showed a very similar growth of silicon carbide as found in section 6.2.1. Figure 6.27 shows the structure of the test piece after 65 h of firing. In this test piece no silicon grains were left. It was noted that in the test pieces fired in pure argon after 65 h still a little silicon was present. In principle the structure is the same as found before. More detailed observations show, however, that in various pores small silicon carbide whiskers are present. Figure 6.28 shows such whiskers (No 1). No 2 in-

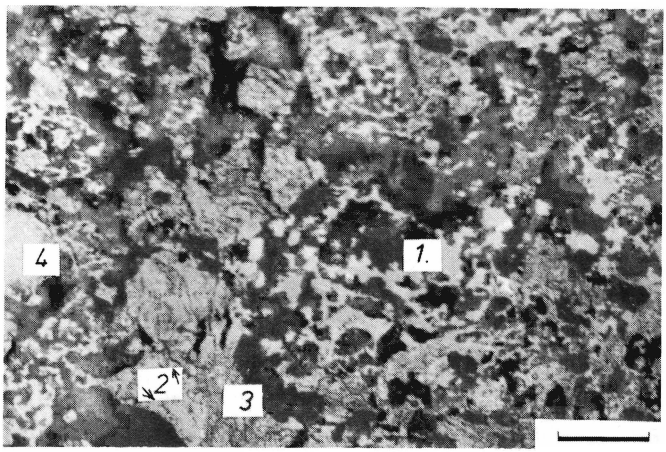

FIGURE 6.27 - Formation of silicon carbide after 65 h of firing at 1300°C in argon + 2 ppm of O_2. 1 - silicon carbide formed by the solid-solid reaction; 2 - unchanged carbon; 3 - silicon carbide in carbon; 4 - mixture of silicon nitride and silicon carbide. Bar = 30 μm.

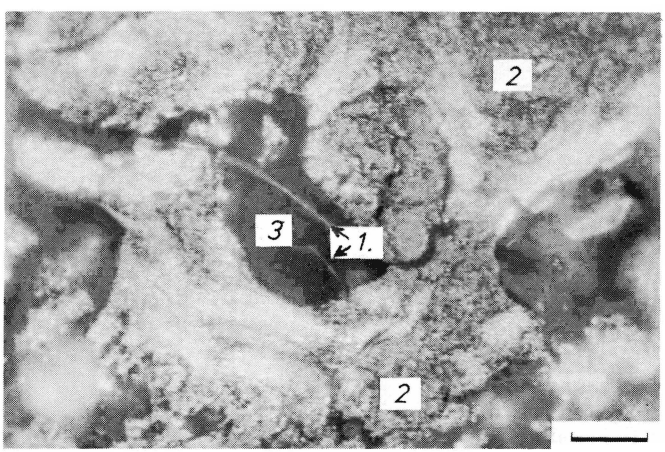

FIGURE 6.28 - Formation of silicon carbide whiskers. 1 - silicon carbide whiskers; 2 - silicon carbide in carbon; 3 - pore. Bar = 10 μm.

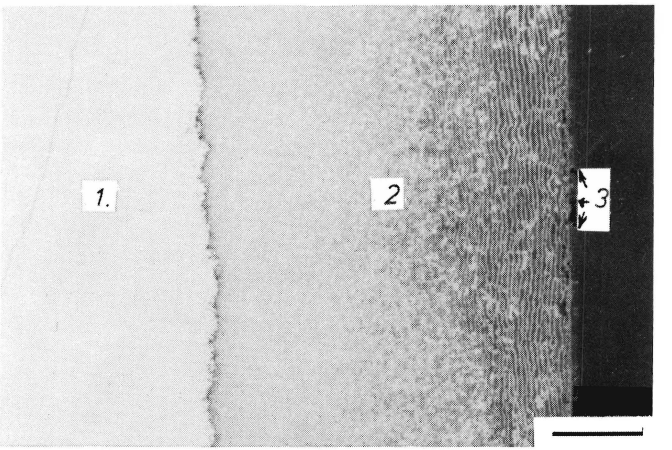

FIGURE 6.29 - A silicon carbide layer at the surface of the silicon single crystal after 70 h of firing at 1300°C in argon + 200 ppm of O_2. 1 - silicon; 2 - silicon carbide bands; 3 - whiskers. Bar = 30 μm.

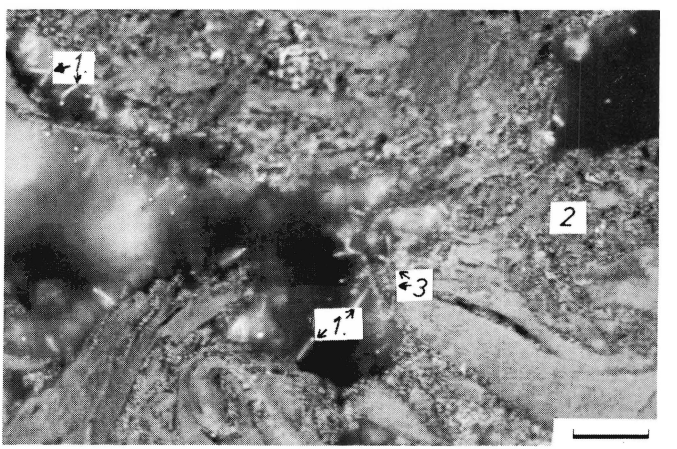

FIGURE 6.30 - A pore in the carbon platelet on top of the silicon single crystal after 70 h of firing. 1 - silicon carbide whiskers; 2 - silicon carbide in carbon; 3 - growing nucleus for the whisker. Bar = 10 μm.

dicates silicon carbide formation in the pores of the carbon.

6.4.2 - Experiment with a silicon single crystal and carbon

A diffusion couple made as described in 6.2.2 was fired at 1300°C for 70 h in an atmosphere of argon + 200 ppm of oxygen. In figure 6.29 a part of the silicon single crystal is shown with a layer of silicon carbide. Comparing this picture with figure 6.11 it can be seen, that the silicon carbide layer is now in direct contact with the silicon. Again some sort of primary bands are visible but much thinner than before. The measured thickness in this case is about 1 µm, whereas a thickness of about 3 µm is measured for the bands formed in pure argon. Also a smaller band to band distance is found; in this case distances lower than 1 µm are measured. On the outer surface small whiskers can be seen (3). The structure of the silicon carbide layer near the silicon is rather disrupted; this might be due to the whisker formation which takes place perpendicular to the silicon surface. In figure 6.11 a silicon carbide layer of 30 µm was found after 95 h of firing. In figure 6.29 a silicon carbide layer of 117 µm was found after 70 h of firing, which indicates a higher reaction rate in the latter experiment.
At the surface of the carbon plate which was placed on top of the silicon, silicon carbide whiskers (No 1 in fig. 6.30) are observed. Figure 6.30 shows a pore in the carbon plate near the contact surface between the silicon and the carbon. Silicon carbide formation in the porous carbon (2) is observed, and especially from these areas silicon carbide whiskers seem to grow into the pore (3).

6.4.3 - Discussion of the results

The experiments show that addition of a small amount of oxygen to an inert atmosphere influences the silicon carbide formation to a great extent. The reaction rate is increased by the oxygen as is shown in figure 6.26 and as can be seen from the thickness of the layers of primary bands on the silicon surfaces after firing in argon or in argon + 200 ppm of oxygen (see figures 6.11 and 6.29). The curve of figure 6.26 shows that the reaction rate becomes markedly higher after about 20 h. In the initial stage the reaction rate is a little lower than in pure argon. This may be due to a fast formation of silicon nitride which

takes place in the first hours of firing as can be seen from figure 6.25. Point 4 in figure 6.27 indicates a transformed silicon grain, which consists now of a mixture of silicon carbide and silicon nitride; this illustrates the competitive growth of silicon carbide and silicon nitride under the given circumstances. In figure 6.27 it is much more difficult to identify the former silicon grains than in figure 6.7, where the mixture was fired in pure argon. No specific growth of primary bands is observed in figure 6.27. It seems that the bands have grown together forming larger grains, which is in agreement with the results obtained from the diffusion couple experiment (see figure 6.29, the left side of area 2).
The formation of silicon carbide whiskers as observed in the figures 6.28, 6.29 and 6.30 may be due to gas-gas or solid-gas reactions.

The found reaction mechanisms, namely formation of dense layers, silicon carbide formation in the carbon pores, and whisker growth, are in agreement with the thermodynamic theory given in section 5.3. The higher reaction rate will be due to the existence of more silicon in the gas phase than in the pure argon atmosphere, and the appearance of some CO in the atmosphere. The existence of Si, SiO and CO in the gas phase makes a direct gas-gas reaction possible. Due to the presence of a little nitrogen in the gas mixture silicon nitride formation from the gas phase will be possible as well.

6.5 - Summary

The experiments described in this chapter fully confirm the theory given in the previous chapter. The experiments show that all the formation mechanisms proposed will occur under the circumstances considered. The reaction rate of the silicon carbide formation is positively affected when a little oxygen is present. With the oxygen content we applied (200 ppm), no formation of Si_2ON_2 was observed. This indicates that the very low oxygen and nitrogen partial pressures needed for Si_2ON_2 formation as proposed by Colquhoun et al [6-12]) are not found in our case, at least not with the analysing techniques used.

The experiments described here show that it is possible to produce silicon carbide from silicon grains and very fine carbon in a suitable

atmosphere. The microstructure of the thus made silicon carbide is suitable for forming the matrix (see also chapter 4) of a refractory brick. The reaction rate is rather low at the temperature which was studied in this chapter. As was found, the addition of some oxygen in the atmosphere in the furnace results in a faster reaction. In that case also some whiskers will be formed, which may be helpful, since it tends to form a more network like structure. Such a network will easily surround the refractory grains and keep them together.

In the last chapter of this thesis the results of the first industrial brick making with the described bond and the results of some experiments with these bricks in blast furnaces will be discussed.

L i t e r a t u r e

6- 1) *Hüttinger, K.J.* — *Chem.Ing.Tech. 43 (1971) 1145-1188*

6- 2) *Lee, J.G.; Cutler, J.B.* — *Am.Ceram.Soc.Bull. 54 (1975) 195-198*

6- 3) *Walker, Y.D.E.* — *Silicon carbide 1973, Proc. 3rd Int.Conf., Miami Beach, Sept. 1973. New York, Columbia Univ.Press, 1974, 403-410*

6- 4) *Atkinson, A.; Leat, P.J.; Moulson, A.J.; Roberts, E.W.* — *J.Mat.Sci. 9 (1974) 981-984*

6- 5) *Brokhin, J.S.; Funke, V.F.; Samsonov, G.V.* — *Hard metals production techniques research USSR, London. Pergamon Press, 1964, 226-239*

6- 6) *Atkinson, A.; Moulson, A.J.; Roberts, E.W.* — *J.Am.Ceram.Soc. 59 (1976) 285-289*

6- 7) *Atkinson, A.; Moulson, A.J.* — *Science of Ceramics No 8 (1976) 111-121*

6- 8) *Jennings, H.M.; Richman, M.H.* — *J.Mat.Sci. 11 (1976) 2087-2098*

[6-9] *Veldkamp, J.D.B.* — *Philips Res.Repts.Suppl., 1974, No 4, p. 23-25*

[6-10] *Amato, J.; Martorana, D.; Rossi, M.* — *Powder Metall. 18 (1975) No 36, 339-348*

[6-11] *Popper, P.; Ruddelson, S.N.* — *Trans.Brit.Ceram.Soc. 60 (1973) 603-626*

[6-12] *Colquhoun, I.; Wild, S.; Grieveson, P.; Jack, K.H.* — *Proc.Brit.Ceram.Soc. No 10 (1973) 207-227*

7.1 - Brick Production

For our studies bricks were produced along the lines described in chapter 4. In series of experiments it was tried to find the best recipe for producing direct-bonded bricks. For the experiments SiC grains were used with a maximum grain size of D_{max} = 3 mm. The binder consisted of silicon grains ($D_{max} \leq 60$ µm). The carbon residue was formed out of a heavy tar.
The materials were carefully mixed together and pressed into a brick in a hydraulic press. For our experiments a size of brick of 260 x 135 x 60 mm^3 was used. The bricks were fired for 48 hours within the temperature range indicated in chapter 4.
After firing the characteristics of the bricks were measured. It was found that an excess in residual carbon gave optimal SiC formation. In figure 7.1 the relation between the total amount of SiC in the bricks and the remaining free carbon after firing is given.
From this curve it can be seen that, when about 4 % (m/m) of carbon is remaining in the brick after firing, nearly all the Si present has reacted with the carbon. The summation of the silicon content and the carbon gives 97 % (m/m). The remaining 3 % (m/m) can be related to impurities in the raw materials used. From figure 7.2 (page 132) it can be seen, that a matrix consisting of SiC is formed in between the SiC grains. No free Si could be found in the matrix.

After the initial investigations carried out on a laboratory scale experiments in a pilot plant were carried out at the production plant of Annawerk GmbH (Rödental, West Germany).
The recipe, the mixing, pressing and firing procedures were optimized in such a way, that routine production was possible. Rather large quantities of this type of brick were produced at Annawerk for experiments in different blast furnaces. In the next sections the characteristics will be discussed as well as the experiments with these bricks in some of the blast furnaces of Hoogovens IJmuiden BV.

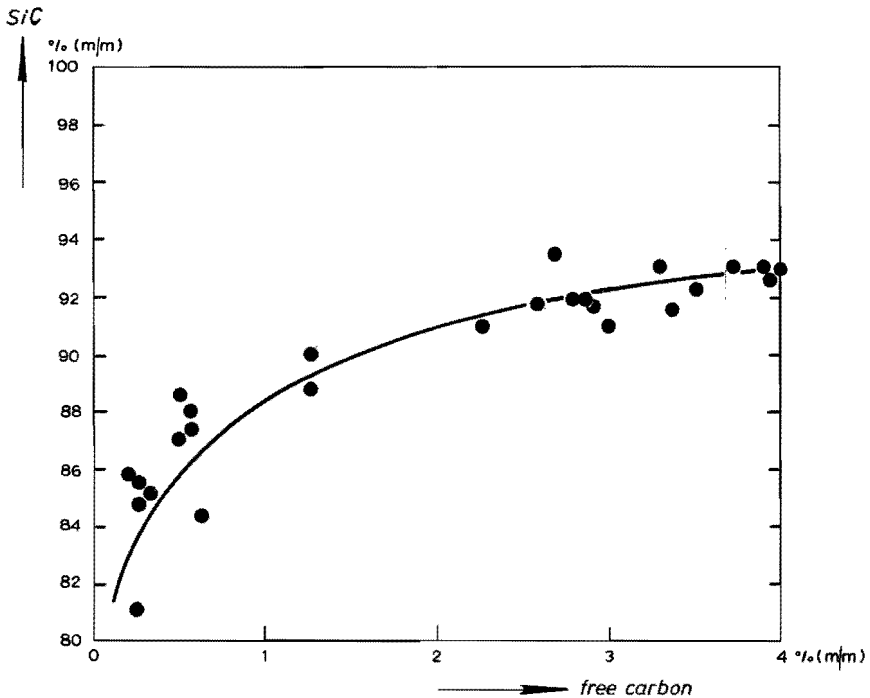

FIGURE 7.1 - The relation between the total SiC and the remaining free carbon after firing.

7.2 - Properties of the Bricks Produced in Practice

7.2.1 - Physical and mechanical properties

For the construction of a blast furnace stack, bricks of different shapes are used. When large differences in size and shape occur, often differences in the physical and mechanical data are found. In our case the dimensions and shapes of the bricks are about the same. Due to this it is allowed to compare all data measured on the bricks produced. Table 7.1 gives the mean values ($\bar{X}$) and the standard deviations (σ) of the physical and mechanical properties of the bricks. As a reference the data of the oxynitride-bonded brick are given as well. The data can also be compared with those established on other types of bricks, which are given in the tables IIa and IIb of Appendix II.

TABLE 7.1 - Properties of the bricks produced

property		oxynitride-bonded		direct-bonded	
		$\bar{x}$	σ	$\bar{x}$	σ
ρ	$g.cm^{-3}$	3.21	0.03	3.18	0.04
d_s	$g.cm^{-3}$	2.53	0.02	2.52	0.03
π_w	% (V/V)	21.0	0.8	20.0	1.2
π_s	% (V/V)	20.0	0.6	18.0	1.9
CCS	$MN.m^{-2}$	168	3.8	124	2.6
M [$MN.m^{-2}$] / Δd [mm]	20°C	54 - 0.4	3.1*	39 - 0.4	4.5*
	400°C	56 - 0.4	2.4	39 - 0.4	5.0
	800°C	54 - 0.4	4.5	36 - 0.4	4.2
	1000°C	44 - 0.2	6.4	39 - 0.4	5.2
	1200°C	26 - 0.2	4.8	45 - 0.5	4.6
	1400°C	18 - 0.2	7.1	42 - 0.6	6.0

* Only the mean value of the bending-through has been given, since the value is rather inaccurate.

The mechanical and thermomechanical requirements proposed in chapter 1 and 3 will be discussed now.

The bricks should be abrasion resistant at high temperatures. As was mentioned in section 3.3.1 an abrasion resistant grain together with a strong bond between the grains is necessary. The silicon carbide grains are very abrasion resistant. Thus the abrasion resistance can be characterized by means of the bending strength of the brick (the hot modulus of rupture). Table 7.1 shows a rather high modulus of rupture for the direct-bonded brick.

From table 7.1 it can be seen that the modulus of rupture of the direct-bonded brick is somewhat lower than of the oxynitride-bonded one for temperatures below 1000°C. Above the temperature of strength of the direct-bonded brick is markedly higher. According to the theory developed in 3.3.1 it can be stated, that the abrasion resistance of the direct-bonded brick above 1000°C will be higher than of the oxynitride-bonded one.

The brick should be thermal-shock resistant as well. From the data given in table 7.1 it is still impossible to calculate the thermal-shock resistance for the direct-bonded brick. Therefore, the heat conductivity, the heat capacity, the Youngs modulus, and the thermal expansion should

be known as well. In table 7.2 these data are given.

TABLE 7.2 - Special data for direct-bonded silicon carbide bricks

properties			direct-bonded SiC
λ	$W.m^{-1}.K^{-1}$	$20^{o}C$	35
		$1000^{o}C$	11
c_p	$J.kg^{-1}.K^{-1}$ *		$26 . 10^{3}$
E	$N.m^{-2}$ **		$12.4 . 10^{9}$
α			$0.4 . 10^{-5}$

* Value derived from literature.
** From data measured by Annawerk by means of a sonic resonance measuring method.

With the data given in tables 7.1 and 7.2 it is possible to calculate R_R at $1000^{o}C$ with relation (3.1). The value thus found is:

$$R_R = 52.7 . 10^{-9} \quad m^3.s^{-1}.K^{-1}.$$

This value is 3.5 times the value of the oxynitride-bonded SiC, which value was given in table 3.3. Due to this calculation it is found, that the direct-bonded SiC brick has the best thermal-shock resistance of the five types of brick investigated (the types of brick were: magnesite, corundum, high duty fireclay, oxynitride-bonded SiC and direct-bonded SiC). The main reason for this is the high conductivity compared to that of the other types of brick. In figure 7.3 the thermal conductivity of the four most important bricks are given in comparison with the conductivity of a semi-graphite brick.
The thermal conductivity measured for the direct-bonded brick is near to the theoretical value for SiC as given by [7-1]) for β-SiC, 15.5 $W.m^{-1}.K^{-1}$ at $1000^{o}C$, and for recrystallized SiC [7-2]) with a value of 18 $W.m^{-1}.K^{-1}$ at $1000^{o}C$. The latter material had a porosity of 18 % (V/V). George [7-3]) published conductivity measurements on hot pressed silicon carbide, which indicate much higer values for this material. For a test piece with 8 % (V/V) of Si and a porosity of 15 % (V/V) a conductivity of 50 $W.m^{-1}.K^{-1}$ was found at $700^{o}C$. According to the given curve a value of about 40 to 45 is expected at $1000^{o}C$. These values are much higher than those mentioned in [7-1]) and [7-2]) and those found with our investigations.

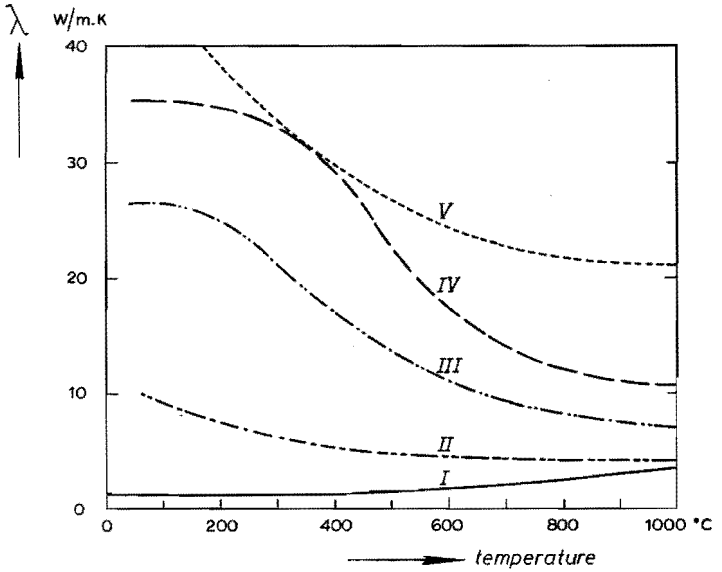

FIGURE 7.3 - Thermal conductivity as function of temperature. I - high duty fireclay; II - corundum; III - oxynitride-bonded silicon carbide; IV - direct-bonded silicon carbide; V - semi-graphite.

7.2.2 - Measurement of the chemical resistance

The alkali and slag resistance of the direct-bonded brick was measured according to the description given in section 3.3.3. The alkali resistance was tested by means of the crucible shaped test brick. 30 g of K_2CO_3 was brought into the crucible and the crucible was sealed with a lid made out of the same brick. The crucible was fired for 4 h at 1100°C. After the test the crucible was cut into two halves. The inner surface was studied microscopically. Figure 7.4 shows the inner surface of the crucible with the remaining K_2CO_3. This photograph has to be compared with figure 3.7. Figure 3.7 shows the surface of the oxynitride-bonded brick after the same test. Both pictures have a magnification of 45 times. The oxynitride-bonded brick shows a loss of bond over a depth of about 2 mm. The direct-bonded brick shows no loss of bond at all. The bond can be seen up to the surface of the crucible.
T-shaped test pieces were cut out of the test bricks. They were used for the finger test as described in 2.4.2. The slag composition used, was as

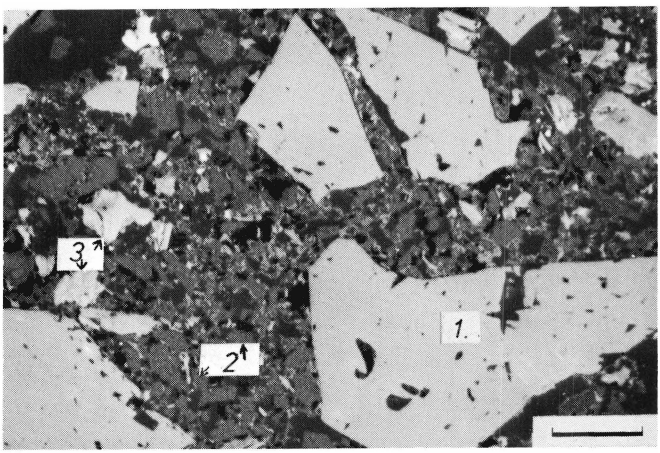

FIGURE 7.2 - SiC formed as a bond between the SiC grains. 1 - SiC grains added to the mixture; 2 - SiC formed during the firing procedure; 3 - free carbon. Bar = 75 μm.

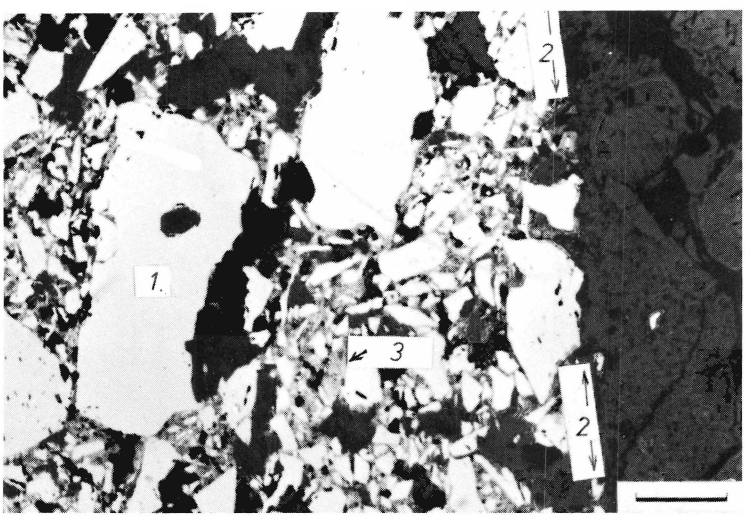

FIGURE 7.4 - The contact surface between the silicon carbide brick and K_2CO_3 (2). White grains are SiC grains (1), light gray material between the grains is the SiC bond (3). Bar = 266 μm. *(see also page 49)*

described in section 3.3.3. (N.B.: normal blast furnace slag with an addition of 5 % (m/m) of K_2CO_3.) The test pieces were soaked in the slag for 1 h at 1450°C. The direct-bonded silicon carbide bricks showed no measurable loss of cross-section. Also microscopic investigations showed no attack of the bond by the slag.

7.2.3 - Conclusions

The results of the laboratory tests on the produced direct-bonded bricks show:

- a highly abrasion resistant brick even at high temperatures;
- better thermal-shock resistance than of any of the other bricks tested;
- very good chemical resistance.

The physical data given in table 7.1 show a larger variation in values for the direct-bonded bricks, than for the oxynitride-bonded ones. This is due to the lack of experience in producing this type of bricks. Data of the last batches produced at the end of the first production period already showed less variation and slightly higher densities and higher modulus of rupture data at room temperature (up to 45 $MN.m^{-2}$) than the first batches.

According to the laboratory data the bricks seem to be a good proposition for the lower blast furnace stack.

7.3 - Experiments in the Blast Furnace Stack

In 1974 a major repair of blast furnace No 4 of Hoogovens was carried out. Blast furnace No 6 was reconstructed in the period 1975-1976. The characteristics of both furnaces are given in table 7.3. In both cases silicon carbide was used as refractory material in the middle and lower stack. In blast furnace No 4 oxynitride-bonded silicon carbide was built with a test panel of 2 m^2 of direct-bonded silicon carbide bricks installed just above the furnace belly.

In the middle and lower stack of blast furnace No 6 only direct-bonded silicon carbide was used.

Blast furnace No 4 came in production again in January 1975, blast furnace No 6 at the end of April 1976.

TABLE 7.3 - Characteristics of blast furnace No 4 and No 6

		No 4	No 6
hearth diameter	m	8.5	11
average daily production	10^3 kg	3000	4600
middle and lower stack lining		SiC Si_2ON_2 (bond)	SiC SiC (bond)
distance between the plate coolers in the stack	mm	312	312

Temperature measurements in the wall showed only very little wear in the first 9 months of operation for both furnaces. After 9 months and a production of about 7 . 10^5 ton of hot metal the first core drilling took place. The highest position of drilling was at point A indicated in figure 7.5a. This position is comparable with the position of the test panels in blast furnace No 6 as discussed in chapter 3. The measured wear at that level was 20 mm. Microscopic investigation of the core showed severe attack of the bond. The binding phase was replaced by alkali compounds in the same way as discussed in chapter 3. The micrograph of the core was similar to that shown in figure 3.12. The wear of the oxynitride-bonded silicon carbide near the belly was higher, a loss of about 200 mm was found near point C in figure 7.5a. The wear of the test panel consisting out of direct-bonded bricks was of the same order (near point B in figure 7.5a). Drillings after 16 and 22 months of operation showed no further wear near point A.

The wear near the belly was about 250 mm after 22 months of operation. After 8 months and a production of 8.8 . 10^5 ton of hot metal the first core drilling took place in blast furnace No 6. The highest position of drilling was about 1 meter below point A in figure 7.5b. The measured wear at that level was 50 mm. Microscopic investigation of the core showed very little damage of the remaining brick. The silicon carbide bond was unaltered. The impurities which had been present in the bond had disappeared. Therefore, the porosity was a bit higher than of an unused brick. Figure 7.6 shows a micrograph of the core. The core was still hard and strong after removal from the furnace in contrast with the cores drilled out of blast furnace No 4. The oxynitride-bonded bricks were soft; the silicon carbide grains could easily be removed from the core. The wear in blast furnace No 6 near the belly was about

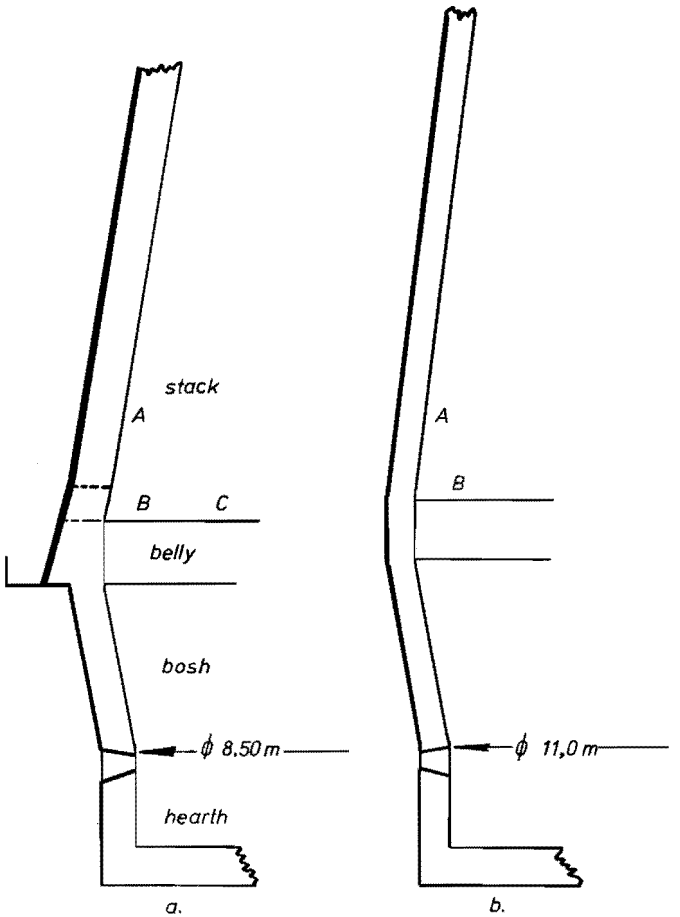

FIGURE 7.5 - General characteristics of the linings of blast furnaces No 4 and No 6.

a. Blast furnace No 4.
A - position comparable with the position of the first test panels in blast furnace No 6, see also section 3.4; B - lowest point of drilling in the oxynitride-bonded bricks; C - position of the direct-bonded brick test panel.

b. Blast furnace No 6.
A - position comparable with A in figure 7.5a.

80 mm, which is less than found in blast furnace No 4. The remaining brickwork was still strong, in contrast to the brickwork of blast furnace No 4, where soft bricks were found. The microscopic and X-ray

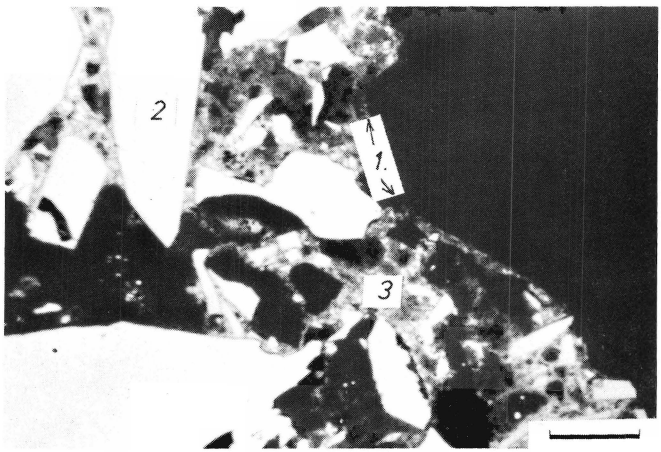

FIGURE 7.6 - Micrograph of the hot face of a core drilled specimen from blast furnace No 6 near point A.
1 - hot face; 2 - silicon carbide grains; 3 - silicon carbide bond. Bar = 30 μm.

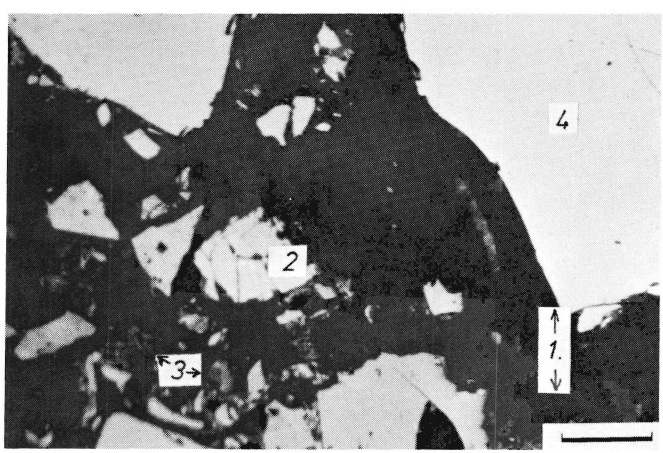

FIGURE 7.7 - Micrograph of core drilled from blast furnace No 6 just above the belly near point B.
1 - hot face; 2 - silicon carbide grains showing some cracks; 3 - silicon carbide bond. Bar = 30 μm.

analyses showed no real alteration of the brick, again the impurities had disappeared from the bond.
In a joint near the hot face some metallic iron was found, which had damaged the silicon carbide (formation of FeSi). In the brick KOH and KCN were found also. The silicon carbide grains were partly cracked near the hot face. Some of them seemed to be scratched out of the bond as can be seen from figure 7.7.
The experiments in blast furnace No 4 showed a linear wear along the furnace height. It is assumed that such a wear pattern also will be found in blast furnace No 6. In that case it is possible to estimate the wear at the height where the silicon carbide panels had been before the relining in 1976. The wear was found to be about 20 - 30 mm. Figure 7.8 shows the comparison between the wear in the former campaign and in the present one. The curves show that the wear in the present campaign is about 10 times smaller than before.

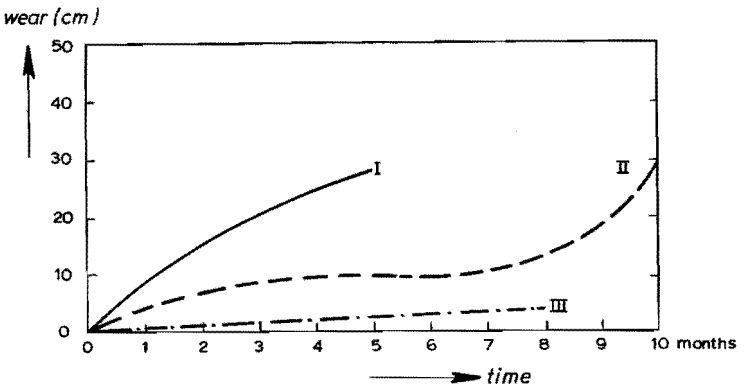

FIGURE 7.8 - Wear of different types of bricks in the first 9 months of operation in blast furnace No 6.
I - impregnated high duty fireclay; II - oxynitride-bonded silicon carbide; III - direct-bonded silicon carbide.

7.4 - Final Remarks

The laboratory experiments carried out with the four different types of brick show:
- that the abrasion resistance of the silicon carbide based bricks is

very good. At high temperatures (above 1000°C) the abrasion resistance of the direct-bonded bricks is better than that of any other brick tested.

- that the thermal-shock resistance of silicon carbide based bricks is much better than the thermal-shock resistance of corundum and high duty fireclay bricks. The thermal-shock resistance of the direct-bonded brick is about 3.5 times as good as of the oxynitride-bonded brick. At higher temperatures this difference will even increase, since the hot modulus of rupture of the direct-bonded brick remains stable, whereas above 1000°C the hot modulus of rupture of the oxynitride-bonded brick decreases.
- the resistance against potassium and blast furnace slag seems to be good for silicon carbide and perhaps for corundum based bricks. It was observed that the corundum showed some damage due to alkali bursting and the transition of α-Al_2O_3 into β-Al_2O_3. The oxynitride bond showed to be attacked by potassium compounds and by the blast furnace slag. The bond disappeared as was found in the laboratory tests as well as in practice. The direct-bonded silicon carbide bricks showed no damage in the laboratory tests. Even under the microscope no attack could be observed.

In practice silicon carbide based bricks seem to be a good solution for the blast furnace stack. In this thesis it is shown, that the production of direct-bonded silicon carbide bricks is possible. It was also shown that a good control of the furnace atmosphere while firing these bricks is of utmost importance for obtaining the required bonding system in the bricks.

The data obtained from the experiments in practice are too few yet, to conclude already whether direct-bonded silicon carbide bricks are to be prefered to the oxynitride-bonded ones. A final conclusion can be drawn after the current campaigns of blast furnace No 4 and No 6 have passed.

The laboratory tests clearly showed the advantages of the material. A disadvantage is the fact, that silicon carbide is soluble in iron. Therefore, its use will be limited to those areas in the furnace, where metallic iron is not yet present or is not in a liquid state. It is quite possible that the rather severe wear at the interception of the stack and the belly in both blast furnaces (No 4 and No 6) is caused by the

presence of metallic iron as was observed in the samples from blast furnace No 6.

It will be clear that the use of direct-bonded silicon carbide bricks is not limited to the use in the blast furnace stack. These highly abrasion and thermal-shock resistant bricks will be useful at high temperatures in other metallurgical and ceramic furnaces as well.

L i t e r a t u r e

[7-1] *Appendix II*	*Silicon carbide 1973, Proc. 3rd Int. Conf., 1973. New York. Columbia Univ. Press, 1974*
[7-2] *Starvic, Z.; Hue, M.*	*Keram. Zts. 27 (1975) No 3*
[7-3] *George, W.*	*Proc.Brit.Ceram.Soc. 40 (1973) 147-167*

APPENDIX I

LIST OF SPECIAL WORDS CONCERNING STEELMAKING AND REFRACTORIES

CHAPTER 1

Abrasion	- The wear of a surface by the mechanical action between solids.
Blast furnace	- Counter current reactor in which solid iron ore is converted into liquid crude iron.
Belly	- The part of the blast furnace of maximum cross-section between stack and bosh.
Bosh	- The truncated central part of the blast furnace, narrowing from the belly at the top to the tuyere belt at the bottom.
Burden	- The mixture of iron ore, coke, gravel, limestone and dolomite charged to the blast furnace.
Bustle pipe	- The common main surrounding a blast furnace, by means of which preheated air is distributed through the goose-necks to the tuyeres.
Campaign	- The production period between two major relinings. The campaign ends when a total relining of the furnace is carried out.
Carbon bricks	- A refractory brick consisting essentially of carbon.
Cowper (hot blast stove)	- A refractory construction in which the air for the blast furnace is preheated.
Fireclay	- A clay which is resistant to high temperatures, containing mainly kaolinitic clay minerals, free silica and which is nearly free from impurities of other constituents.
Graphite	- An allotropic hexagonal form of carbon. In the refractory world often used for bricks made of graphite grains bonded with tar and pitch, and calcined.
Hearth	- The lower part of the blast furnace in which the molten iron and slag is retained.

Hot blast main - Main connecting the hot blast stoves with the bustle pipe.

Hot metal - Liquid crude iron processed by means of a blast furnace.

Iron spot - A dark coloured spot on a refractory brick formed from particles of iron or its compounds present in a brick.

Pig iron - Solid crude iron; casting iron.

Semi-graphite - Not fully graphitized carbon. For instance petrol coke after calcining at temperatures between 1600°C and 2000°C.

Stack, Shaft - The truncated central part of the blast furnace widening from the charging system at the top to the belly at the bottom.

Slag - Non-metallic material formed during the treatment or purification of a metal, or substance resulting from the attack of a refractory product by materials in contact with it.

Thermal shock - A sudden change in temperature liable to cause spalling (see also chapter 2).

Tuyere - The device connected to the goose-neck, through which air is injected into the blast furnace.

Tuyere belt - The upper part of the hearth containing the tuyeres.

CHAPTER 2

Hot face - The face of the brick which is exposed to the furnace inside, and the burden in the furnace.

Standard size brick - A rectangular shaped brick with the following dimensions: length 230 mm; width 114 mm; thickness 74 mm.

Texture - Macroscopic relationship between the various shapes and sizes of pores and grains in a refractory product.

CHAPTER 3

Alkali bursting - Disintegration following a permanent increase in volume due to the formation of alkali compounds in the brick.

Brickwork - The wall construction consisting of bricks and jointing material (mortar).

Flat plate cooler - Water cooled rectangular mantel plates inserted in the blast furnace lining.

Grog - Burned fireclay, crushed for use in the mixtures for producing bricks.

High duty fireclay brick - A brick made from fireclay, with a low porosity and an Al_2O_3 content of about 42 % (m/m).

Thermal spalling - The cracking or fracture of a refractory product caused by differential expansion due to thermal shock, the effect of a steep temperature gradient or a cristallographic transition.

CHAPTER 4

Coking temperature - The temperature at which a pitch or tar containing material is fired to calcine, the tar or pitch into coke like carbon.

Green - Unfired.

Green brick - Refractory material pressed into the shape of a brick but not yet fired.

Matrix - Is the space between the refractory grains > 150 μm. It consists for a high percentage of a glassy phase, very fine particles and pores.

Reaction firing - During this firing a chemical reaction takes place, which is the essential for the final properties of the brick. In the electro- and fine ceramic industry often the word reaction sintering is used. In the firing procedure used for this thesis no sintering takes place, but the bond for the brick is due to the chemical reaction taking place.

Topology - Geometrical description of matter and space.

Topo ceramic model - The geometric conception for describing ceramic bodies.

T a b l e IIa - Characteristics of the bricks investigated for the choice of the type of bricks

property			graphite	semi graphite	high duty fireclay	magnesite	corundum	silicon carbide	corundum (99 %)
main constituent			99 % (m/m) C	99 % (m/m) C	42 % (m/m) Al_2O_3	95 % (m/m) MgO	95 % (m/m) Al_2O_3	92 % (m/m) SiC	99.5 % (m/m) Al_2O_3
bond			pitch	pitch	glass	silicate	mullite	oxynitride	direct
ρ	g/cm^3		2.21	2.15	2.76	3.56	3.82	3.21	3.94
d_s	g/cm^3		1.54	1.65	2.26	2.98	3.29	2.53	3.18
π_w	% (V/V)		30.0	22.0	17.0	16.5	14.0	21.0	19.3
π_s	% (V/V)		24.0	15.0	13.0	15.5	13.0	20.0	18.9
CCS	MN/m^2		14.5	26.2	66	95.8	266	168	62.1
M [MN/m^2] / Δd [mm]		20°C	3.7 - 0.3	7.3 - 0.5	16 - 0.3	19.0 - 0.4	44 - 0.5	54 - 0.4	17.4 - 0.3
		400°C	5.8 - 0.4	8.8 - 0.4	20 - 0.3	9.1 - 0.2	48 - 0.5	56 - 0.4	18.4 - 0.3
		800°C	4.0 - 0.4	8.4 - 0.4	16 - 0.3	5.7 - 0.2	47 - 0.5	54 - 0.4	15.9 - 0.2
		1000°C	4.2 - 0.5	8.8 - 0.4	13 - 0.3	9.7 - 0.2	48 - 0.7	44 - 0.2	14.6 - 0.2
		1200°C	4.4 - 0.5	6.9 - 0.4	8 - 0.8	5.5 - 0.5	28 - 0.4	26 - 0.2	11.8 - 0.2
		1400°C	3.8 - 0.6	8.6 - 0.5	4 - 1.0	3.3 - 1.0	18 - 0.3	18 - 0.3	2.9 - 0.4
λ	W/m.K	20°C	90	50	1.2	8	5	22	-
		100°C	-	-	-	-	-	-	2.8
		1000°C	35	30	0.9	4	2	7	-
α		$.10^{-5}$	0.18	0.38	0.50	1.18	0.8	0.5	0.83
E	N/m^2	$.10^9$	1.3	1.3	4.2	10	38	12	-
c_p	J/K.kg	$.10^3$	13.9	8.7	27.1	28.1	11.4	26.1	-

T a b l e IIb - Types of brick used in the test panels of blast furnace No 6

property		I	II	III	IV	V
main constituent		92 % (m/m) SiC	67 % (m/m) SiC	90 % (m/m) SiC	85 % (m/m) SiC	45 % (m/m), 45 % (m/m SiC C
bond		oxynitride	ceramic	Al_2O_3, TiO_2	ceramic	pitch
ρ	g/cm^3	3.21	3.12	3.21	3.17	2.35
d_s	g/cm^3	2.53	2.42	2.56	2.53	1.19
π_w	% (V/V)	21.0	22.4	21.7	20.2	15.0
π_s	% (V/V)	20.0	20.8	21.2	19.1	6.9
CCS	$MN.m^{-2}$	168	50	80	95	35
M [$MN.m^{-2}$] / Δd [mm]	20°C	54 - 0.4	23 - 0.4	23 - 0.2	nd	13 - 0.5
	400°C	56 - 0.4	29 - 0.4	38 - 0.3	nd	17 - 0.5
	800°C	54 - 0.4	29 - 0.4	37 - 0.3	nd	16 - 0.6
	1000°C	44 - 0.2	46 - 0.4	41 - 0.3	nd	11 - 0.6
	1200°C	26 - 0.2	23 - 0.5	36 - 0.3	nd	8 - 0.8
	1400°C	18 - 0.3	8 - 0.6	19 - 0.3	nd	7 - 0.8

nd = no data

S U M M A R Y

In this thesis a model is developed to describe the wear mechanism of the lower blast furnace stack lining. The three main causes of wear are: erosion, corrosion and thermal-shock. The phenomena can be translated into properties which the lining material should have. These properties have been measured by means of laboratory tests for a number of refractory materials of which reasonable resistance was expected. In this way a ranking of various types of bricks was established. The ranking showed silicon carbide bricks to be most promising for use in the blast furnace stack.

All the bonding systems investigated, however, of silicon carbide bricks available on the market are attacked in the blast furnace. The silicon nitride/oxynitride bond gave the best performance, but it was also attacked, therefore, research was carried out to develop a direct-bonded silicon carbide brick.

In this thesis that possibility has been studied. Thermodynamic considerations showed the possibility of silicon carbide formation even below the melting point of silicon, when the silicon carbide is formed out of its elements. Based on thermodynamical calculations it is shown, that five different reaction mechanisms might be possible. The occurrence of the reaction mechanisms proposed was studied in an experimental furnace in which good defined atmospheres could be maintained. The experiments showed, that the five reaction mechanisms proposed do occur depending upon the gas atmosphere used. It was established that not only a direct solid-solid reaction does occur, but also reactions take place between silicon vapour and solid carbon, SiO vapour and solid carbon, solid silicon and CO, and between SiO and CO vapour. Silicon carbide formation for the latter three possibilities only occurs when the oxygen partial pressure is low enough, otherwise SiO_2 will be formed. For very low partial pressures of oxygen it acts like a catalyst for the silicon carbide reaction. The promising results of the first commercially produced direct-bonded silicon carbide bricks and their behaviour in the blast furnace are discussed.

In dit proefschrift wordt een model ontwikkeld, waarmee de slijtage van het onderste deel van de hoogovenschachtwand kan worden beschreven. De drie hoofdoorzaken van de slijtage zijn: erosie, corrosie en thermische schok. De genoemde fenomenen kunnen vertaald worden in eigenschappen waaraan de vuurvaste bemetseling van de hoogoven moet voldoen. Deze eigenschappen zijn met behulp van laboratoriumproeven bepaald voor een aantal in aanmerking komende materialen. Op deze wijze is een rangschikking verkregen, waaruit bleek, dat van siliciumcarbide onder de gegeven omstandigheden de beste resultaten te verwachten waren.

Alle bindingstypen van op de markt verkrijgbare siliciumcarbide-stenen bleken echter onder hoogovenomstandigheden aangetast te worden. Van de verschillende bindingstypen bleek de siliciumnitride/oxinitride nog de beste eigenschappen te bezitten. Ook de nitriden worden echter aangetast, daarom werd het verdere onderzoek gericht op de ontwikkeling van direct gebonden siliciumcarbide-stenen.

In dit proefschrift wordt de mogelijkheid hiervan bestudeerd. Aan de hand van thermodynamische beschouwingen wordt aangetoond, dat de vorming van siliciumcarbide uit haar elementen al mogelijk is bij temperaturen beneden het smeltpunt van silicium. Aangetoond werd dat, op grond van de thermodynamische gegevens, vijf reactiemechanismen te verwachten zijn. Met behulp van experimenten in goed gedefinieerde gasatmosferen werden de vormingsmechanismen van siliciumcarbide bestudeerd. De experimenten lieten zien, dat de vijf mechanismen afhankelijk van de gasatmosfeer werkelijk optreden. Aangetoond werd dat, naast een directe vaste stof-vaste stof reactie, reactie mogelijk is tussen vaste koolstof en siliciumdamp, vaste koolstof en SiO-damp, vast silicium en CO-damp en tussen SiO en CO. De laatste drie reacties geven alleen SiC-vorming, wanneer de zuurstof-partiaaldruk voldoende laag is. In dat geval werkt de zuurstof als een soort katalisator.

Tot besluit worden de bemoedigende resultaten van de produktie van direct gebonden siliciumcarbide-stenen en hun gedrag in de hoogoven besproken.

D A N K W O O R D

Het in deze dissertatie beschreven onderzoek werd verricht in de research- en bedrijfslaboratoria van Hoogovens IJmuiden BV. De produktie van stenen voor de proeven in de praktijk werd uitgevoerd door Annawerk Keramische Betriebe GmbH, Rödental - West-Duitsland.
De Directie van de Hoogovens-laboratoria ben ik bijzonder erkentelijk voor de mogelijkheid die zij mij geboden hebben om dit onderzoek te verrichten en te publiceren.
Veel dank ben ik verschuldigd aan de heren H.A.J. Kieftenbeld en E.F. Schotman, die een belangrijk aandeel hebben gehad in het onderzoek en de uitwerking van de resultaten. De kritische begeleiding van het onderzoek door ir. A. Waasdorp, ir. J. van Laar, drs. J.A.M. van Langen en ir. B. Zuidema heb ik zeer gewaardeerd. Ir. S. van Goudoever ben ik zeer erkentelijk voor het kritisch doorlezen van het manuscript.

Ohne die wertvolle Zusammenarbeit mit Annawerk Keramischen Betrieben GmbH wäre die Entwicklung der Steine nicht möglich gewesen. Den Enthusiasmus womit Annawerk unsere Idee direkt-gebundener Steine herzustellen begrüsst hat, war von grosser Bedeutung für die weitere erfolgreiche Zusammenarbeit.
Die viele Besprechungen mit die Herren Professor E. Gugel, Dr. H.G. Nitzsche, U. Klein, G. Senftleben und Dr. A. Fickel sind von grosser Bedeutung gewesen für meine Arbeit. Ich danke die Herren Gugel, Nitzsche und Fickel für die kritische Begleitung bei der Anfertigung meiner Dissertation.

Mar Heijndijk en de heer A.A. Verkooyen dank ik hartelijk voor hun bijdrage in de totstandkoming van het manuscript.

STELLINGEN

1. Door Hasselman wordt een karakterisering van de temperatuurwisselbestendigheid van keramische materialen gegeven, waarbij ten onrechte géén rekening wordt gehouden met het ontstaan van temperatuurgradienten in het materiaal bij plotselinge veranderingen van de oppervlaktetemperatuur.

   Hasselman, D.P.H. Voordracht, XIX Int. Feuerfest-Kolloquium, okt. 1976

2. Asvrije koolstofstenen worden in een hoogoven niet door kaliumdamp of door kaliumverbindingen aangetast. Ten onrechte nemen Hawkins et al. aan dat kaliumdamp met de koolstof zal reageren.

   Hawkins, R.J.; Monte, L.; Waters, J.J. Ironmaking Steelmaking (Quarterly); 1 (1974), No. 3, 151-160

3. α-SiC wordt niet in meetbare hoeveelheden gevormd beneden 1410°C; er vormt zich vrijwel uitsluitend β-SiC. Boven 1410°C ontstaat hoofdzakelijk α-SiC. *Dit proefschrift*

4. In het oxystaalproces ontstaat tijdens de periode van maximale ontkoling ten gevolge van geëmulgeerde staaldeeltjes een extra oppervlak, dat ongeveer de afmeting van 7 voetbalvelden bezit, terwijl het stilstaande bad slechts een oppervlak heeft van circa 1/3 van het doelgebied.

5. De lichtgekleurde dicht gesinterde zone in een versleten teergebonden magnesietsteen uit een oxystaalconverter bestaat niet uit gerekristalliseerde periclaas, maar uit een mengsel van onveranderde periclaas en gerekristalliseerde silica.

   1. *Howe, R.A.; Mc.Gee, T.D.; Osterholtz, C.E. Am.Ceram.Soc.Bull. 55 (1976) No. 2, 205-209*
   2. *Kim, S.M.; Lu, W.K.; Nicholson, P.S. Mc.Master Symp. Hamilton, Canada, 1976*

6. Een beschrijving van de fysische verschijnselen aan het contactoppervlak van alveolen en stofdeeltjes in de longen met behulp van de halfgeleidertheorie zou het inzicht in het ontstaan van longaandoeningen ten gevolge van stof vergroten. *Klosterkötter, W.; Robock, K. Am.Ind.Hygiene Ass.J. (1975), 659-668*

7. De beschrijving van de materie wordt in eerste benadering steeds gecompliceerder bij toenemende ordening.

8. Het normaliseren van bepalingsmethoden is alleen gericht op het verkrijgen van eensluidende analyseresultaten tussen laboratoria. Het mag nimmer de ontwikkeling van nieuwe en betere methoden in de weg staan.

9. De strategie van een steekproefschema dat gebruikt wordt voor afnamekeuring dient zodanig te zijn ingericht, dat de technische eis die aan het te keuren produkt gesteld wordt, door de keuze van de steekproefomvang niet wordt beïnvloed.

1. DIN 51061
2. ISO/TC 33/SC 6, N 226

10. Het gebruik als determinatiekenmerk van een samengetrokken onderste bladbasis bij het genus Otozamites (Bennettitales) is vaak niet betrouwbaar. *Ash, S.R. Palaeontographica Abt. B. 149 (1975), 150*

11. Het schrijven van een leerboek is als lesgeven voor een lege klas.

12. De plannen van staatssecretaris Hendriks om het aantal ziekenhuizen in de IJmond drastisch te beperken, zijn een schoolvoorbeeld van gebrek aan beleid. *Perspublikaties januari 1977*